# MONITORING, ANALYSIS, AND SIMULATION OF PHOTOVOLTAIC HEAT ISLAND EFFECT IN TURKEY: SEKBANDEMIRLI SOLAR POWER PLANT FIELD STUDY

A THESIS SUBMITTED TO
THE GRADUATE SCHOOL OF NATURAL AND APPLIED SCIENCES
OF
MIDDLE EAST TECHNICAL UNIVERSITY

BY

EMRE DEMİREZEN

IN PARTIAL FULFILLMENT OF THE REQUIREMENTS
FOR
THE DEGREE OF DOCTOR OF PHILOSOPHY
IN
EARTH SYSTEM SCIENCE

JANUARY 2022

Approval of the thesis:

**MONITORING, ANALYSIS, AND SIMULATION OF PHOTOVOLTAIC HEAT ISLAND EFFECT IN TURKEY: SEKBANDEMIRLI SOLAR POWER PLANT FIELD STUDY**

submitted by **EMRE DEMİREZEN** in partial fulfillment of the requirements for the degree of **Doctor of Philosophy** i**n Earth System Science, Middle East Technical University** by,

Prof. Dr. Halil Kalıpçılar
Dean, Graduate School of **Natural and Applied Sciences** _____

Prof. Dr. Bülent G. Akınoğlu
Chair of the Program, **Earth System Science** _____

Prof. Dr. Bülent G. Akınoğlu
Supervisor, **Earth System Science, METU** _____

Assist. Prof. Dr. Talat Özden
Co-Supervisor, **Electrical and Electronics Engineering, Gümüşhane University** _____

**Examining Committee Members:**

Prof. Dr. İsmail Yücel
Civil Engineering, METU _____

Prof. Dr. Bülent G. Akınoğlu
Earth System Science, METU _____

Assoc. Prof. Dr. Adem Bayram
Civil Engineering, Karadeniz Technical University _____

Prof. Dr. Aynur Eray
Physics Engineering, Hacettepe University _____

Assoc. Prof. Dr. Onur Taylan
Mechanical Engineering, METU _____

Date: 18.01.2022

**I hereby declare that all information in this document has been obtained and presented in accordance with academic rules and ethical conduct. I also declare that, as required by these rules and conduct, I have fully cited and referenced all material and results that are not original to this work.**

Name Last name : Emre Demirezen

Signature :

# ABSTRACT

## MONITORING, ANALYSIS, AND SIMULATION OF PHOTOVOLTAIC HEAT ISLAND EFFECT IN TURKEY: SEKBANDEMİRLİ SOLAR POWER PLANT FIELD STUDY

Demirezen, Emre
Doctor of Philosophy, Earth System Science
Supervisor: Prof. Dr. Bülent G. Akınoğlu
Co-Supervisor: Assist. Prof. Dr. Talat Özden

January 2022, 158 pages

Today, solar energy conversion technologies, which are among the methods of obtaining renewable, sustainable, and clean energy, show rapid development. One of the most common technologies is Photovoltaic Solar Power Plant (PVPP), which provides electricity by direct conversion of the energy carried by the sunlight (or daylight). These power plants are socially accepted in environmentally-friendly and economical energy production. However, there are some debates about the environmental impacts of these power plants. One of the issues at the focus of these debates is whether dark-colored photovoltaic solar module (panel) arrays in large numbers used to build these power plants alter the natural ground reflectivity (albedo) of the land where they are installed. For this reason, they may also affect the local air temperature cycles of the region where they are located. This environmental problem, referred to as the Photovoltaic Heat Island Effect (PVHIE) in the literature, arises from the optical and thermal properties of photovoltaic modules interacting with their close environment. A three-year field project and study was carried out to observe this effect in a PVPP constructed in the

Sekbandemirli rural area in the Tavşanlı district of the Kütahya province in Turkey. The relevant weather data collected by the meteorological stations installed on specific locations inside and outside Sekbandemirli PVPP were analyzed using statistical (ANOVA and Tukey's HSD), correlational (Pearson and Spearman), graphical (percentage column distribution, daily and monthly line charts, and representative illustrations) and simulation-based (the microclimate simulation software *ENVI-met*) methods. Accordingly, the heat island formations, which can be expressed as "transient", whose frequency of occurrence changes daily and seasonally, have been found at the Sekbandemirli PVPP field center. The air temperatures recorded at the field center show the differences between "(-3) – 6°C" compared to those recorded at the reference location outside the field. The higher daytime ambient air temperatures up to 6°C difference at the field center significantly indicate the evident (and positive) PVHI formations, although a less effective (up to -3°C) cooling effect (negative PVHIE) prevails mostly at nighttimes. This thesis is the first study on PVHIE in Turkey and the world, in line with the methods used within its content.

Keywords: Heat island effect, Air temperature, Weather station, Solar power plant, Photovoltaic module

# ÖZ

## TÜRKİYE'DE FOTOVOLTAİK ISI ADASI ETKİSİNİN İZLENMESİ, İNCELENMESİ VE BENZETİŞİMİ: SEKBANDEMİRLİ GÜNEŞ ENERJİSİ SANTRALİ SAHA ÇALIŞMASI

Demirezen, Emre
Doktora, Yer Sistem Bilimleri
Tez Yöneticisi: Prof. Dr. Bülent G. Akınoğlu
Ortak Tez Yöneticisi: Dr. Öğretim Üyesi Talat Özden

Ocak 2022, 158 sayfa

Günümüzde yenilenebilir, sürdürülebilir ve temiz enerji elde etme yöntemleri arasında bulunan güneş enerjisi dönüşüm teknolojileri, hızlı bir gelişim göstermektedir. Bu teknolojilerin en yaygın olanlarından birisi, güneş (veya gün) ışığının taşıdığı enerjinin doğrudan çevrimi ile elektrik eldesini sağlayan Fotovoltaik Güneş Enerjisi Santrali (FV-GES)'dir. Bu santraller, çevre-dostu ve ekonomik enerji üretiminde toplumsal olarak kabul görmüştür. Ancak bu santrallerin çevresel etkileri hakkında bazı tartışmalar mevcuttur. Bu tartışmaların odağındaki konulardan biri, bu enerji santrallerini inşa etmede kullanılan büyük sayılardaki koyu renkli fotovoltaik güneş paneli dizilerinin, kuruldukları doğal arazinin doğal yüzey yansıtabilirliğini (albedo) değiştirip değiştirmediği üzerinedir. Bu nedenle, bulundukları bölgenin yerel hava sıcaklık döngülerini de etkileyebilirler. Literatürde Fotovoltaik Isı Adası Etkisi (FV-IAE) olarak geçen bu çevresel sorun, yakın çevresiyle etkileşim yapan fotovoltaik güneş modüllerinin optik ve termal özelliklerinden kaynaklanmaktadır. Bu etkiyi gözlemlemek için Türkiye'nin Kütahya iline bağlı Tavşanlı ilçesindeki Sekbandemirli kırsal kesimine kurulmuş bir güneş enerjisi santralinde üç yıl süren

bir saha projesi ve çalışması yürütülmüştür. Sekbandemirli GES içinde ve dışında belirli noktalara kurulan meteorolojik istasyonlar ile toplanan ilgili hava durumu verileri istatistiksel (ANOVA ve Tukey's HSD), korelasyonel (Pearson ve Spearman), grafiksel (yüzedesel sütun dağılımı, günlük ve aylık çizgi grafikleri ve temsili çizimler) ve simülasyon tabanlı (mikroiklim simülasyon yazılımı *ENVI-met*) yöntemler kullanılarak analiz edilmiştir. Bu doğrultuda, Sekbandemirli FV-GES sahasının merkezinde, oluşma sıklığı günlük ve mevsimsel olarak değişen, "geçici" olarak ifade edilebilecek ısı adası oluşumları bulunmuştur. Saha merkezinde kaydedilen hava sıcaklıkları, saha dışındaki referans alınan lokasyonda kaydedilen hava sıcaklıklarına göre çoğunlukla "(-3) - 6°C" arasında farklar göstermektedir. Çoğunlukla geceleri daha az etkili (-3°C'ye kadar) bir soğuma etkisi (negatif FV-IAE) baskın olmasına rağmen, gündüzleri saha merkezinde 6°C'ye varan daha yüksek ortam hava sıcaklıkları, anlamlı olarak belirgin (ve pozitif) FV-IA formasyonlarına işaret etmektedir. Bu tez, içeriğinde kullanılan yöntemler doğrultusunda, FV-IAE konusunda Türkiye'de ve dünyada yapılan ilk çalışmadır.

Anahtar Kelimeler: Isı adası etkisi, Hava sıcaklığı, Meteorolojik istasyon, Güneş enerjisi santrali, Fotovoltaik güneş paneli

*I dedicate all the effort put into this thesis to my family, teachers, and friends*

## ACKNOWLEDGMENTS

I would like to thank my thesis supervisor, Prof. Dr. Bülent G. Akınoğlu, for his valuable contributions from the idea development to the project management and the coordination among the project team (and the Thesis Monitoring Committee members) of this study, which was conducted for the first time in its field in Turkey.

In addition to developing the content of the thesis work, I would also like to thank my co-supervisor, Assist. Prof. Dr. Talat Özden, who communicated with the relevant stakeholders, made the required agreements on behalf of the project team accordingly and personally took care of the technical infrastructure preparations at the Sekbandemirli field to launch this thesis study as a field research project.

I would like to thank Prof Dr. Raşit Turan, the founder of ODTÜ-GÜNAM, and my director during my administrative position. In addition to his suggestions and comments during the Thesis Proposal Defense, the possibilities for utilizing the ODTÜ-GÜNAM's infrastructure services by Prof. Turan's approval are very beneficial in shaping the thesis.

I would also like to thank Prof. Dr. Ayşen Yılmaz, Prof. Dr. İsmail Yücel, Prof. Dr. Özlem Özdemir, Prof. Dr. Aynur Eray, Assoc. Prof. Dr. Adem Bayram, and Assoc. Prof. Dr. Onur Taylan for their valuable ideas and suggestions for improving the thesis in terms of content and scope in the thesis juries (Thesis Proposal Defense, Thesis Monitoring Committees, and Thesis Defense).

During the field project application stages of the thesis, the project manager of the Teknik Grup company, Tolga Eryaşar, provided convenience in the extension of the data collection and monitoring process and fast support in solving technical problems at the field, apart from the service purchased from the company.

Alparslan Yavuz, the Sekbandemirli PVPP operating company owner, kindly gave us permission to conduct our field projects in their power plant, and Oğuz Aydın, one of the engineers of this company, was spared time for both our field visit and remote communication.

Ahmet Hamdi Aksoy, Hakan Akınoğlu, and Cengiz Karaman made the visual designs of some figures in the content of the thesis.

Middle East Technical University funded the scientific research projects of this thesis with the project numbers BAP-07-02-2017-006 and TEZ-D-105-2020-10169).

Turkish State Meteorological Service provided the Tavşanlı weather station data utilized within the data analysis of this thesis.

I would also like to thank the professors and colleagues whose names are mentioned below (or whom I may have forgotten to mention) for their suggestions and support regarding the preparations of the content of this thesis:

Prof. Dr. Aysıt Tansel, Prof. Dr. Güzin Erlat, Prof. Dr. Haluk Erlat, Dr. Özlem Aydoğan, Tayfun Hız, Ayşegül Karabulut, Buket Gökbakan, Bilge Tunçel, Elşen Aydın, Asmin Aşkın, Beyza Durusoy, Zeynep Tuğçe Özkarslıgil, Gence Bektaş, Dr. Nilsun Hasançebi, Ömer Öncü, Yasemin Yıldırır, and Bouchra Laarabi.

## TABLE OF CONTENTS

## LIST OF TABLES

TABLES

## LIST OF FIGURES

FIGURES

## LIST OF ABBREVIATIONS

ABBREVIATIONS

| | |
|---|---|
| AC | : Alternating Current |
| AHI | : Atmospheric Heat Island |
| ANOVA | : Analysis of Variance |
| BIPV | : Building-Integrated PhotoVoltaics |
| CCGT | : Combined Cycle Gas Turbine |
| COP | : Conference of the Parties |
| CSP | : Concentrated Solar Power |
| CPU | : Central Processing Unit |
| DC | : Direct Current |
| ECHAM | : An atmospheric general circulation model, developed at the Max Planck Institute for Meteorology |
| EIA | : Environmental Impact Assessment |
| EMO | : The Chamber of Electrical Engineers |
| EROI | : Energy Return on Investment |
| ESMAP | : Energy Sector Management Assistance Program |
| EU | : European Union |
| EVA | : Ethyl Vinyl Acetate |
| GENSED | : Solar Energy Industrialists and Industry Association |

GHG : Green House Gas

HIE : Heat Island Effect

HJT : Heterojunction Technology

HSD : Honest Significant Difference

IBC : Interdigitated Back Contact

IEA : International Energy Agency

IR : Infrared

IRENA : International Renewable Energy Agency

LCOE : Levelized Cost of Electricity

ODTÜ GÜNAM : Middle East Technical University – Center for Solar Energy Research and Applications

PERC : Passivated Emitter and Rear Contact/Cell

PV : PhotoVoltaic

PVHIE : PhotoVoltaic Heat Island Effect

PVPP : PhotoVoltaic Power Plant

REN21 : Renewables 2021 Global Status Report

RCP : Representative Concentration Pathway

SHI : Surface Heat Island

SSP : Shared Socioeconomic Pathway

TEİAŞ : Turkish Electricity Transmission Corporation

TFEC : Total Final Energy Consumption

TMMOB : The Union of Chambers of Turkish Engineers and Architects

TOPCon : Tunnel Oxide Passivated Contact

TSMS : Turkish State Meteorological Service

T.R. : Turkish Republic

UAE : United Arab Emirates

UBLHI : Urban Boundary Layer Heat Island

UCLHI : Urban Canopy Layer Heat Island

UHI : Urban Heat Island

UK : United Kingdom

UN – SDGs : United Nations Sustainable Development Goals

UNFCCC : United Nations Framework Convention on Climate Change

US : United States

US-EPA : United States - Environmental Protection Agency

WHO : World Health Organization

WMO : World Meteorological Organization

WWF : World Wildlife Fund

WS : Weather Station

## LIST OF SYMBOLS

SYMBOLS

| | |
|---|---|
| °N, E, S, W | : degrees North, East, South, West |
| acc | : Accuracy |
| Eq. | : Equation |
| $I_{mp}$ | : Maximum power current |
| $I_{sc}$ | : Short circuit current |
| K | : Poisson constant |
| m | : meter |
| m/s | : meter per second |
| MWh | : Megawatt-hour |
| $p_0$ | : Standart atmospheric pressure |
| $p$ | : Actual atmospheric pressure |
| P | : PVPP Electrical Power Output |
| $P_{max}$ | : Maximum power |
| Sw | : Shortwave |
| $T_{M\ (or\ m)}$ | : Module temperature |
| $V_{mp}$ | : Maximum power voltage |
| $V_{oc}$ | : Open circuit voltage |
| WS | : Weather Station |

$WS_{WDi}$ : : Wind direction measured by the relevant (i) Weather Station

$WS_{WSi}$ : Wind speed measured by the relevant (i) Weather Station

$WS_{Ti}$ : Air temperature measured by the relevant (i) Weather Station

$\theta$ : Potential air temperature

# CHAPTER 1

# INTRODUCTION

It can be said that among the various environmental problems that have occurred at the global and regional level in the world to date, the one whose impact area is as clear as "climate change". Today, "global warming", which has a negative impact on many issues from agricultural applications to energy provision and use, from health sciences to sociology, from economic development to textiles, has emerged as one of the most conspicuous results of climate change. The concept of “warming” here does not only emphasize the increase in air temperature in the atmosphere. At the same time, this situation also includes the increase in the frequency of observation of extreme weather and climate events, as well as disasters such as drought, flood, avalanche, erosion, forest fire, throughout the world geography and at the local level.

## 1.1 Global and Regional/Local Impacts of Climate Change

Atmospheric radiative forcing of $CO_2$ gas, which has the highest share in greenhouse gas emissions that trigger climate change, showed the fastest increase following the beginning of the Industrial Revolution (Figure 1.1). Consequently, the 1-2°C increase in the surface air temperature over land and global mean surface temperature (land and ocean) values towards 2020 (Figure 1.2) has caused the unique climatic characteristics of many different geographies of the world to change.

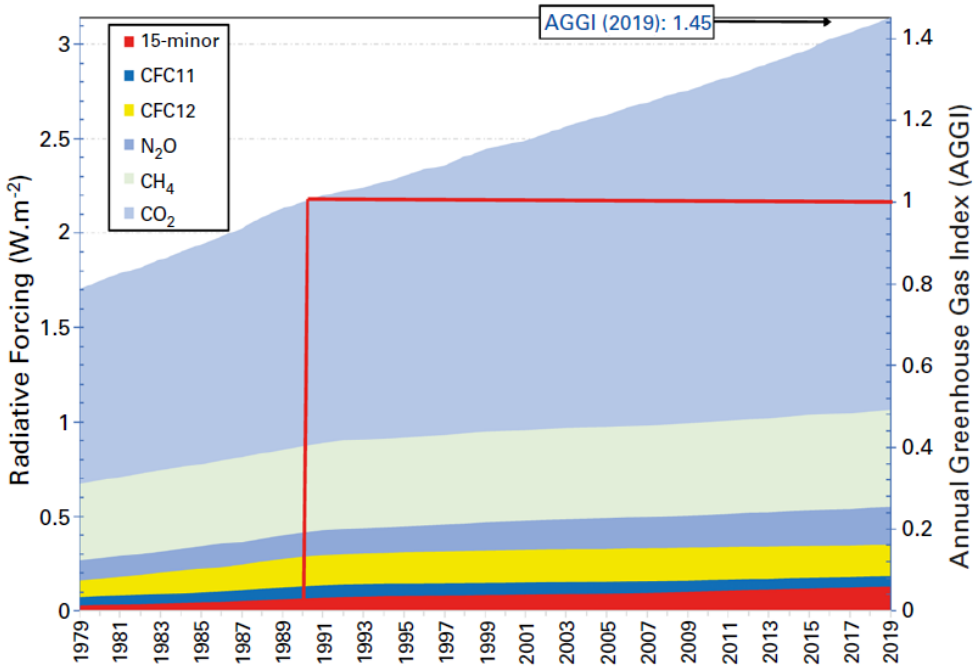


Figure 1.1. Atmospheric Radiative Forcing and Greenhouse Gas Index between 1979-2019 [109]

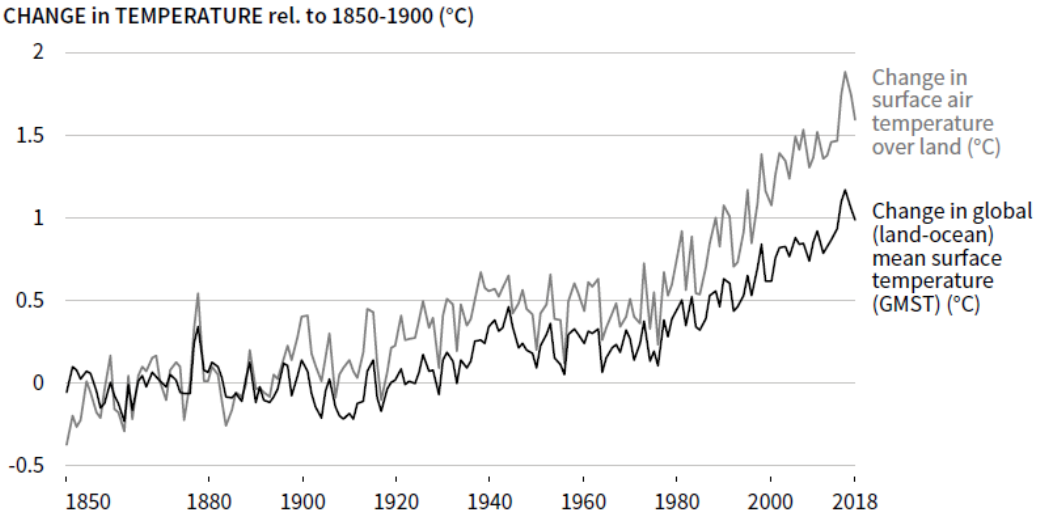


Figure 1.2. Temperature Change between 1850-2018 [46]

According to the World Meteorological Organization's State of the Global Climate 2020 report [108], the years between 2014-2020 (including 2020) were recorded as the six warmest years. On June 20, 2020, the temperatures reaching 38.0°C in the northern region of the Arctic Circle were recorded in the Verkhoyansk region in northeastern Russia. The upward trend in sea-level rise is accelerating, and the ability of the oceans to mitigate climate change weakens because of the increase in ocean heat storage and acidification. In September 2020, the minimum sea-ice extent in the Arctic region was recorded as the second-lowest level. In the Laptev Sea in the Arctic Ocean, the earliest sea-ice retreat was observed by satellite. As reported by this report from WMO, the mass loss in the Antarctic region tended to accelerate around 2005 and now has about 175 to 225 Gt of ice per year. The report also noted that 2020 was unusually active for the North Atlantic hurricane season, and hurricanes, extreme heatwaves, severe droughts, and wildfires caused many deaths and economic losses of tens of billions of US dollars. In addition, during the first half of 2020, there was a migration intensity around 9.8 million, mostly due to hydro-meteorological hazards and disasters. In addition to the extreme weather impacts, the entire food supply chain has been affected by the disruption of COVID-19 in the agriculture sector, and food insecurity has increased.

These effects of climate change, which are detected in different geographical settlements and locations of the world, also affect Turkey with its regions. Thus, various projections, forecasts, and scenarios focused on climatic alterations are prepared and discussed. Some findings are included in the "Türkiye'nin Yarınları Projesi" [110] dated April 2010 of the World Wildlife Fund Turkey. It is estimated that there will be rapid temperature increases in Turkey and Konya Basin starting from 2030, reaching around 4°C in winter and 6°C in summer. Proportionally higher temperature increases in summer will not show significant regional differences. However, it is stated that during the winter season, the temperature increases in the inner parts of the country and particularly in the Eastern Anatolia Region will be higher compared to the coastal regions.

Some predictions on precipitation, snow thickness, river flow rates, and flow regime are also included in the WWF Final Report. The simulations of the ECHAM5 model demonstrate that an increase in precipitation is expected in the northern parts of Turkey, and a significant decrease is expected in the southern regions (Figure 1.3).

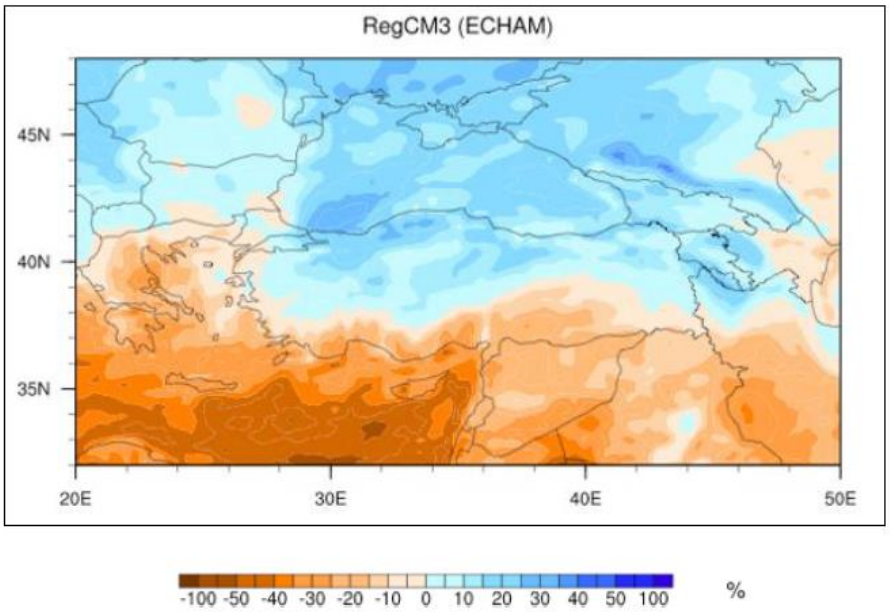


Figure 1.3. Winter Season Precipitation Comparison between 1961-1990 and 2071-2099 projection *(based on the ECHAM5 model simulations)* [110]

Furthermore, the decrease in the snow thickness in the region because of the increase in temperature in Eastern Anatolia may cause seasonal surface water flow changes. The amount of surface water flow in the region will increase in connection with a decline in the expected snow accumulation in the winter season. Conversely, the surface water flow decreases due to reduced snow accumulation during the seasonal transition period (winter to spring). As a result of this situation, it will change the flow regimes of the Euphrates and Tigris, two of the region's and Turkey's major rivers, and fed by surface water flow in Eastern Anatolia. The flow rates of these rivers will increase in winter months and decrease in spring months.

## 1.2 Importance of Solar Energy Conversion Technologies towards Renewable and Environmental Energy Production and Provision

The growth in total final energy demand (TFEC) worldwide between 2009 and 2019, as indicated in the REN21 report [78], can be understood from the increase in total final energy consumption (TFEC) (Figure 1.4). Fossil fuels, nuclear energy, and traditional biomass account for 3/4 of this increase. However, three issues have come to the fore in energy production and supply methods, especially due to the industrial activities carried out in line with the national energy policies of developed and developing countries, which cause anthropogenic climate change: Regulation of the current carbon emission activities thanks to “Net-Zero Emission / Carbon-Neutral” targets; "Energy Efficiency" studies, which include applications within the scope of more efficient energy utilization; and "Renewable Energies", which are environmentally friendly and that, unlike fossil fuels, are renewed by natural cycles without their use being limited to the reserves on Earth. Moreover, the 7$^{th}$ subject of the United Nations' Sustainable Development Goals, which came into force in January 2016 and consisted of 17 main titles in the social, economic, environmental, and cultural framework, is "Affordable and Clean Energy".

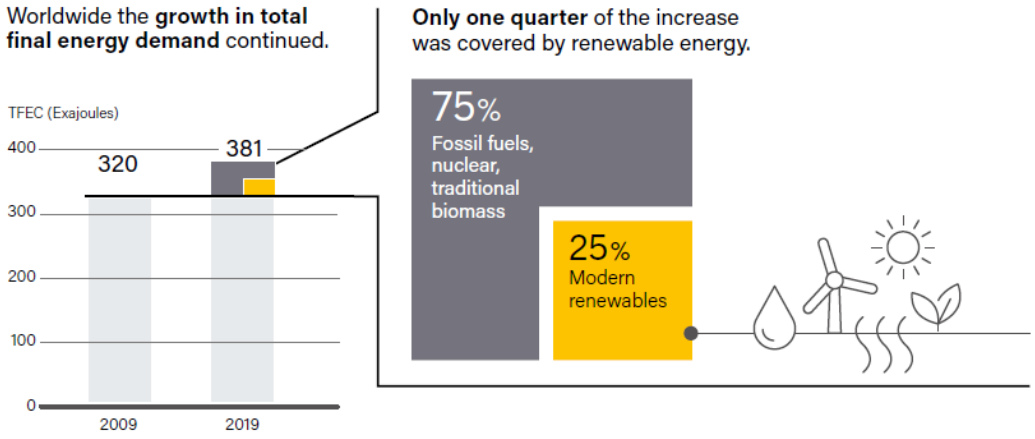


Figure 1.4. Modern Renewables Share in Total Final Energy Consumption between 2009-2019 [78]

There are five primary natural resources under the renewable energy title: Solar, wind, hydropower, geothermal, and biomass. In addition, there are some applications such as hydrogen, wave energy, and hybrid systems in this category. These sources are used in the conversions between thermal, mechanical, chemical, and electrical energy types through various energy conversion methods.

It can be said that the share of renewable energy sources is increasing gradually in reducing the negative environmental impacts (including climate change) that occur in energy production with the use of fossil fuels, on the atmosphere, water resources (oceans, seas, lakes, rivers, groundwater, etc.) on earth and green areas (forests, rural areas, natural habitats, etc.). As an indication of this growing share, the graph of the use of energy resources in electricity production for developing and advanced economies, published in the report of the International Energy Agency [47], can be examined (Figure 1.5). The increase in the use of renewable energy in both the economy types between 2010 and 2050 is remarkable.

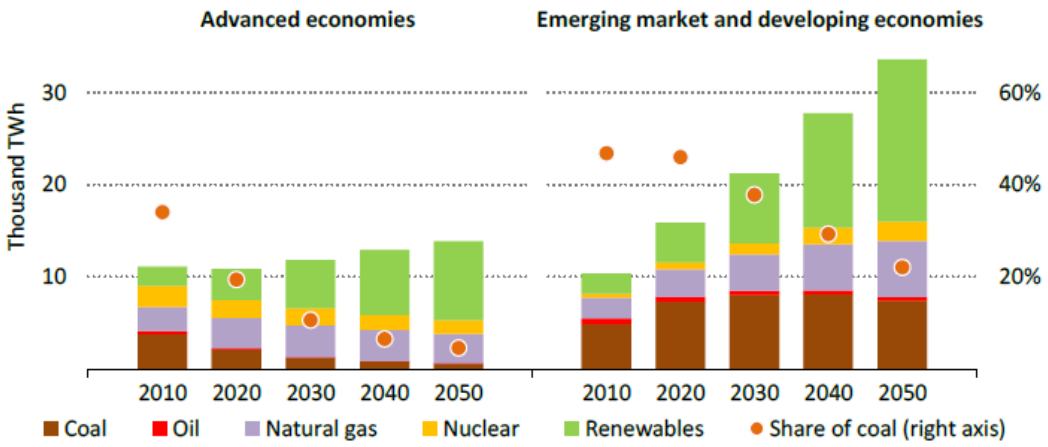


Figure 1.5. Electricity Generation by Year and Energy Resource [47]

Among renewable resources, the Sun’s energy is based on the fusion reactions that occur within its structure. The amount of the Sun’s electromagnetic radiation (including ultraviolet, visible, and infrared radiation (IR) band ranges and having a wavelength range from 100 nm to 1 mm) that reaches a unit area on Earth's orbit before it enters the Earth's atmosphere (in space) is called the *Solar Constant*. And its value is 1366 W/m². This value decreases to 1000 W/$m^2$ on the Earth's surface depending on some processes such as absorption, diffusion, and reflection in the atmosphere after sun rays enter the atmosphere (at solar noon on a clear day in the summer months).

Solar energy, which reaches the earth in two primary forms of energy as light and heat, can be converted into different types of energy via various environmentally friendly and practical energy conversion applications and technologies. In this direction, benefits can be provided in the form of passive and active heating and cooling with solar heat, water heating with solar heat, and electricity generation by sunlight or heat. Passive solar heating is related to the building designs and the selection of materials used, taking into account the amount of solar radiation reaching the facades of buildings by considering the four seasons. In the active heating and water heating systems, intermediary devices such as solar collectors, hot water pumps, or fans are used. The systems that provide electricity from the Sun are grouped under two technology titles: “PhotoVoltaic (PV)” technologies work with the principle of converting sunlight directly into electricity through solar cells and module/panel devices. As for the "Concentrated Solar Power (CSP)" systems, mechanical and electrical energy is obtained by focusing the sunlight on a particular receiver via several optical instruments such as mirrors and lenses to produce intense heat. There are also “hybrid systems” that refer to the hybrid use of these systems with other renewable energy technologies (e.g., wind turbines).

With solar PV and wind energy conversion systems, the worldwide electricity consumption has been on a higher trend in the last 20 years compared to other renewable energies (Figure 1.6).

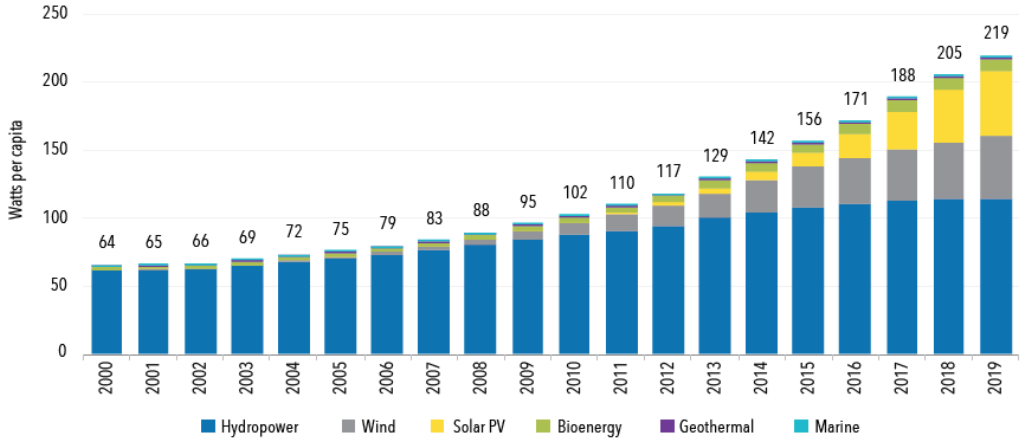


Figure 1.6. Global Electricity Consumption by Renewable Resource between 2000-2019 [44]

Furthermore, these systems are preferred in both the countries that have strong and weak opportunities to benefit from these energies, depending on their geographical location and resource potential. Plus, environmental awareness and social acceptance of all these countries' citizens and governments contribute to solar PV and wind energy proliferation day by day. As an indicator, the change in the LCOE of the four sub-energy technologies of these systems towards 2020 is given (Figure 1.7).

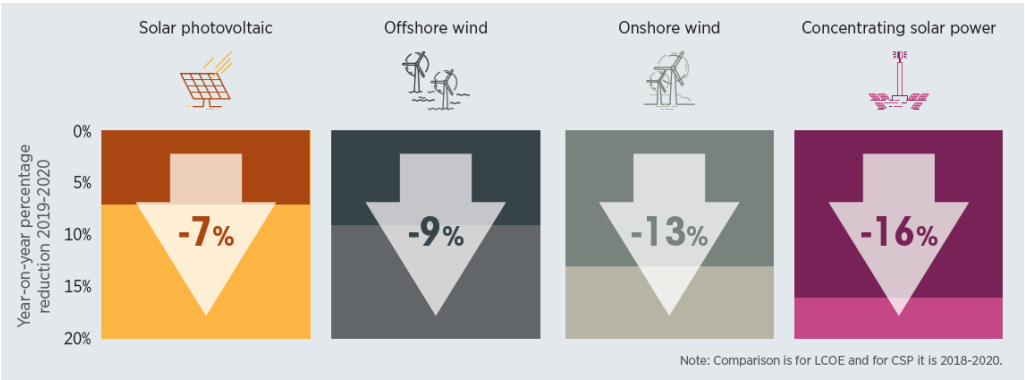


Figure 1.7. Reduction of Global Weighted-Average LCOE in Utility-Scale Solar and Wind Energy Technologies [45]

A similar development of these systems, which have a trend of growing installed power in the world, is also present in the capacity increase for electricity generation in Turkey by energy resource between 1990 and 2020 (Figure 1.8). The share of solar energy among installed power values by energy sources in 2020 is close to 6.5 MW (Figure 1.9).

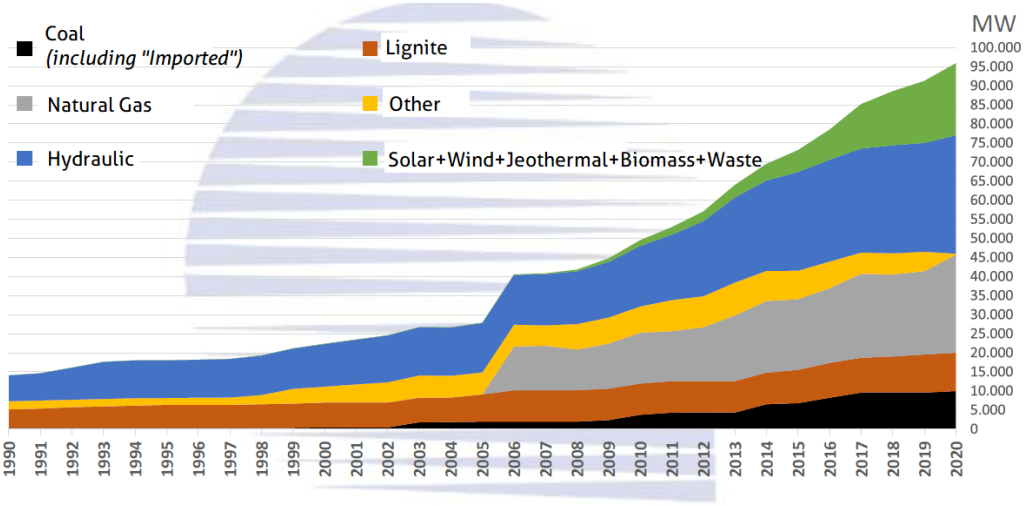


Figure 1.8. Turkey's Electricity Generation by Energy Resource between 1990-2020 [93]

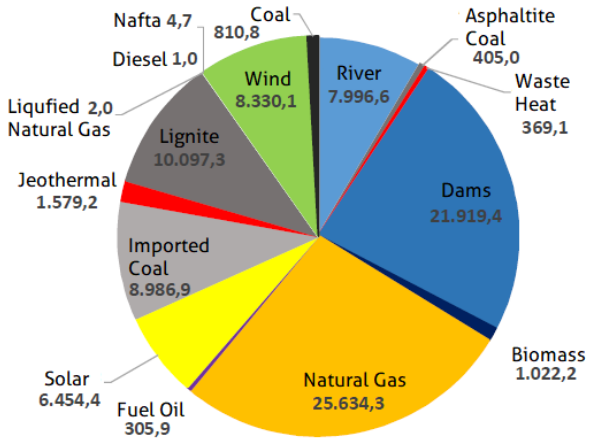


Figure 1.9. Turkey's Installed Power (MW) Distribution by Energy Resource in October 2020 [92]

Renewable energies also take their place in Turkey's climate, environment and energy policies. In the *Turkey Climate Change Strategy 2010-2023* of the T.R. Ministry of Environment, Urbanisation and Climate Change [88], it is stated that the share of renewable energy in total electricity generation will be enhanced to 30% by 2030. Regarding this enhancement, it is mentioned that the entire hydropower potential will be evaluated, wind and geothermal electricity production capacities will be increased, and electricity generation from solar energy will be encouraged. In the strategy, it is indicated that all domestic resources will be utilized as much as possible in parallel with the energy provision security and climate change targets. Also, the sanitary hot water systems will be supported by solar energy collectors.

## 1.3 Solar Photovoltaic Power Plants

There are two basic conversion technologies for large-scale land-use of solar energy: Concentrated Solar Power Plants (CSPPs) and Photovoltaic Power Plants (PVPPs). In CSPP technology, the rays coming from the Sun throughout the day are transferred to a receiver via mirror, lens, or reflector systems. The intense heat obtained from the Sun's rays transferred to this receiver provide the electricity used mostly at the industrial level. These systems are divided into four groups as Power Tower, Parabolic Troughs, Linear Fresnel, Power Tower, and Parabolic Dish types. Especially since tower-type CSPPs have to be installed in very large and idle areas, the countries with such lands within their borders in the world geography prefer using this technology. With about 50 projects on CSP [16], Spain ranks first in solar electricity conversion with this method. Spain is followed by the USA with 22 projects; China with 16 projects; India with 7 projects; South Africa with 6 projects; Morocco with 5 projects; Australia with 4 projects; Italy with 3 projects; France and Saudi Arabia with 2 projects each; Turkey, Germany, Denmark, Egypt, Canada, Mexico, Chile, Thailand, and Algeria with 1 project each.

An example of a CSPP working with the principle of focusing the Sun's rays on a power tower type receiver with mirror type solar tracking devices called "Heliostat" is given in Figure 1.10.

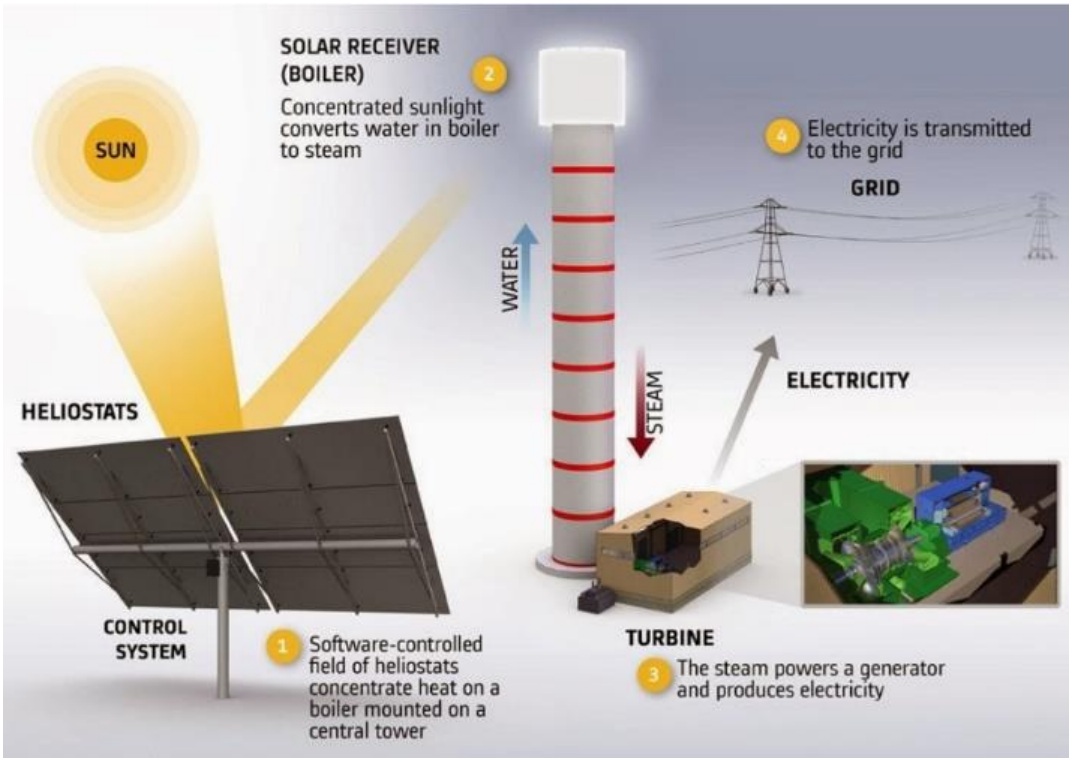


Figure 1.10. Power Tower-type CSPP system [1]

PVPPs are on the way to becoming one of the most preferred technologies not only within the scope of solar energy utilization but also among renewable energy power plant installations, both economically, environmentally, and socially.

These power plants are established by electrical and mechanical connections/assemblies of several components, from the semiconductor devices called “solar PV cell” (the smallest components) to long solar PV module arrays connected with power electronic circuits and electrical grids (Figure 1.11). PVPPs can also be installed on smaller or larger lands than the areas occupied by CSPPs,

according to the electrical power output planned to be obtained from the plant. There are different areas of use, from the transmission of the electricity produced from these power plants to the settlements such as villages, towns, cities; to its use in agricultural applications (for example, irrigation), which is referred to as "agrivoltaic / agrophotovoltaics" in the literature.

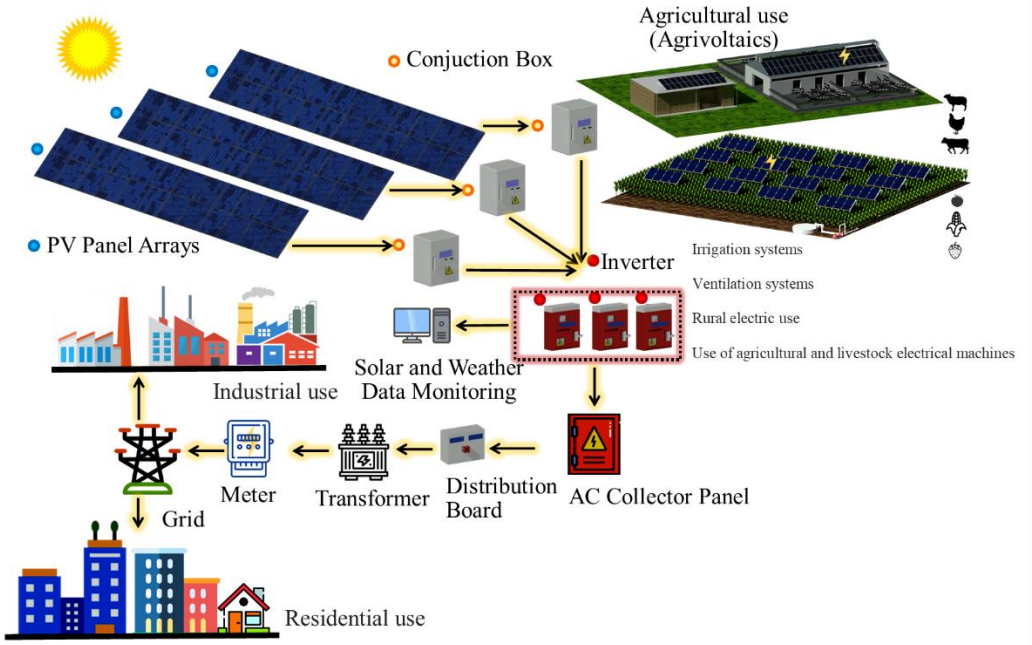


Figure 1.11. Solar Photovoltaic Power Plant System Components

### 1.3.1 Solar Modules and Other Components

In designing a Solar PhotoVoltaic Power Plant (PVPP) infrastructure, one of the essential components for installing the power plant is solar PV modules. Solar modules are manufactured by serially connected individual semiconductor solar cells, which convert the incoming solar radiation reaching their surfaces into electrical power, creating a DC and potential difference. At this point, it should be noted that solar modules should maintain their long-term functionality in the applications such as rooftop/BIPV, vehicle-integrated, etc., as well as in ground-mounted solar projects such as PVPPs (20-25 years). For this, solar cells connected in series are required to be framed with the materials such as encapsulant material (EVA), tempered glass, aluminum frame, insulated back sheet. This design is also necessary to protect the solar modules against extreme climatic and environmental conditions. The "junction box" located behind the solar modules is the piece that acts as a transfer point in the transmission of the electricity produced from the solar modules to the string. The working principle of a solar cell and the PV effect can be seen in Figure 1.12a; the basic elements used in the construction of a solar module can be seen in Figure 1.12b; the drawings showing the design steps from solar cells to solar array can be seen in Figure 1.12c. By making the appropriate electrical connections of the solar cells, solar modules are fabricated; and by combining the modules, solar panels and panel arrays in PVPPs are formed.

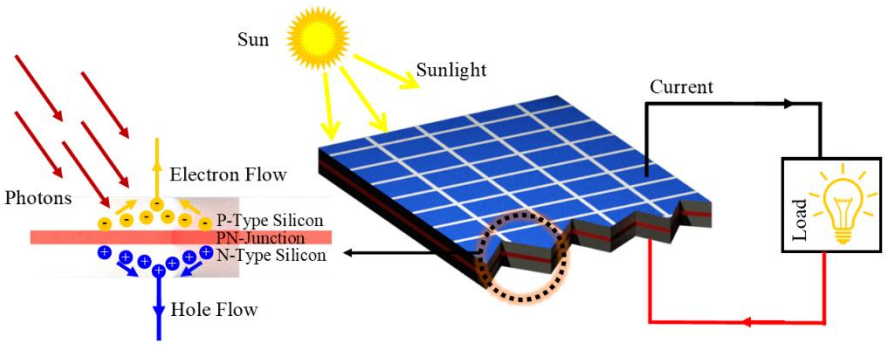


(a)

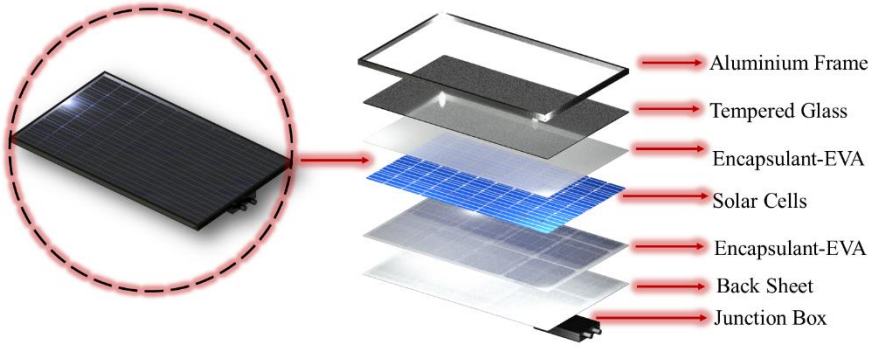


(b)

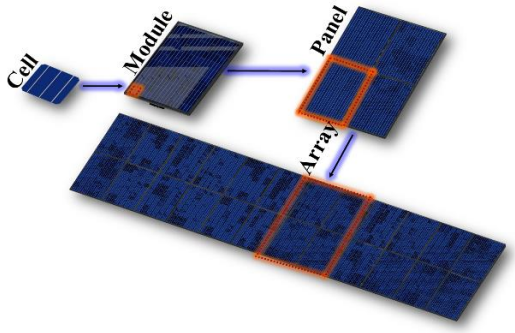


(c)

Figure 1.12. PV Effect (a), PV Module Components (b), and Assembly Steps from PV Cell to Solar Panel Array (c)

When determining the specifications of solar modules, many factors are taken into account, from the solar cell type (such as monocrystalline, polycrystalline, thin-film) and the fabrication technology (e.g., PERC, IBC, Bifacial, HJT, TOPCon) to the structural properties of the module frame materials. Within these specifications, apart from the main electrical parameters such as $P_{max}$, $V_{mp}$, $I_{mp}$, $V_{oc}$, $I_{sc}$, the "operability" values of modules under environmental conditions such as *operating temperature interval* and *temperature coefficient*, which expresses the efficiency change depending on the ambient temperature conditions, are also given. The temperature coefficient is considered in accordance with the solar cell temperature tested at 25°C under Standard Test Conditions. This coefficient shows how much efficiency loss will be at the solar module power output relative to the increase in ambient temperature. In Figure 1.13, the module efficiency intervals of some PV module technologies are categorized.

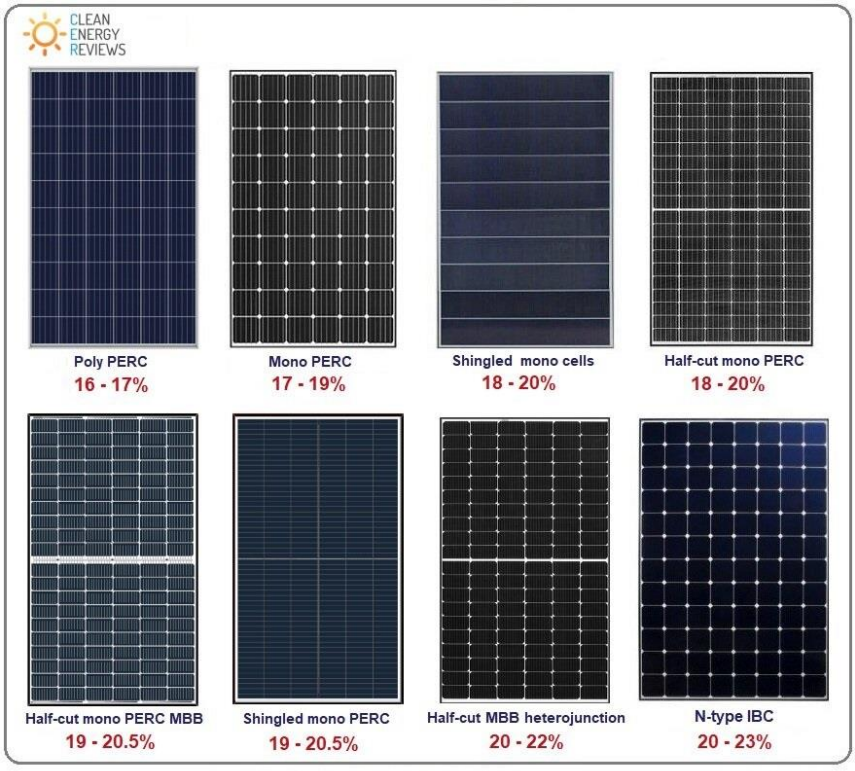


Figure 1.13. PV Module Technologies and Their Efficiency Interval [87]

When looking at the dimensions of the modules mainly used in PVPPs and rooftop applications, the values in the surface area range between 1.7 - 2 $m^2$ are preferred, while smaller modules can be manufactured in the applications such as street light- or traffic sign-integrated PV. In the applications for providing energy to satellites, the modules in larger sizes can be manufactured. To place the solar modules onto the land surface in a PVPP installation; or onto the roof in a rooftop application, they are mechanically assembled with carrier systems made of materials such as steel and aluminum.

Solar modules, which can meet price-performance criteria, come to the fore in the solar energy market. The parameter that is evaluated in the first place in terms of module performance according to its price and that expresses the solar energy conversion rate is “module efficiency” accordingly. This rate is usually between 15-25% for commercial modules on the market. A slight increase in module efficiency enables the savings from a large number of solar modules and panel arrays that can produce the desired amount of power/energy to be taken from the plant as electrical output while the PVPPs are operational, as well as from land use. Today, there are many private sector companies that contribute to price-efficiency comparison tables in module design and manufacturing.

Some devices in power electronics are used to deliver and distribute the electricity generated from solar panel arrays to customers and end-users. The direct current (DC) obtained from solar modules is transferred to the devices called “inverters” via “junction box” integrated on them and “solar connectors" connected to “junction box”. There are varieties of inverters such as string, central, micro-inverter, power optimizer, and these devices provide current conversion from DC to AC. While making connections between the PVPP system components and establishing the grid integration of the system, some precautions are also taken to be protected from low/high voltage, disasters such as lightning, fire, etc. Following the operationalization of PVPPs, data collection - monitoring, and maintenance services are activated. Incoming solar radiation data reaching the power plant are measured by “pyranometer”, and local weather data (air temperature, wind speed/direction,

relative humidity, etc.) in the region where the power plant is located are collected via the measurement instruments “weather station” and its sensors. This collected data can be monitored through various web portals and interfaces after the necessary authorizations. On the other hand, the operations such as PV module surface cleaning, routine part replacements, thermal imaging, and module deformation check are carried out within the maintenance services. These services include inspecting and repairing macro or micro-cracks on solar modules, leakages in electrical connections, and loose cables.

### 1.3.2 Photovoltaic Power Plant Types by Utilization Method and Geography

“On-Grid” systems are designed by giving a certain amount or more of the electricity produced in this type of power plants to the grid. In “Off-Grid” PVPP, this amount or excess electricity is transferred to a device such as a battery, which can usually be reused later (Figure 1.14). The electricity produced in both systems can be transferred to the applications at urban or industrial level. Besides, on the one hand, rooftop/BIPV PV applications often involve residential sector energy conversion through building roofs or façades where the system is installed (houses, apartments, factories, government/private offices, institutional buildings, etc.). On the other hand, ground-based PVPPs can be utilized in agricultural and rural applications such as “agrivoltaics”.

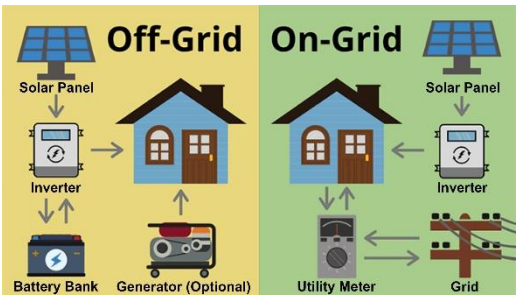


Figure 1.14. Off-Grid and On-Grid PV System [31] *(modified)*

Hybrid power plants are designed by combining On-Grid and Off-Grid PV systems or by orienting solar panel arrays in such a way that they can be installed in the same power plant area as other renewable energy sources such as wind turbines. Considering that the same efficiency cannot be obtained from renewable resources throughout the day depending on 24-hour time zones and geographical/ seasonal climate conditions, these hybrid systems can be advantageous. For example, a PVPP field that cannot produce electricity at night can be supported with wind turbines if it is located in an area receiving wind at all hours of the day. In this way, wind turbines working thanks to kinetic energy provided by the wind can fulfill the function of solar modules that cannot produce electricity at night or during the daytime when sufficient solar radiation does not reach the site (such as cloudy, foggy, rainy weather conditions). Conversely, in sunny/clear (or when there is enough daylight) weather conditions where the wind speed is very low or the air currents in the region cannot transfer mechanical energy to the turbine blades at a level to produce electricity, the solar modules can be operational again to ensure that the electricity produced from the hybrid power plant is not interrupted.

In almost every country in the world, ground-based PVPPs are the most preferred solar PV systems among all solar power plant projects, including CSPs, in terms of providing solar electricity with different methods and being installed in different geographies. Before the projects related to PVPPs are put into operation, various preliminary evaluations are made regarding location/site selection and land/soil structure, as well as some solar analysis, design, and calculations. Some of the main titles in the "project planning and organization" phase of this evaluation process are given below:

- Collecting billing information, determination of subscriber type, determination of contract power, etc. before performing field analysis and measurements required for the design of PVPP
- Deciding on the appropriate PVPP application method based on the Regulations

- Preliminary work for the simulation of PVPP
- Preparation of PVPP feasibility (budgeting and EROI calculations)
- Preparation of the PVPP application (required application documents, call letter, assessment, preparation for the PVPP connection agreement process, etc.)
- Other necessary processes/transactions after the acceptance of the project

In addition to the project stages above, the following issues are also addressed within the scope of the roadmap of PVPP installation, planning, and organization:

- Assessment of the area's relationship, where the PVPP will be constructed, with natural life, ecological factors, and weather/climatic conditions (habitat and wildlife conservation, fauna and flora/vegetation, surface soil type, weather event frequencies, environmental impact assessment, etc.)
- Supplying the measurement devices and equipment used to specify the solar energy and radiation potential (sunlight duration/hours analysis by considering the elevation and slope of the land surface, some estimations about shading factors, etc.) of the PVPP site via a geographic (spatial) analysis
- Comparisons between the techniques for calculating incoming solar radiation potential reaching the PVPP site and several solar radiation databases (meteonom, NASA-SSE, etc.)
- Making calculations to determine the operating temperature of the PV modules to be used in PVPP
- Evaluation of the sufficiency of the energy produced in the power plant on a daily, monthly, seasonal and annual basis, with some electrical production estimation calculation techniques, according to the applications in which it will be utilized
- Examining simulations that can be made with PVPP software tools (PVSyst, PV-SOL, Helioscope, etc.) and microclimate/weather modeling software (e.g., WRF) to contribute to the preparations above

- Other preparatory work such as PVPP project drawing, electrical and static calculations
- Determining the grid connection method, taking the location, purpose of use, and infrastructure of the PVPP into account

Ground-based installations are mostly preferred for PVPPs in terms of ease of installation, cost-effectiveness, and flexibility in determining the site on Earth's surface. However, for fulfilling the purposes such as the conserving of ecological life and natural areas on land; meeting the energy needs in the geographies where extreme climatic conditions prevail; minimizing the increasing space requirement for these systems, PVPPs can be installed and operated in different geographical regions with the contribution of innovative technologies (Table 1.1):

- **Desert-type PVPP**s installed on the desert lands that are very large and do not have ecological mobility
- **Polar-type PVPP**s established to meet the energy needs of the settlements in the polar regions and the projects and operations carried out there
- **Floating PVPP**s installed on water resources such as seas, lakes, oceans for saving from the use of terrestrial land

Table 1.1. Advantages and Disadvantages of PVPP Power Plant Applications

| **PVPP Application** | Advantages | Disadvantages |
|---|---|---|
| *Ground-based* | - Ease of installation and material transportation<br>- Terrestrial land diversity on the Earth geography<br>- Ease of grid integration and storage<br>- Different utilization methods (residential, agrivoltaics, industrial, etc.)<br>- Ease of monitoring (by satellites, weather stations, etc.), cleaning and maintenance | - Possible environmental impacts on natural life and ecosystem<br>- Terrestrial land degradation due to the rapid increase in global land use<br>- Operational difficulties depending on sunshine hours, weather events, landscape elevation and slope<br>- Soiling on PV modules due to, e.g., atmospheric aerosols |
| *Desert-type* | - Terrestrial land abundancy and low environmental and ecological impact<br>- Long sunshine hours and intense solar radiation<br>- Installation easiness thanks to no or low elevation and slope changes on land surface<br>- Ease of monitoring thanks to clear weather conditions | - Decreases in PV module efficiency due to hot climatic conditions and high air temperatures<br>- Decreases in PV module efficiency due to intense soiling by dust/sand storms<br>- Difficulties in material transportation, cleaning and maintenance services due to locational differences between deserts and settlement areas |
| *Polar-type* | - Terrestrial land abundancy and low environmental and ecological impact<br>- No or low soiling (especially compared to desert PV applications)<br>- Installation easiness thanks to no or low elevation and slope changes on land surface<br>- Operational easiness thanks to mostly stable weather conditions | - Decreases in PV module efficiency due to snow accumulation by heavy snowfalls<br>- Difficulties in material transportation, cleaning and maintenance services due to locational differences between deserts and settlement areas<br>- Limited possibilities for grid integration and storage |
| *Floating* | - Large water body (lakes, seas, etc.) surfaces<br>- Installation easiness thanks to no elevation and slope changes on water surface<br>- Environmental benefits such as reducing evaporation on water surface, decrease in terrestrial land use, etc.)<br>- PV module orientation advantages for sunshine hours and incoming solar radiation<br>- Water availability for PV module efficiency (cooling) and cleaning | - The most challenging conditions (compared to other installation types) in material transportation, cleaning, and maintenance services provided from land to water bodies<br>- Limited possibilities for grid-integration and storage (compared to ground-based and desert-type PVPPs)<br>- Operational difficulties due to extreme weather events (e.g., storms) on water bodies<br>- Decrease in light penetration into water body and possible environmental concerns related to aquatic life and ecosystem |

### 1.3.3 Installed and Developing Capacity Panorama in the World and Turkey

Taking the *Solar Power Europe - Global Market Outlook for Solar Power 2021-2025* report [84] as a reference, as of the end of 2020, the worldwide total installed solar PV capacity has reached 773.2 GW with an increase of nearly 140 GW compared to the previous year. Among the information presented in the report, cumulative solar power, which has grown by about 500 times since the beginning of the 2000s, was emphasized with the contribution of the feed-in-tariff law that came into force on grid-connected solar applications in Germany. In the same report, the price decrease per MWh in electricity generation was compared to some primary energy sources (CCGT, coal, nuclear, wind, solar) in the 10 years between 2010 and 2020. In other words, solar electricity, which was at the highest pricing level among other sources with 300 $/MWh in 2010, showed the fastest decline in 10 years and went down to 37 $/MWh. This cost is followed by electricity generation from wind (from around $130/MWh to $ 40/MWh) and from CCGT (from around $ 80/MWh to $ 59/MWh). There has been no significant change in coal-sourced generation over the 10 years ($ 112/MWh in 2020). As for nuclear energy, it has followed an upward trend from its cost of around $ 100/MWh in 2010 to $ 163/MWh in 2020.

The *International Energy Agency's Renewables 2020 - Analysis and Forecast to 2025* report [48] shows that solar PV net capacity is already growing in almost every country and region in the world. In addition, in line with some scenario projections (Main and Accelerated), it has been stated that these capacity additions will continue to increase in the near future. In the report, the 5-year capacity development since 2015 is shown as a "historical" situation, while the post-2020 increase projections are given under the headings of "Main" and "Accelerated". China, which has historically led the growth trend of Solar PV, was followed by Europe and the USA. According to the projections for the near future, which are predictive, it is seen that with China maintaining its leadership, and Europe can leave the USA behind and take second place (Figure 1.16).

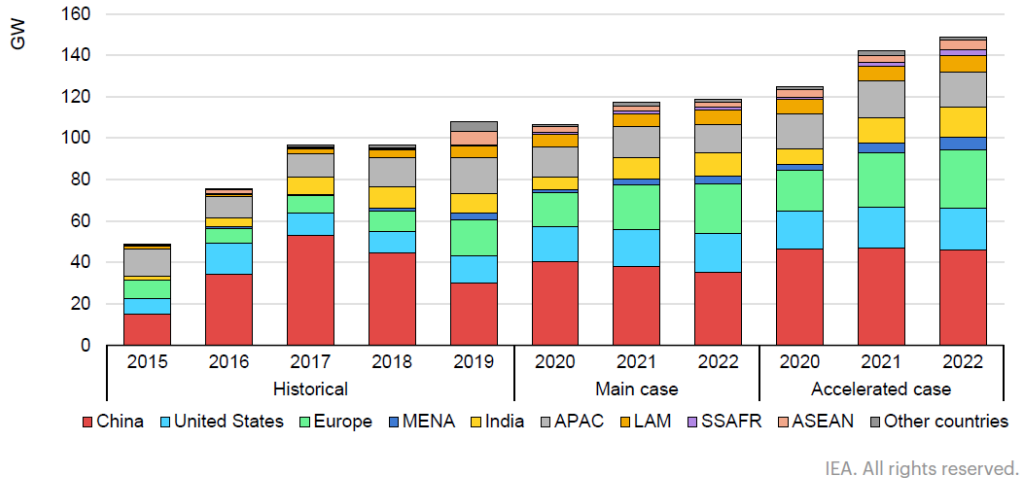


Notes: MENA = Middle East and North Africa. APAC = Asia and Pacific (not including China). LAM = Latin America. SSAFR = sub-Saharan Africa. ASEAN = Association of Southeast Asian Nations.

Figure 1.15. Historical and Two Scenario-based Additions for Solar PV Net Capacity by Country/Region [48]

When looking at the expected average global annual capacity additions in accordance with the growth scenarios, it is given in Figure 1.17 that the highest increase will be in utility-scale solar PV in 2022 and between 2023-25, followed by commercial and residential solar PV.

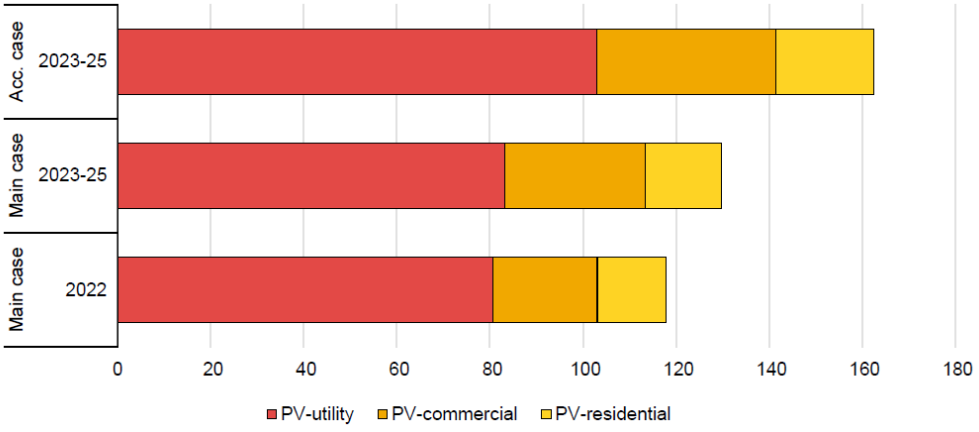


Figure 1.16. Two Scenario-based Utility, Commercial, and Residential Additions for Average Global Annual Solar PV Capacity [48]

Under this title, the remarkable development of Rooftop PV projects in various parts of the world can also be mentioned. While the total capacity in Europe was below 20 GWp in 2009, it has increased nearly 6 times in the next 10 years [49]. In this rapid progress, the capacity increase of Germany, Italy, the UK, France, and Spain, respectively, has a significant role. As another example, the rooftop solar PV installations in Australia in February 2018 exceeded 115 MW [32]. When considering India, despite the problems caused by the COVID-19 pandemic, it has been stated that an 883 MW rooftop PV capacity increase has been realized in the country in the first 9 months of 2020 [56]. The 7.4 GW rooftop solar capacity increase in Vietnam from November to December 2020 is the most remarkable enhancement in the country's uptrend in this area, which has been inconsistent since September 2019 [89].

When switching from the solar projects and installations panorama in the world to the one in Turkey, the following information can be given: GENSED [101] reported in April 2021 that the solar energy installed power in Turkey approached 7 GW in line with TEİAŞ data. It has been stated that 515.4 MW of the investments made for the total installed capacity is for licensed projects, and 6.448.6 MW is for unlicensed projects. It can be said that the application conditions are effective in making an investment more than 10 times in unlicensed solar energy power plant projects compared to the licensed ones. In case the electricity generation capacity of the power plant to be established exceeds 1 MW, the production license and Environmental Impact Assessment report are requested. Moreover, at least 6 months of meteorological solar measurements and statistics related to the project must be collected before the licensed power plant applications (there is no requirement in unlicensed projects). The license period for licensed projects is 49 years. The government provides a 10-year purchase guarantee for unlicensed projects.

In the *Solar Power Europe* [84] report, in the solar market scenarios of 2021-2025, Turkey is among the top 20 countries under solar PV additions. Turkey ranks 16$^{th}$ among these years, surpassing the UK, the UAE, Italy, and Mexico, with 7 GW according to the low scenario, 9 GW according to the medium scenario, and 13 GW according to the high scenario (Figure 1.18).

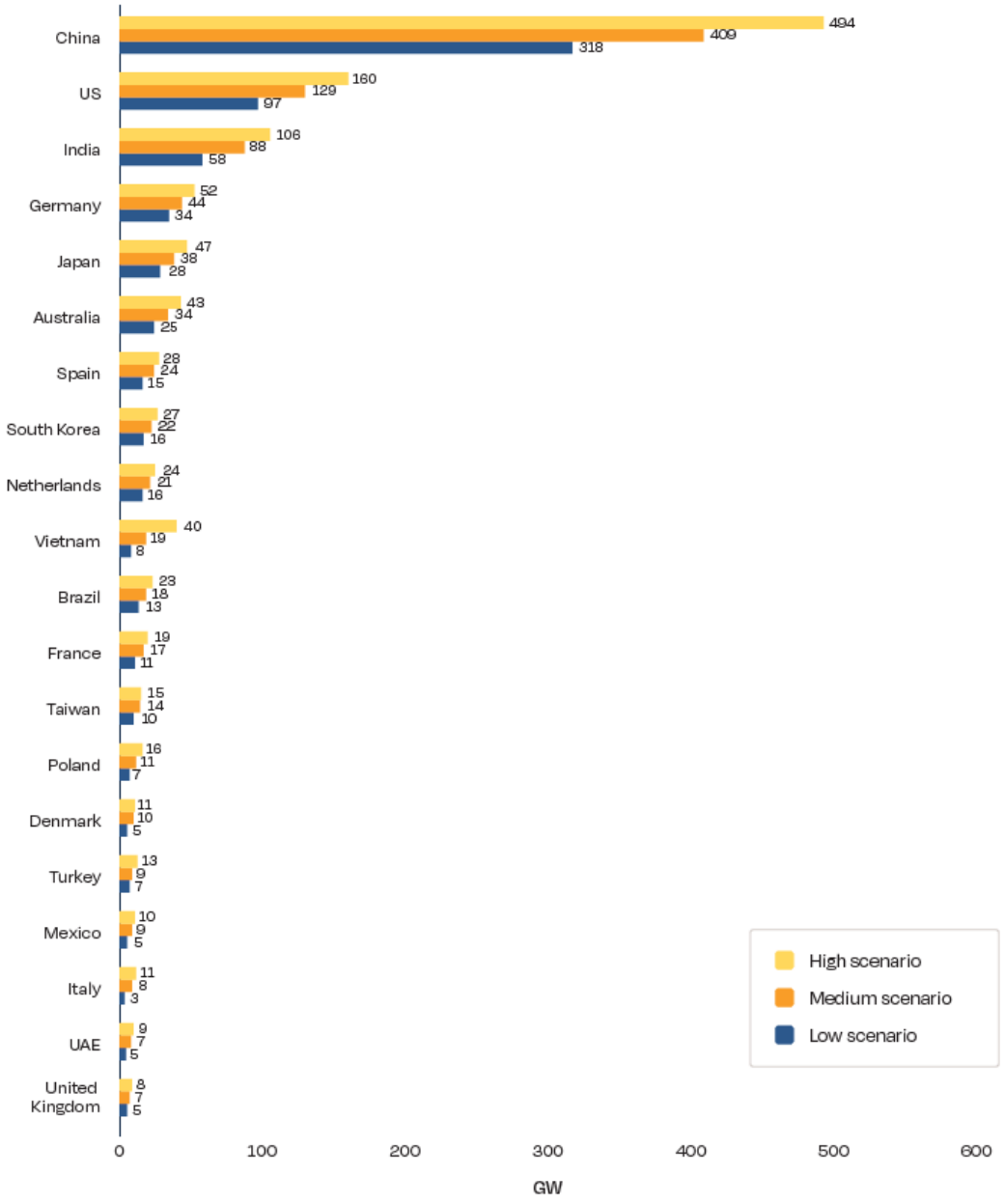


Figure 1.17. Countries' 2021-2025 Solar PV Addition Potentials based on Three Scenarios [84]

### 1.3.4 Environmental Impacts of Photovoltaic Power Plant Installations

Compared to fossil fuels and finite energy types such as coal, crude oil, and natural gas, environmentally friendly and clean natural renewable resources such as solar, wind, hydropower, geothermal, hydrogen, biomass have a common worldwide acceptance. Besides, the power plants established to obtain energy types such as electricity, heat, and steam, mechanical power from these resources may also have some environmental side-effects.

Tsoutsos et al. [100] examined various environmental impacts within solar technologies' construction and operation processes (solar thermal heating, PV power, and solar thermal electricity) as separate topics about 15 years ago. In this study, the following impacts were particularly emphasized related to PV power generation:

- Impacts that may occur on the natural ecosystem and soil productive area in the installation of PV systems, depending on the installation preferences such as topography, area coverage, land type, location, etc.
- Routine or accidental pollutant discharge caused by PV system components such as modules
- "Visual impact" problem caused by the PV systems installed near natural beauty areas
- Natural resource depletion that may be caused by the need for bulk materials used in PV modules, depending on their efficiency and the types of technologies used in their production
- Air pollution, which may occur due to manufacturing and transport operations, albeit in small quantities
- Environmental noise that may occur, especially during the construction processes of PV systems
- Waste management requirement for chemical substances used in PV systems (e.g., batteries)
- Module-recycling issue

Turney and Fthenakis [98] prepared some categorization and comparison tables between the installation and operation of PVPPs and traditional power (i.e., fossil fuels) over 32 environmental impacts. Beneficial advantages or detrimental disadvantages of PVPPs compared to traditional power are indicated in each impact category in these tables. And the priority is leveled for each impact in question (low, moderate, high). The content of this information, which is compiled in 3 general tables, is as follows:

a) Impact categories associated with human health and well-being (hazardous chemicals emissions; noise; recreational resources; visual aesthetics; climate change; land surface occupation)
b) Impacts on habitat and wildlife (hazardous chemical problems such as acid rain, oil spills, etc.; physical risks and dangers related to cooling water systems, birds' fly paths, roadways, railways; habitat-related issues as fragmentation, local quality, land transformation, and climate change)
c) Impacts on land use and hydrogeology (soil erosion; surface water runoff and water quality; waste management, groundwater recharge, and water purity)

Among the topics discussed under this title, ground-based PVPPs affect the microclimate / local climate of the region where they are installed, especially after their installation, in relation to the size of the area they cover on the land surface. The focal point of these discussions is the unnatural changes or alterations observed in the factors such as cloud cover, precipitation regime, surface reflectance (albedo), wind patterns, atmospheric deposition in a region-specific natural microclimate system due to a PVPP installed artificially with a large number of solar panel arrays. This is also because of the variation in the radiation exchange between the surface and the atmosphere because of the change in land surface albedo due to panel installations, as stated in Armstrong et al.'s study [5]. At the same time, plant-soil carbon cycling is also affected by PVPP-based microclimatic effects, as also discussed in the content of this study.

Hernandez et al. [39] contributed to the researches in this field in the literature by publishing another study detailing the environmental problems associated with the construction, operation, and decommissioning phases of utility-scale solar energy (including CSP) applications. The study includes different impacts that may occur in some or all periods of these three stages. Removing vegetation, land leveling, etc. in the construction phase; use of a large land area in construction and operation processes; water consumption for water cooling needs during operation; power plant removal at decommissioning stage; environmental degradation issues, which emerge due to some toxicants and flammable materials used in all three stages, are shown in a table-figure in the study. Within the impact area of these issues, more than 20 potential responses and impacts on the environment and ecology are also given in the same table-figure.

In addition to these most discussed examples of solar energy utilization systems, there are also possible current problems that have recently entered the literature. Some of those are; the difficulties of the process of distributing the electricity generated in solar power plants via transmission lines and corridors; impacts of toxic substances that can mix with water due to the construction and cleaning materials used in floating PV systems like land-based ones, on the underwater habitat; and the negative consequences of floating systems on light penetration and radiation budget processes between the water surface and the atmosphere. PhotoVoltaic Heat Island Effect, which observes as unnatural temperature oscillation and variation trends on the microclimate because of solar panel array-based natural surface albedo alteration, and which is the central subject of this thesis, has taken its place among different environmental debates in the literature in the last 20 years. Impact areas of this type of heat islands are not limited only to the adverse consequences of the local weather and climate in the region where solar power plants are installed. They also have undesired harmful effects that may affect, for example, flocks of birds traveling on migration routes. There are also studies in the literature examining the environmental impacts of PVPPs on a region/location-specific basis. Among them, the following can be examined:

- Those who emphasize that environmental and socio-economic impacts on a regional basis should be considered while determining policy-making strategies and making regulations in this field in Romania, where solar energy utilization infrastructure is developing [104] [105].
- Those who explain that the development of solar energy systems in West Texas (the USA) [20], which has large arid and semi-arid rural areas and favorable climatic conditions, should be continued by considering environmental upside and downside situations, etc.

The summary in the "Highlights" section of the study of Tawalbeh et al. [91], which can be shown as a general compilation of the studies under this title and enables the subject to be viewed from a contemporary perspective, can be reviewed. The four main findings in this section can be expressed as:

- PV systems cannot be specified as being completely eco-friendly and zero-emission
- PV systems have negative environmental impacts associated with the use of land and water, containing hazardous/toxic component materials, pollution and noise, and visuality
- Design, sustainability, and recycling improvement will be the focus of PV system designs in future
- Incentives and researches that can close the gaps in the PV systems' adverse environmental effects and they can contribute to constituting a considerable platform for legislations in future

All these environmental side effects and impacts have been discussed collectively or separately while the solar project engineers and operators have been constructing the ground-based solar energy conversion systems requiring much more natural ground/land surface area due to installation capacity increment. One of the distinct impacts is in the focus of this thesis: Photovoltaic Heat Island Effect (PVHIE).

To understand a less-studied weather-based phenomenon in the international literature and conduct the first study of this environmental issue in Turkey, the following chapters of this thesis are shaped by the content and objectives below.

The concept of microclimate and local weather are introduced on the basis of the Earth's energy budget and climate zones in Chapter 2. Following this, the formation structure of urban heat island (UHI) types, possible artificial sources, categorization and measurement methods; PVHIE; physical heat release processes of PV modules causing this heat island type are expressed and graphically given in this chapter. A brief literature review on UHI ve PVHI effect can also be found in this chapter.

Chapter 3 presents the preparations and equipment of Turkey's first field projects (PVPP field selection, measurement devices, project support, etc.) to detect and observe possible PVHI formations in the selected geographical location of the study.

The field measurements collected from the data monitoring technique in Chapter 3 are statistically, graphically, and correlationally analyzed in the next three chapters (4-6) to interpret the significant numerical results indicating the daily and seasonal transient PVHI formations.

Considering the quantitative results obtained in the previous chapters, a holistic microclimate modeling system, *ENVI-Met*, is used to simulate the PVPP and its close environment with the local weather parameters as solar radiation, surface reflectivity (albedo), and air temperature (Chapter 7). Thus, a comparison and compatibility assessment can be made between the numerical results and simulation-based outputs of PVHIE.

The thesis analysis and result parts between Chapters 4 and 7 are summarized with the concluding remarks given in Chapter 8. This chapter also includes some key-point recommendations (particularly for ground-mounted PVPP applications) to reduce the environmental impacts of PVHIE.

# CHAPTER 2

# HEAT ISLAND EFFECT

"Global warming" is one of the most apparent factors that cause regional consequences of climate change, which has a worldwide and wide impact area to be observed. In line with the reasons explained in the first chapter of this thesis, especially with the intense industrialization activities brought by the Industrial Revolution, the trend of atmospheric temperature increase at an unprecedented rate in the history of civilizations is monitored. This trend's progress up to know is shaped by the issues common to each geography, such as the production-consumption activities of countries, the efficiency of local resource usage (for example, the strategies and policies followed for energy saving), their sensitivity to environmental protection.

Unfortunately, despite many scientific and technological developments in the 20$^{th}$ and 21$^{st}$ centuries; the *Kyoto Protocol*, which was adopted in 1997 and entered into force in 2005 and includes 192 parties; the *Paris Agreement* (UNFCCC-COP 21), a legally binding international treaty, which was adopted by 196 parties at the end of 2015 and entered into force approximately one year later Global Warming has continued to rise at an unstoppable rate. Scientists and researchers develop various scenario forecastings based on the triggering factors (e.g., GHG emission rates) of global warming and temperature rise rates in the Earth's atmosphere. Among these scenarios developed, there are optimistic and moderate ones and those that emphasize that the problem will bring a severe global threat out in the near future. In Figure 2.1, the new type of "Socioeconomic Pathways (SSPs)" and the older "Representative Concentration Pathways (RCPs)" scenarios, which started in the first quarter of the 21$^{st}$ century and branched out around 2040 according to different estimations, can be seen.

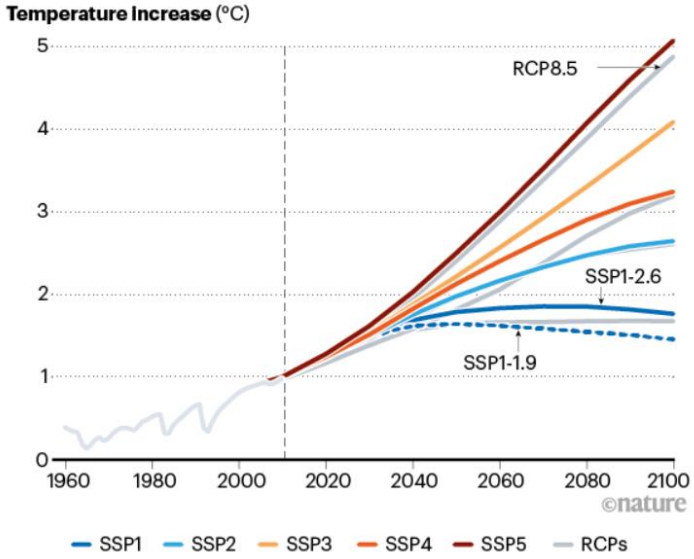


Figure 2.1. SSP- and RCP-based Temperature Increase Scenarios [95]

The scenario curves in Figure 2.1 show that the temperature increase, which did not exceed 1°C until the first quarter of the 20$^{th}$ century, will remain below 2°C in this century with the best estimates. In the most pessimistic scenario in SSP5, it is estimated that this magnitude can reach up to 5°C. The observation frequency of extreme climate and weather events such as heatwaves, severe droughts, intense floods, hurricanes and rainstorms, glaciers/sea ice melting, and sea-level rise has increased in different geographies of the world due to the hydrological cycle and atmospheric circulation, which have been altered by the effect of global warming at a relatively low level of 1-2°C until today. Considering this situation, when the scenarios predicting higher temperature increases in Figure 2.1 are considered, it can be said that these events will occur more frequently while their impact area is spreading day by day. Possible alterations in microclimatic or local weather-based events predicted by various scenario projections do not only disturb the balance of the atmospheric environment. At the same time, these alterations cause concerns and risks to grow in water-based and land-based issues such as changes in the Earth's energy budget, reduction in drinking and freshwater, crop loss, ecosystem degradation/habitat destruction, increase in wildfires.

## 2.1 Microclimate and Local Weather

The climates on Earth as a planet arise as the five essential components (spheres) interact with each other: “Atmosphere” representing air environment; “Hydrosphere” representing water bodies and reservoirs; Cryosphere, which represents the glacier environment such as ice, permafrost; “Lithosphere” representing the upper rocky layer; “Biosphere” representing life-based habitats, ecological system, and environments. “Earth's Energy Budget”, which describes the general distribution of incoming solar radiation reaching the Earth on the Earth surface (continents and oceans), has a major role in the formation of interactions between these spheres. In Figure 2.2, NASA's overall picture, Earth's Energy Budget, is shown proportionally. This figure also shows the balance between the radiant energy (mostly containing the visible light part of the electromagnetic spectrum) reaching the Earth from the Sun and the radiant energy reflected and emitted from the Earth surface and atmosphere to space.

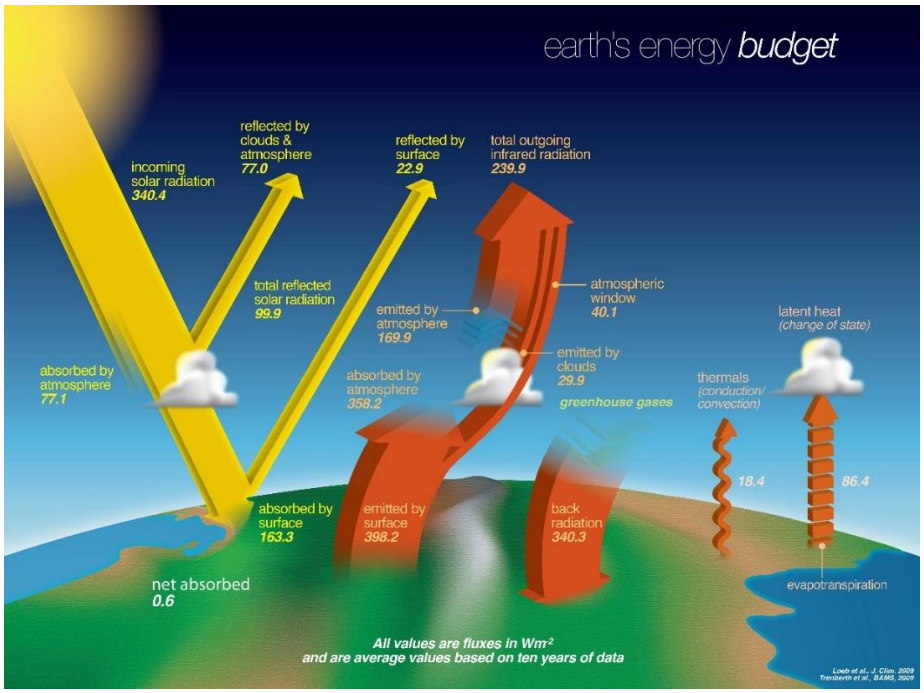


Figure 2.2. Earth’s Energy Budget [107]

The "Climate Zones" classification has emerged as a result of the investigation of Earth's tilt and rotation, atmospheric circulations (Hadley Cell, Polar Cell, etc.), water cycle, wind (airflow) patterns and ocean current, land intensity, water resource distribution, and intensity and prevalence areas of many other climatic and geographic factors at regional level in the four seasons. While developing this system, these two scientists discovered that vegetation distribution throughout the world strongly links with regional climate. At the emergence of these zones, German climatologist and botanist *Wladimir Köppen* and German meteorologist and climatologist *Rudolf Geiger* developed the *Köppen-Geiger Climate Classification System* (between 1884 and 1936). While developing this system, these two scientists discovered that vegetation distribution across the globe strongly links with regional climate. The fact that temperature and precipitation, which have a crucial role in shaping the plant type and density of the Earth flora on the land, are also two essential climatic factors, has been specific information that *Köppen and Geiger* benefited from while establishing the infrastructure of their classification system. The basic inferences of the system are as follows:

- Vegetation distribution on the Earth's geography is closely related to climate.
- The growth of region-specific plants is temperature and precipitation, which are also the two main climate factors. Higher air temperatures and rainfall rates can be defined as climatic conditions in regions with more forest areas; Desert-type continental areas receive less rainfall.
- It has been divided into five climate zones, taking the climates into account, vegetation growth, and distribution on the geographies around the world. These zone groups are also divided into subgroups within themselves.
- In preparing the climate classification map, categorization was made with the color distribution on the world map.
- The classification in most of the zones is prepared as temperature-based. In addition, Zone B is defined over "aridity".

*Köppen-Geiger Climate Classification Map*, created with the main five climate zones and their subgroups, is given in Figure 2.3.

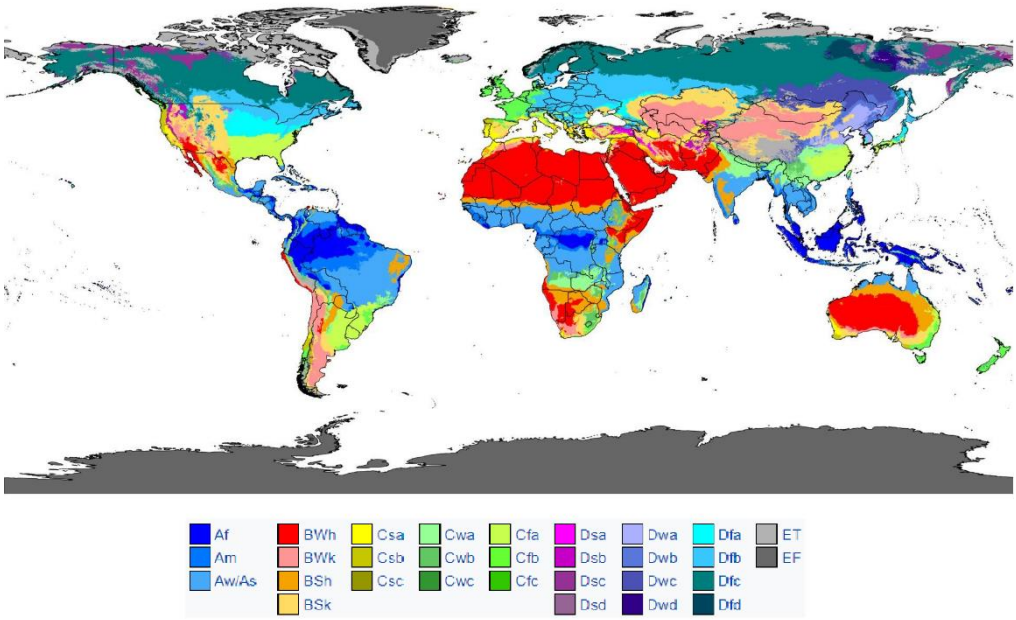


Figure 2.3. Köppen–Geiger Climate Classification Map [10]

According to the colorings in Figure 2.3, the five main groups indicated by shades of blue (except light blue) are “Tropical (or Equatorial) Zone A”; “Arid (or Dry) Zone B” denoted in red, pink, or orange; “Warm (or Mild) Temperate Zone C” with shades of green; “Continental Zone D” indicated by purple, violet, or light blue; and last but not least is “Polar Zone E” represented by shades of gray. Subgroups of these zones, indicated by upper- and lower-case letters at the bottom of the map, are categorized by temperature and dryness. For example, in Zone A, the regions with no dry season are indicated as "Af"; those with a short dry season are denoted as “Am”; and those with a dry season in winter are designated as “Aw”. In Zone B, “BWh” indicates hot-arid deserts, and “BWk” indicates cold-arid deserts; “BSh” indicates hot-arid steps, and “BSk” indicates cold-arid steppes. Zone ET and EF, which are specific to polar geographies, show tundra and snow-ice regions, respectively.

In the source of the map in Figure 2.3 mentioned in the References section of this thesis, the year range in which various revisions were applied to the map can be seen. When this range is considered, it can be said that the Köppen-Geiger Climate Classification System continues to be referenced by climate scientists and scientists today. Besides, “highland climate”, which is referred to as Zone H and specific to mountain-level elevations, has also been added to the map within the later revisions.

The fact that the five main climate types are divided into sub-zones in the Köppen-Geiger Climate Classification is meaningful in introducing the concept of "microclimate". Microclimates are a definition used to explain the climatic conditions of the subzones mentioned above in relatively small areas in many different regions of the geography they cover, within the height range of at most a few meters. These small areas can be defined as terrestrial, marine, or glacial environments. It can be said that many natural and artificial factors such as vegetation cover, soil type, topography and elevation, land surface (ground) reflectivity, waterbody, urbanization in these environments have an effect on the formation of area-specific microclimate. The cooling effect of a lake or reservoir in the atmosphere of its environment; the impact of dense buildings, pavements, vehicular traffic, etc. on the local air temperature increase in cities; trees in places with dense forest fields and their effect on moderating temperature conditions in the atmosphere, can be given as some particular examples of these effects. Changes in temperature, humidity, wind direction/speed noticed/felt during a trip between a metropolitan area and a nearby rural area, and microclimatic differences between neighboring settlements can be given as other examples of this issue.

In summary, although a region where these areas are located has its own prevailing climate conditions, the factors mentioned above can cause alterations and variations in these conditions. For this reason, microclimates may occur. Monthly, weekly, daily, and hourly weather forecasting for the cities of many countries worldwide is informative news that everyone knows and follows. However, making forecasts on the basis of the districts of these cities is related to the microclimate formations of these districts within their borders.

Microclimates can also show their effects on the agricultural product diversity and yield of the region where they occur. In this regard, the situation in two provinces in Turkey, which has suitable geography in terms of microclimate diversity, can be given as an example: Mersin is in the Mediterranean Region of the country, and products such as wheat, lentils, and chickpeas are grown as common in the city. In addition, thanks to the advantage brought by the microclimatic environment, bananas can also be grown in the Anamur district of the city. As another example, tangerines, mostly grown in the Mediterranean, Aegean, and Marmara regions of the country, can also be grown in the inner parts of Rize province in the Black Sea Region, which have unique microclimatic conditions.

Microclimates are interrelated with the formation of local weather conditions. On the one hand, by looking at the microclimate of an area, an overview of seasonal weather event changing trends can be obtained there; on the other hand, the microclimatic changes of the area related to the basic variables such as temperature, humidity, dew/frost point, wind direction and speed, atmospheric pressure, air turbulence, evaporation/transpiration of the local weather can be determined. The "Föhn Effect" that can be observed in mountainous regions, which is explained within the scope of the climate and meteorology course contents of educational institutions such as schools and universities, is one of the most popular examples of these microclimatic changes (Figure 2.4).

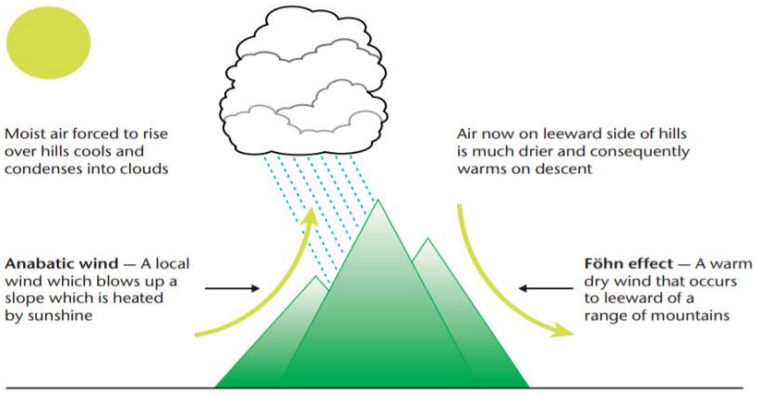


Figure 2.4. Föhn Effect [61]

In metropolitan cities, the number of which has increased gradually with the urbanization activities, local climatic features, and weather conditions that have been altered can be observed compared to the natural/rural regions in these cities' close/adjacent areas. Depending on this situation, "urban microclimate", a sub-type of microclimate, emerges. Urban microclimates, which are used to describe the climatic structure of the particular atmosphere in the canopy and boundary layers of megacities and metropolitan areas, also bring some environmental concerns. The "Urban Heat Island Effect" might be considered as the most conspicuous of these concerns that environmental scientists, engineers and agencies, city and regional planning experts, architects and civil engineers, municipal executives, and many others see as a growing environmental threat due to expansion of city boundaries.

## 2.2 Urban Heat Island Formations

The US-EPA states that urban heat islands are formed due to heat absorption and retention in cities with dense constructions on the land surface area such as buildings and pavements [77]. Due to these two physical processes in artificial surfaces, higher air temperatures may be felt, especially in urban centers, compared to neighboring/outlying rural and natural surroundings. These temperature differences are expressed as follows in the *Reducing Urban Heat Islands: Compendium of Strategies - Urban Heat Island Basics* report published by the US-EPA [115]:

> *"The annual mean air temperature of a city with one million or more people can be 1.8 to 5.4°F (1 to 3°C) warmer than its surroundings, and on a clear, calm night, this temperature difference can be as much as 22°F (12°C)."*

Touching on the heatwaves, which show their effect at more frequent, severe, and longer levels in the summer months with the impact of climate change, the US-EPA also emphasizes that UHIs cause increases in energy costs such as air conditioning, air pollution, and heat-related illnesses. [77]

### 2.2.1 Urban Heat Sources

It can be said that urban heat sources come first among the most critical factors that prepare the ground for the formation of an “urban microclimate” in Section 2.1. The concept of “source” mentioned here should not be confused with a resource for thermal energy production and utilization. For example, buildings such as houses and residences, which are designed and constructed by taking into account the position of the Sun in the sky according to the seasons and time zones of the day, enable to benefit from solar energy by the advantages of passive heating or cooling (shading effect, insulation, thermal mass, heat absorption or distribution). However, “heat sources” that cause an altered climatic environment directly within the boundaries of a city or metropolitan area can be considered as interaction points between the urban fabric and the atmosphere that surrounds this fabric. These points represent building roofs, pavements, sidewalks, highways, roofs of vehicles in heavy traffic, etc.

Before the classification and observation/detection methods, which will be detailed in the sub-sections following this title, it is helpful to say that there are also some tools for defining urban heat sources. Today, natural-artificial fabric changes on Earth's terrestrial surface can be viewed thanks to the various popular geospatial and mapping software programs such as *Google Earth / Maps, Apple Maps, Windows Maps, Bing Maps, Yandex Maps*, that are prepared and used by using satellite and various remote sensing technologies. These software programs, which have a wide user base from expert researchers to citizens interested in the subject as a hobby, offer general or detailed land views that can be scaled with zoom in or out options in bird's eye or "Street View" mode. In this way, for example, within the borders that encircle an entire city or within a specific residential location/area, the types of urban sources mentioned above and each of which are heat interaction points, and their densities on the urban fabric of the city can be easily determined.

Solar or artificial radiation reaching a surface interacts with an object and its surface through some basic physical processes, depending on the components (or on the material it's made from) in the structure of this object in solid, liquid, or gas form. Before detailing the UHI formation and observation processes, it is beneficial to summarize these processes:

- **Absorption:** Absorption is a physical property of how much electromagnetic radiation (e.g., IR) a material can absorb. Plastic and ceramic can be given as examples of materials with this property. The IR energy absorbed by the objects is transferred to the surrounding environment of the object by three basic physical processes: Radiation, Convection, and Conduction.
- **Transmission:** The transmission property indicates the amount of IR energy reaching an object's surface(s) that can pass/transfer through the object. For example, Germanium is a good transmitter in terms of IR transmittance, and thanks to this feature, it is used in lens designs in IR cameras.
- **Reflection:** A little different from the features above, reflection shows how much of the IR energy reaching the surface of an object is reflected. Metals such as polished gold, aluminum, and nickel are highly reflectable materials. Reflectivity can also be defined by the term "albedo", and the reflectivity strength of a surface can be determined with a value between 0 and 1 for the reflection or albedo coefficient.

The incident energy reaching the surface of the objects can be found by summing the three physical properties of the object above. The IR energy absorbed by an object increases its thermal energy (unlike transmitted and reflected energy). At a constant temperature and in a vacuum environment, no energy exchange is observed between an object and its surroundings. In this case, for the object's temperature to remain the same, the energy absorbed by this object and the energy radiated must be equal to each other. Here, the energy radiated by the object is actually "emitted energy". In other words, the stronger the object can absorb IR energy, the stronger it can emit IR energy. This property is expressed by “Emissivity”.

The emissivity feature, which plays a critical role in the formation of UHIs, is generally in the order of 0.9 to 1.00 for the materials used to form the urban fabric of many metropolitan areas around the world. In other words, the emissivity values of these materials are quite high. At this point, it can be expected that the albedo values of these materials are also low. However, it should be noted that low albedo value and high emissivity value do not always mean more heat release or more intense UHI formation. For example, natural areas having low surface albedo and high specific emissivity rates, such as water bodies or forests, reduce UHI formations. Water has high specific heat capacity, low heat absorption, and retention. Moreover, the softening properties of the harsh climates of the trees in the forests, their biological processes, such as photosynthesis, the ecosystem they host are the factors contributing to UHI reduction. In Table 2.1, albedo and emissivity rates are given for some natural surfaces found in nature and some materials frequently used within the urban fabric.

Table 2.1. Albedo and Emissivity Rates of Natural and Urban Fabric Surfaces [85]

| **Surface / Material** | ***Emissivity*** | **Natural Surface** | ***Albedo*** |
|---|---|---|---|
| Asphalt | 0.96 | Forest | 0.05 - 0.15 |
| Concrete Roof | 0.97 - 0.98 | Grassland | 0.10 - 0.25 |
| Flagstone | 0.96 | Sand | 0.15 - 0.40 |
| Granite | 0.98 | Snow | 0.50 - 0.95 |
| Green Roof | 0.93 | Water | 0.05 - 0.12 |
| Metal Roof | 0.99 | | |
| Roof Tile | 0.98 - 0.99 | | |
| Sand | 0.96 | | |
| Sidewalk Brick | 0.96 | | |
| Tile | 1.00 | | |
| Tree and Lawn | 0.97 | | |
| Water | 1.00 | | |
| Wooden Board | 0.95 | | |

### 2.2.2 Categorization and Measurement Techniques

The Canopy Layer, which defines an area up to the upper limits of the city buildings where the city residents reside; and the Boundary Layer, which extends to the upper limits of the atmosphere on the city, are the zones where the detection and measurement of UHI formations can be made. At this point, it is beneficial to summarize the components of incoming solar radiation reaching the canopy layer of a metropolitan area:

- **Diffuse Radiation:** The "diffuse" component of incoming solar radiation entering the Earth's atmosphere, which is mostly considered negligible in calculations, is the radiation scattered from the structures such as several air molecules & aerosols, water vapors, clouds, dust particles, pollutants in the air.
- **Direct Radiation:** It is the radiation component that directly reaches the Earth surface without any scattering. For this reason, the expression "direct" is used for this type of radiation.
- **Global Radiation:** It is defined as the total incoming shortwave radiation falling on a surface above ground. It is also the sum of direct (beam) and diffuse radiation.

The concept of radiation is also the total amount of photons emitted from a single source. Irradiation is the amount of radiation calculated on the surface that these photons reach. Similar to the components of solar radiation summarized above, the components of solar irradiance are given below:

- **Direct Normal (Beam) Irradiation:** The measurement of the solar irradiation at a geographical location’s surface of the Earth with a surface element perpendicular to the Sun

- **Diffuse Horizontal Irradiation:** The terrestrial irradiation scattered or diffused by the atmospheric factors and particles and measured on a horizontal surface
- **Global Horizontal Irradiation:** This irradiation is measured as the total shortwave radiation received by a surface horizontal to the ground.

Before moving on to UHI categorization, it is useful to specify some factors that pave the way for UHI formations in metropolitan areas by comparing them with rural areas: Metropolitan city constructions (such as building façades, pavements, and vehicle roads) that receive intense incoming solar radiation, especially in hot summer months and during the daytime, have more heat absorption and retention compared to the natural field surfaces of rural areas. In addition, less water evaporation and penetration (more surface runoff) occur in metropolitan areas, which have an environment that is mostly weak in terms of vegetation and green fields and dense in terms of impervious surfaces, compared to rural areas rich in plant diversity and flora. Again, in connection with these conditions, plant transpiration is also less. For these reasons, the air temperature curves in the form of "island", which is the starting point of the heat island nomenclature, emerge with an increasing trend from rural and suburban areas to metropolitan city centers, as can be seen in Figure 2.5. The rising trend of these temperature curves shows decreases in green spaces, parks, and ponds where vegetation is enhanced in cities.

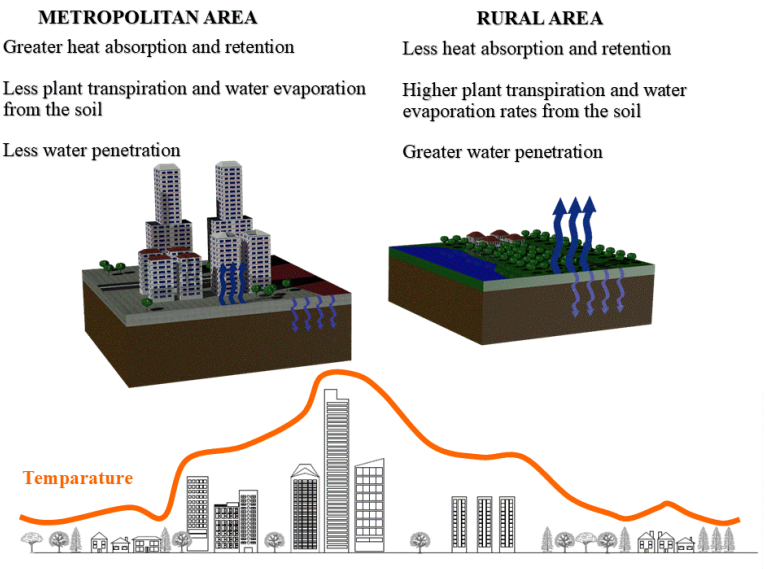


Figure 2.5. Metropolitan-Rural Area Comparison and UHI Temperature Intensity Curve

The Canopy Layer, which defines an area up to the upper limits of the city buildings and where the city residents reside, and the Boundary Layer, which extends to the upper limits of the atmosphere on the city, are the zones where detection and measurement of UHI formations can be made. These zones are also defined when studying which meteorological conditions and events are observed within the mesoscale and microscale limits of the atmosphere. UHIs, which can also be defined as an “altered microclimatic event”, arise from artificial sources in the microscale environment of a city and show their influence in a wide impact area extending to the mesoscale (upper atmospheric layer) boundaries of the city. At this point, it should be emphasized that the airflow cycle in the city is closely related to the UHI observation frequency in line with the natural wind conditions (speed and direction) in the region where the city is located and the urban design (green spaces, ventilation corridors, etc.). Figure 2.6 shows in which zones the UHI formations occur, depending on the urban sources, within a metropolitan area's mesoscale and microscale meteorology.

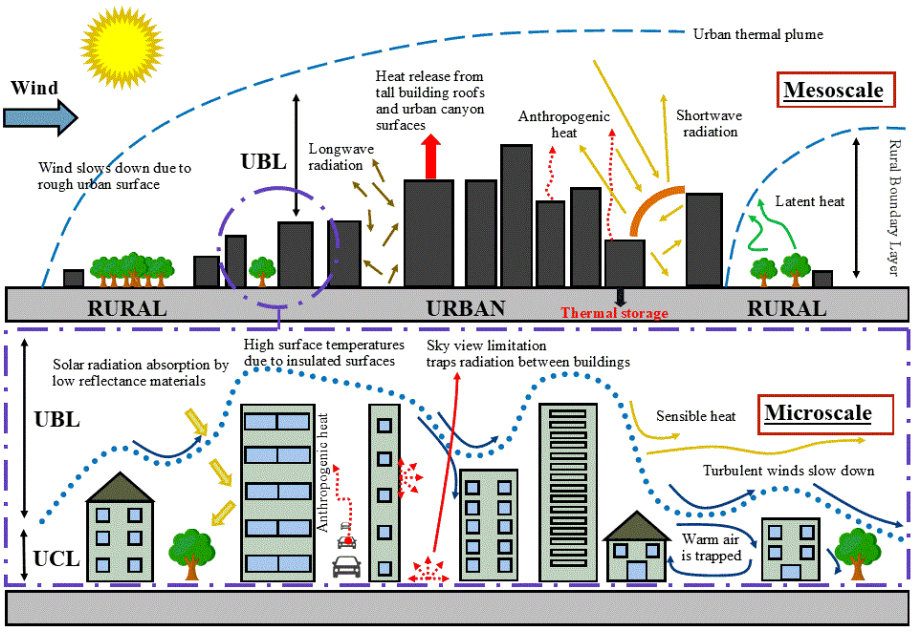


Figure 2.6. UBL and UCL Heat Island Sources [53] *(modified)*

The Urban Boundary Layer (UBL) and Urban Canopy Layer (UCL), the boundaries specified in Figure 2.6, are the two primary zones considered in monitoring the atmospheric and meteorological conditions and weather events in an urban area. In this direction, the heat islands detected within the boundary layer limits of cities (and at the macro level) are called UBLHI; the heat islands detected within the limits of the canopy layer (and at the micro-level) are called UCLHI. Both types of heat islands are mainly caused by radiation and heat alterations due to dense construction in the city. Some of these alterations affecting mesoscale and microscale meteorology can be seen in Figure 2.6. In metropolitan cities where higher ambient temperatures are recorded than in neighboring rural areas, the Urban Thermal Plume, which can be defined at the boundaries of the urban atmosphere including UCL and UBL, and also seen in Figure 2.6, is formed because of the rise of the heated air. The point and non-point sources at the mesoscale and microscale levels that cause Urban Thermal Plume and UCLHI and UBLHI Effects given in Figure 2.6 are explained in more detail below:

**Buildings:** Especially in metropolitan areas, high-rise buildings, skyscrapers, etc., which are located very close to each other in the distance and in line with a city planning increasingly dense in city centers, can be given as examples under this heading. In the façade and roof constructions, materials with low reflectance, high heat absorption/retention capacity, and preparing the ground for the formation of insulated surface can be specified as point sources in UHI formations. Therefore, such manufacturing materials used in the construction of city buildings greatly impact the intensity and observation frequency of the Surface Heat Island (SHI) and Atmospheric Heat Island (AHI) formations, which will be included later in this Chapter. Buildings made with this material, which continues to absorb heat due to incoming shortwave radiation reaching their surfaces all day long, cool at night, releasing the heat they retain during the day (longwave (IR) radiation) into the atmosphere, which causes significant increases in nighttime urban air temperatures. This additional heat load in the urban atmosphere can also be expressed as one of the anthropogenic heat types.

**Urban Canyons:** "Urban canyons" are formed as a result of high-rise / tall buildings and skyscrapers being built side by side, and this positioning style is extended along lines such as long streets and boulevards within the scope of city planning (this definition is made as a reference to natural canyons). These canyons, which limit the sky view, cause the inter-building longwave radiation transitions seen in Figure 2.6 or the reflection of the shortwave radiation (reaching the building façades) between the façades. In other words, inside these canyons, which may show both point and non-point source characteristics, there are heat/radiation traps that strengthen UHI formations.

**Vehicle Traffic, Roads, and Pavements:** Particular UHI point sources (anthropogenic heat) for cities are those that cause exhaust (and GHG) emissions from vehicles in traffic, especially during heavy vehicle traffic times, in violation of environmental laws and regulations. In addition, as mentioned in the "Buildings" section above, dark-colored vehicle roofs, which can cause low reflectance and high heat absorption/retention, are among the HIE sources. Besides, considering that

pavements, roads, and highways, which are essential components of pedestrian and vehicle transportation system for a city, extended to almost all sub-regions of the city, again, it can be said that the selection of building material is an issue that needs to be well planned for these components as well.

**Wind and Air Circulation:** Wind and air circulation are two important natural factors that reduce HIE, unlike the UHI sources given above. Dense buildings and the rough urban surface can disperse the wind that enters the cities from a particular direction and slow down the wind speed. Warm air can be trapped in the city by slowing down and even stopping wind and airflow (Figure 2.6). In addition, warm air can be carried in the air by convection as "sensible heat" in relation to the ambient temperature felt by the city residents (Figure 2.6). As for evapotranspiration, it is the sum of plant transpiration and evaporation from the land surface that city residents feel as humidity. It is at lower rates due to less latent heat transfer due to less vegetation in cities (Figure 2.6). For these reasons, it is crucial to make ventilation corridors on suitable locations in urban design and planning stages, taking into account local winds, to ensure efficient natural air circulation and HIE reduction.

UHI formations can be categorized according to the zone in which they occur, as well as the way they are detected on an urban fabric surface (SHI) or in the atmosphere overlying a metropolitan city (AHI). AHI and SHI effects are separated from each other according to the following conditions:

- daily and seasonal presence and intensity;
- how big an air temperature difference they create;
- identification and observation/monitoring methods and equipment;
- graphical interpretation / depiction type

The UHI categorization specified with these titles can be examined in Table 2.2.

Table 2.2. SHI and AHI Categorization [25] [103] [115]

| **Category** | **Surface UHI** | **Atmospheric UHI** |
|---|---|---|
| Time of day and season | *Presence:*<br>All times of the day and night<br>*Intensity:*<br>During the day and in the summer | *Presence:*<br>Small or absent during the day<br>*Intensity:*<br>At night, before dawn, and in the winter |
| Temperature variation | *Day:* 10 – 15 °C<br>*Night:* 5 – 10 °C | *Day:* (-1) – 3 °C<br>*Night:* 7 – 12 °C |
| Identification method / instrument | *Remote Sensing (3D, 2D, ground):*<br>• Satellites<br>• Aircrafts<br>• Some ground systems | *Fixed weather monitoring stations:*<br>• Ground-mounted versions for CLUHI<br>• Tower-mounted versions for BLUHI<br>*Mobile traverses:*<br>• Automobiles for CLUHI<br>• Aircraft for BLUHI<br>*Vertical sensing:*<br>• SODAR (Sonic Detection and Ranging) for BLUHI<br>• Tethered balloons for BLUHI |
| Depiction | Thermal imaging | Isotherm mapping, Temperature graphs |

### 2.2.3 Literature Review of Urban Heat Island Studies

UHIs, which have an important place in the literature in terms of both urban planning and environmental studies, have been examined according to the heat island type (AHI or SHI) in which they are detected in various parts of the world, in accordance with the detection and monitoring methods specified in Table 2.2. Some published articles and proceedings of research studies on this subject in the literature are summarized below.

Athukorala and Murayama [6] performed a spatio-temporal analysis for the Greater Cairo region of Egypt, considering daytime and nighttime land surface temperatures, which are among the determining variables in UHI observations. In line with their studies, Landsat Thematic Mapper, Operational Land Imager and Thermal Infrared Sensor, Moderate Resolution Imaging Spectro-radiometer, Google Earth Engine

(GEE) tools and instruments were used. The researchers, who detected a negative UHI effect, namely the cooling effect, with the mean land surface temperature difference of -3.59°C in the urban area during the day compared to the rural area, found a positive UHI effect with a temperature difference of 2.33°C at night.

Amindin et al. [3] made land surface temperature, urban thermal field variance index, and UHI index mapping by using Landsat (4,5,7,8) satellite images in line with a UHI intensity determination and distribution analysis covering 21 years (1995-2016) for the Ahvaz city in Iran. The land surface temperature examined in this study was also associated with the decrease in green space in the Ahvaz region in 21 years.

Lu et al. [58] examined the link between the land cover in the Xi'an city (China) and spatio-temporal variations in the thermal environment using Landsat images from 1995 to 2020. According to the study results, an increase in mean SHI intensity of around 2°C was detected over 25 years. In the study, it was stated that the densities of impervious surfaces compared to green spaces have a significant impact on land surface temperature. It has also been noted that increasing urban green areas reduces the negative effects of UHIs.

Montaner-Fernández et al. [65], in their study of the city of Santiago, Chile, stated that maximum temperatures had been recorded for more than a century in the last few summers. Moderate Resolution Imaging Spectroradiometer satellite imagery from nine meteorological stations was used within the scope of the study to determine the nighttime (up to 9°C) and daytime UHI formations and spatial variability in Santiago during the summer months of 2005-2017.

Hardin et al. [36] investigated daytime and nighttime temperatures in four major cities in the Northeast by high-resolution spatio-temporal analysis using a large number of weather stations (100-200 per area) between 2006-2013 and between May and September. According to the study results, UHI intensities and regional air temperature variability were significant in dry and hot conditions. UHI formations with the highest intensity occur on nights with dry weather conditions. The highest average nighttime UHI intensity in the study was found in New York City.

Deilami et al. [18] prepared a comprehensive and systematic review of various spatiotemporal factors associated with the UHI effect. In this direction, they examined 75 studies related to the UHI effect. Within the scope of this review, an assessment was made on UHI detection with different methods such as satellite images, land cover classification, and land-use changes, models.

Xu et al. [112] conducted a study on effective air-cooling systems in Singapore's urban microclimate. The authors stated that they developed a heat island modeling tool to simulate the stack effects of split-type air conditioners on high-rise buildings and thermal environment. Accordingly, Computational Fluid Dynamics and solar radiation model coupling were used to simulate air temperature and relative humidity. The study also stated that the thermal environment around the buildings could be improved by increasing the thermal conductivity and reflectivity of the buildings or by decreasing the absorptivity.

Kotharkar and Surawar [55] used traverse survey points to examine the 2012-2014 summer and winter nocturnal mean CLUHI formation intensities for the city of Nagpur in India. In the study, the mean CLUHI in Nagpur was 2.14°C in summer; It was determined as 2.36°C in winter. The authors found that the CLUHI effect predominates in areas with high populations and dense high-rise buildings. The highest CLUHI hotspots were observed in highly-populated and vegetation-weak areas. In the study, it was stated that there is a connection between land cover change and vegetation and CLUHI formations.

In his doctoral thesis, Dihkan [21] examined the UHI effect in some of the country's main coastal and inland cities (Ankara, İstanbul, İzmir, Bursa, Gaziantep, Trabzon, and Erzurum) to prepare a general UHI characteristic for Turkey. In the study, Streutker (2002; 2003) model modification was made, and the temporal variation of SHI between 1984-2011 with remote sensing images was examined. In the cities in the study, the AHI effect was analyzed by using the mobile traverse method. As a result of these examinations, both SHI and AHI effects were detected in all the city centers selected within the scope of the study. In some of these cities, the SHI effect,

which showed an increasing trend between 1984 and 2011, was found. The author associated urban SHI formations with land cover change and anthropogenic impact on urban geometry.

Mirzaei [63] conducted a study on the compatibility of the models used in UHI studies. The author categorized the studies, especially between 2013-2015, in line with their context.

Yılmaz [113] examined the SHI effect in Adana city and its surroundings in Turkey, using Landsat satellite images and meteorological station data. Within the scope of the study, surface temperature models were prepared using thermal bands of satellite images. The differences in the relative surface temperature between the city and its surroundings during the year were analyzed. The study stated that positive SHI was detected in the summer months, whereas a negative SHI effect in the winter months.

Dwivedi and Khire [25] published a study on the technologies used in UHI measurements. In the study, it was informed that surface materials (such as concrete and asphalt) capable of rapid heat absorption (during daytime) and loss (during nighttime) cause increases in urban air temperature. On the other hand, the contribution of natural areas such as water, trees, and green space, which can make slower heat absorption and loss, in keeping cities cool, has been expressed. It has been stated that the methods in which UHIs are detected by ground-based observation and meteorological data are insufficient to provide continuous surface information in the region where they occur. The study also expressed that new UHI detection paths can be provided using the thermal remote sensing method with the developments in satellite, thermal sensor, and aircraft technologies.

Coseo and Larsen [17] used remote sensing and urban climatology-related publications to explain the UHI formation intensities in 8 neighborhoods of Chicago. The authors collected the air temperature measurements in an urban block in each neighborhood in Summer 2010. They experimentally analyzed air temperature variations and extreme heat events at certain times of the day.

In the literature covering UHI-based researches, there are more studies (than the publications above) using several methods (experimental, simulation-based, classification, etc.) for different locations in the world geography. Hadjimitsis et al. [35] studied the UHI effect in Cyprus with ground and satellite measurements. Dorer et al. [22] investigated the impact of urban microclimate (including measured UHI intensities) on building energy demands required for space heating and cooling processes, using building energy simulations and computational fluid dynamics. Stewart and Oke [86] introduced a classification system for the concept of "local climate zone", which can significantly contribute to UHI studies and urban air temperature observations. Kuşçu Şimşek and Şengezer [81] emphasized the importance of green spaces, which have an important role in urban heat reduction in the city of Istanbul, Turkey's largest metropolitan area. Yüksel and Yılmaz [23], on the other hand, published a study on remote sensing and meteorological observations for UHI detection and assessment in the summer months of 1985-2002 in Ankara, the capital city of Turkey.

## 2.3 Photovoltaic Heat Island Effect

UHI effect, which has a wide discussion area between environmental issues at regional and global level, where researches are conducted and published for different geographical locations and with various methods, is also the most conspicuous among the heat island types. However, within the scope of human activities, it has begun to be observed that this effect can also arise from other sources, in parallel with the growth and development in different sectors (e.g., renewable energy sector). One of these sources is PVPPs, whose number and area are increasing with rapid progress in the Earth's natural surface.

The PV Heat Island Effect (PVHIE), which is observed due to the heating-cooling cycles of PV module arrays in PVPP fields, can be detected and monitored more easily compared to UHIs that may occur due to complicated urban fabric surface and

dynamics. Because PV module arrays in a PVPP field are the devices mainly having the same dimensions, manufactured from the same material, and installed with the same positioning (height above ground and angular orientation (tilt angle). As a result, PVHIE can be studied via simpler methods than UHI formations that may arise from a mixed urban geometric surface.

The relationship between ambient temperature and solar PV module efficiency has an essential role in the emergence of PVHIE formations. The ambient (air) temperature of the region/location where PV modules are installed is one of the most influential parameters on module efficiency. Depending on the changes in module efficiency, physical heat release (or loss) processes from the surface of the solar module pave the way for PVHIE formations. The time periods in which these processes increase or decrease daily and seasonally are crucial in determining the intensities of PVHI formations. These topics and, in addition, a summary of the studies in the literature on PVHIE, as given in the UHI section above, are detailed in the sub-sections below.

### 2.3.1 Ambient Temperature and Solar Module Efficiency

In determining the energy conversion and electrical efficiency of solar PV modules, a wide range of components are effective, from the techniques used in the production processes of solar cells, which are semiconductor devices, to the physical properties of the materials used in module manufacturing. The efficiencies of PV modules, which are electrical and mechanical assemblies, may decrease according to the ambient (air) temperature conditions of the environment where they are located after these modules are installed and utilized. At this point, it is helpful to define the "temperature coefficient" given in the specifications of solar PV modules.

The temperature coefficient is expressed as a negative percentile. For example, a temperature coefficient value specified as “-0.5%/°C” describes that each 1°C increase in module temperature will result in a 0.5% decrease in PV module electrical

output. This 1°C increase represents the rise in temperature from 25°C. The reason why 25°C is the reference point is that the PV module efficiency tests are performed at this temperature.

Ambient temperature, one of the most critical factors in the increase of module temperature, can vary depending on the microclimatic conditions in the geographical location where module installations are made. Therefore, especially when installing ground-mounted or building-integrated PV systems, air temperature records during the daytime hours when the PV modules are operational should be considered. In the regions where these records are high, the PV system's electrical power losses may be higher, and some environmental impacts such as PVHIE may occur more prominently. In addition to the fact that the increased module (surface) temperature in hot weather conditions causes a decrease in the electrical output and efficiency of the system, with the additional heat they emit or release to the atmosphere due to their heating-cooling cycles, PV modules can also be a PVHI source. It is given in the following sub-section by which physical processes a PV module releases heat to its surroundings.

### 2.3.2 Physical Processes of Heat Release from Solar Modules

It was explained in Chapter 1 that the energy conversion efficiencies of solar PV modules mostly vary between 15-25%, with some module products (Figure 1.13). A large amount of energy that cannot be converted at these efficiency rates in solar modules emerges as heat. PVEducation.org [41], an online education platform with many topics on PV systems, explains in the following titles that in addition to the external factors (such as ambient temperature), internal (structural) factors may cause the heating of PV modules:

- **Reflectivity of PV Module Surface:** How much of the light reaching the front surface of the PV modules is reflected from the module surface is defined by the module's surface albedo. Reflected light means energy that cannot be converted to electrical power output, although it does not cause module warming. In other words, it shows how much energy is lost in the conversion of incident energy reaching the solar module. For a standard and glass-coated PV module, this ratio is around 4%.

- **PV Module Efficiency and Operating Point:** Module efficiency and operating point describe the light energy fraction, which can convert to electricity. When a solar cell operates with open-circuit voltage and short-circuit current, there is no electricity generation, and all incident energy is converted into heat. Both of these parameters have an effect on the warming of solar modules.

- **Light Absorption Capability of PV Module:** In addition to the operation of solar cells with the principle of light absorption, the ratio of light absorption and reflection taken place in the structural parts of the PV module (e.g., module surface color) is among the factors that play a role in determining the heat generation in the PV module.

- **IR Absorption:** The IR absorption capability (e.g., aluminum frame) of the parts used in the assembly of a PV module is among the factors to be considered in terms of whether there is a heat release by longwave radiation from these parts. IR light passing through modules without absorption is emitted as longwave radiation, i.e., heat, to the surrounding environment.

Depending on the factors above, Figure 2.7 shows the physical processes that solar PV modules make heat release/loss from their inner and surface parts to the environment in which they are installed and the overlying atmosphere.

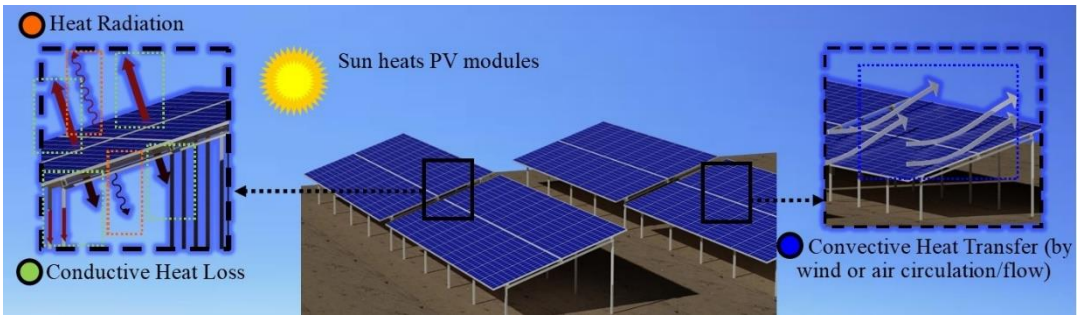


Figure 2.7. Heat Release/Loss Processes from Solar PV Modules

The illustrations in Figure 2.7 also show the heat transfer mechanisms within the fundamental laws of physics. The brief definitions of these heat transfer mechanisms are given below:

**Radiation:** It is the form of heat release that occurs when the thermal energy absorbed by the PV modules during the cooling process is emitted by electromagnetic waves, i.e., longwave (IR) radiation.

**Conduction:** It is the process of transferring the heat released directly over the module assembly, depending on the structural and thermal properties of the PV module parts.

**Convection:** It is the process of transporting the heat released in the PV module via the motion of the air surrounding the module (air circulation, wind flow, etc.).

Among the heat release/loss processes illustrated in Figure 2.7, the heat energy the PV modules emit due to longwave (IR) radiation can also be examined from the thermal camera images in Figure 2.8. On the date which the image of Figure 2.8 was taken (October 8, 2021), the maximum daytime air temperature is 20°C, and 4°C for the daytime minimum).

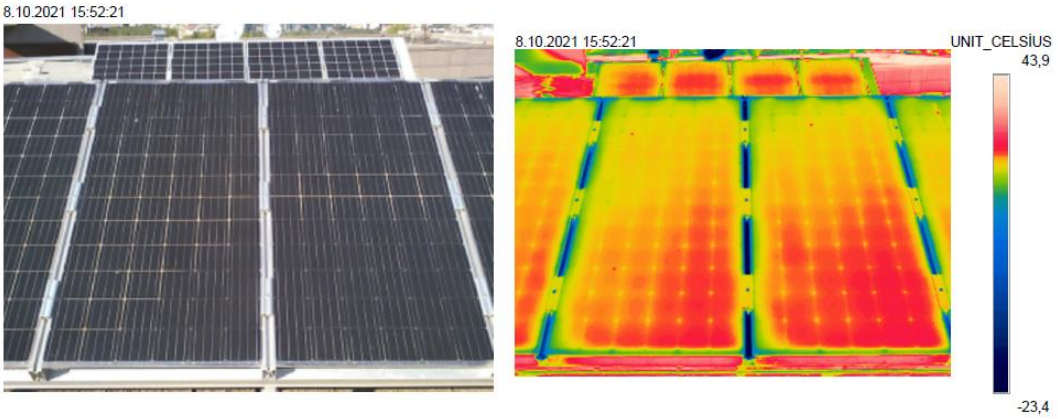


Figure 2.8. Thermal Camera (model *FLIR T530*) Images of a PV Module Array in ODTÜ-GÜNAM Outdoor Test Facility

### 2.3.3 Literature Review of PV Module Thermal Modelling and PVHIE Studies

Various thermal modeling studies are carried out in the literature regarding the performance, efficiency, and degradation of PV modules. Although these studies are mostly carried out to examine the effects of meteorological and various external factors on the operability of the modules and to develop models related to this, they are also important in contributing to recent environmental debates such as PVHIE. After giving some examples of PV thermal modeling studies in the literature under this title, the PVHIE research studies referenced within the scope of this thesis will be summarized:

Tuncel et al. [97] stated that in the regions where long hot seasons are effective, the decrease in PV module efficiency due to high temperatures should be considered. The thermal modeling method can be used for PV performance assessment in this direction. Regarding this issue, the authors worked on a polycrystalline silicon PV module installed in Ankara and benefited from the hourly data of meteorological variables in their research. The authors included the calculated heat capacity value

in their analysis, which is not given in the module specification sheets. They found that the model results were not affected by the heat capacity change.

Tuncel et al. [96] made a mathematical analysis by considering the wind (direction & speed) and temperature variables that are effective in PV module energy conversion. In this way, they studied how accurately PV performance estimations can be made without installing a pilot test and monitoring system. For this purpose, some comparisons were made between the mathematical model and the measurements in the ODTÜ-GÜNAM Outdoor Module Test Facility in Ankara, Turkey. With the comparisons they have made, the authors have determined in which time periods of the day the mathematical model and outdoor measurements are more compatible and in which time periods the model should be developed considering this situation.

Lobera and Valkealahti [57] expressed a dynamic thermal model on the total energy balance of a6 PV module. This model has been verified by the measurements in a solar PVPP as module temperature, solar irradiance, and weather station data collection. The differences between the simulated daytime PV module temperature and the measured PV module temperature in the study were below 2°C.

Siddiqui and Arif [80] carried out multi-physics modeling (including module cooling effect) that can provide 3D thermal and structural performance estimation of a PV module under meteorological conditions, as well as electrical performance. In the study, thermal, structural, and electrical analyses of a PV module were carried out for four different days with different environmental conditions for the city of Jeddah, Saudi Arabia. Furthermore, the cases where the effect of module cooling was included and excluded from the analyses were examined.

Research studies published in line with the above PV module thermal modeling and outdoor measurements comparisons contribute not only to module performance analysis but also to make an environmental impact assessment of environmental side effects such as PV heat island, which may arise due to high numbers of PV module deployment applications.

The published studies on PVHIE in the literature have been prepared since the 2000s, mostly including field study measurements and sometimes modeling. Many of these studies are given a summary in the following paragraphs:

Jiang et al. [50] conducted an experimental study on a PV plant and barren natural field in the Wujiaqu city of the Xinjiang region in China. During the day, the increase in net shortwave radiative forcing compared to the reference site and monitoring the warming and cooling effect amounts at the PV power plant are given. It was also found how much net radiation was converted to electrical energy. Furthermore, the percentage increase in sensible heat flux, which can cause convective heating and an increase in air temperature of the overlying atmosphere (at 2 meters and 10 meters), has been determined. The percentage reductions in latent heat flux have been found. The rates of change in sensible heat flux, ground surface heat flux, latent heat flux, and air temperature, depending on the warming of the PV modules during the day and cooling at night, were calculated separately within the scope of the study.

Wu et al. [111] prepared another similar study for the Qinghai province of China. This research was conducted at Gonghe PV Power Plant in the province to examine the impacts of desert-based PV module deployment on local surface energy exchanges and local microclimate in China. Within the scope of the study, local air temperature and humidity in the reference area, transition area, and inner area of the PVPP were compared using long-term observational data. According to the study results, there was a slight increase and decrease in daytime air temperature and a significant drop in nighttime air temperature. The slight increase in the spring and summer months reached a maximum of 0.34°C; The slight decrease in autumn and winter months was determined as the maximum of 0.26°C. A reduction of nighttime temperature was observed in all four seasons (max. 1.82°C for winter night). It was found that the relative humidity in PVPP tends to increase, except for a slight decrease in the summer months. The most significant increase in humidity was 5.00% and 4.76% (respectively) in winter for reference and transition areas. It was found that diurnal air temperature and humidity values inside the PV power plant were higher than outside the PW power plant.

Fan and Huang [28] investigated the impact of PVPP installation increases on surface spectral reflectance for Qinghai province, China, using the satellite-based Moderate Resolution Imaging Spectroradiometers (MODIS) method. The study was conducted at Desert Sunlight Solar Farm in the Mojave Desert in California, USA. In accordance with the study results, it was revealed that a PVPP caused a 20-25% surface reflectance reduction. This research is important in assessing the relationship between albedo and heat islands from the perspective of PV module deployments.

One of the studies investigating the PVHIE issue within the scope of agrivoltaic applications was contributed to the literature by Barron-Gafford et al. [9]. In this study, which developed an approach with an appropriate integration, considering microclimatic conditions, PV module temperature, and agricultural factors (soil moisture, irrigation water, plant biomass production, etc.), several advantages of PV module shading have been noted (increase of food production; decrease of plant drought and PV module heat stresses).

Again, Barron-Gafford et al. [8] contributed to the studies in the literature that previously examined the UHI-like PVHIE mostly with theoretical or simulation methods by utilizing a field study they conducted experimentally at the University of Arizona, USA. The authors recorded higher temperatures of 3-4°C at a PVPP site than the neighboring wildlands at night.

Fthenakis and Yu [30] examined the impacts of large-scale PVPPs on the local microclimate using computational fluid dynamics. Accordingly, the authors conducted their work by comparing recorded field data (temperature and wind) and 3D simulations of a PVPP with a 1 MW installation capacity in North America. In the study, both field data and simulation results showed that annual average air temperatures in the PVPP center were 1.9°C higher than ambient temperatures. In addition, thermal energy dissipation has been found from the PVPP field to the surrounding environment up to 300 meters. The 18-month data analysis of the study showed that PVHIE emerged when the PV module arrays were cooling, mostly at night.

Millstein and Menon [62] conducted a similar study by designing hypothetical PV module arrays for the Mojave Desert of California, USA. Weather Research and Forecasting (WRF) model was used to analyze the interaction between weather and surface parameters, including surface temperature and surface albedo changes. Similar to the study of Fthenakis and Yu [30], the increases in local afternoon temperatures up to 0.4°C were detected due to the decrease in surface albedo. Also, the PV module arrays affected the local wind patterns within an area of 300 km.

Apart from these studies in the literature, there are also studies examining the effects of BIPV installations on the urban microclimate and the relationship between the UHI effect and these installations. Some examples of these studies are Matai [60], Burg et al. [13], and Masson [59]. Keetels's report [52] published by TU Delft can also be viewed.

# CHAPTER 3

# FIELD STUDY ON PVHIE IN SEKBANDEMİRLİ RURAL REGION

It can be understood from the information given in Chapter 2 that there are few studies in the literature on PVHIE and that the contents of the presented proceedings and published articles are shaped by field studies conducted in certain geographies. In Turkey, no experimental research has been conducted, except for the projects carried out within the scope of this thesis. In other words, the first field projects to investigate this effect for land-based PVPPs, whose number and footprint is increasing day by day in Turkey, a geographically rich country in solar energy potential, were conducted within the scope of this thesis.

## 3.1 Field Location and PVPP Selection

It would be helpful to examine the "Turkey's solar PV power potential", which is taken into account in the selection of the PVPP where the thesis study was conducted and the location where this PVPP is located before moving on to the titles about the methodology, project, and equipment, analyzes and results of the study. Mapping techniques can demonstrate this solar resource potential for the regions and provinces of Turkey.

Maps showing this potential for Turkey are an essential resource that they can refer to give ideas to project investors and stakeholders in the PVPP project processes, which are implemented following the necessary environmental and economic feasibility studies. Since the regional solar radiation distribution on the map can be examined with this mapping method, an idea can be obtained about the climatic and microclimatic differences between the regions.

PV power potential maps of the world and Turkey, funded by ESMAP, prepared by SOLARGIS, and published by the World Bank Group, are given in Figure 3.1. When the annual and long-term daily averages are examined, especially between the polar regions and the equator, and throughout the regions in the middle and southern latitudes, it can be said that Turkey is among the rich countries in solar energy potential. In Europe, it comes first, along with Spain.

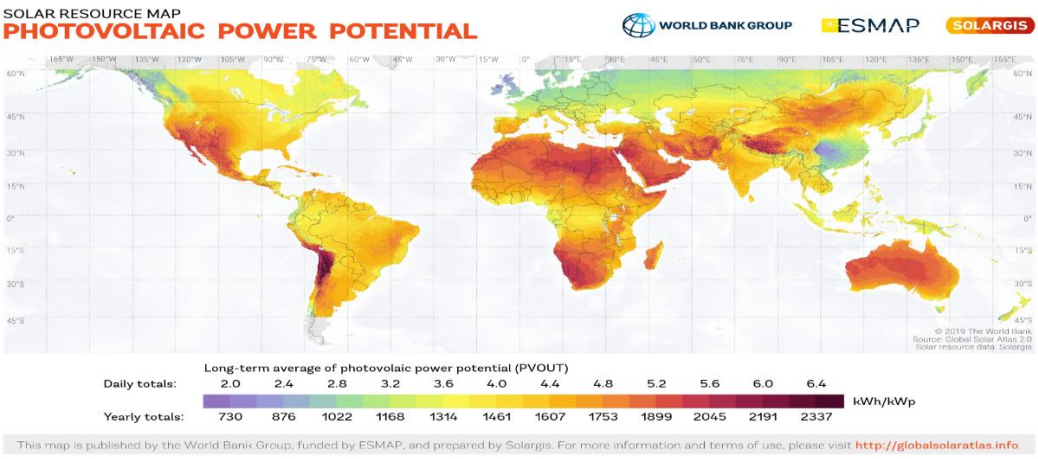


(a)

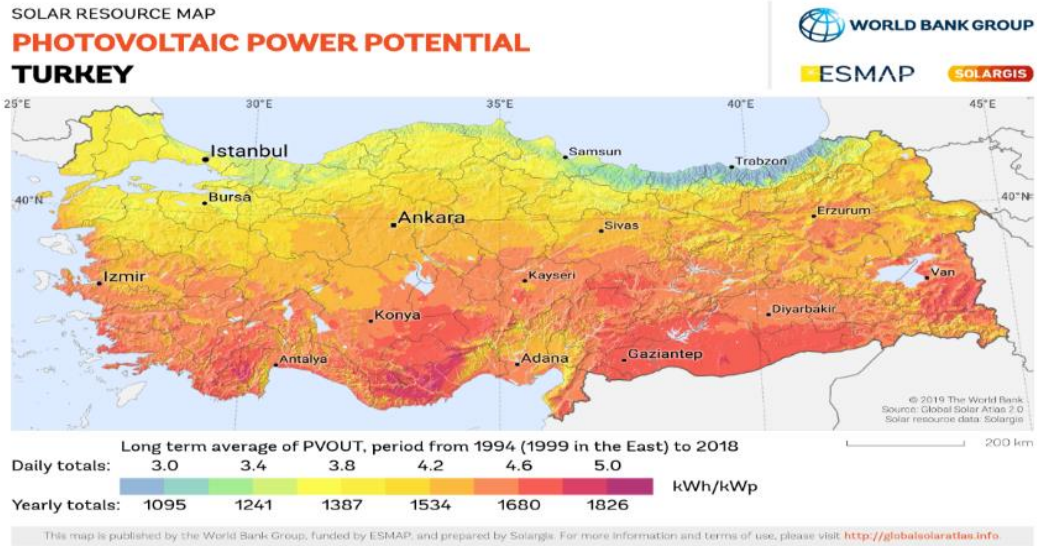


(b)

Figure 3.1. Solar Photovoltaic Power Potential of World (a) and Turkey (b)

The map of Turkey in Figure 3.1 (b) has been stated above for PVPP installations in which regions can be taken as a reference for more output. However, it should be noted that issues such as the following should also be considered in the location selection for PVPP installations: Placement and orientation operations of the PV modules in these power plants on the land; ease of access to the land where the power plant is installed (for equipment transportation, technical control, and maintenance, etc.); determination of suitable land in line with the EIA.

Sekbandemirli PVPP, where the field study in this thesis study was conducted, is located in the province of Kütahya. In Kütahya, located in a geographic transition location between Central Anatolia, Aegean and Marmara regions, these regions' climatic features and seasonal weather conditions can be observed. Sekbandemirli PVPP is located right next to the Sekbandemirli Village (39.52°N, 29.34°E) of the Tavşanlı district of Kütahya, 16 km from the town. Sekbandemirli is also the name of the rural area where the village is located. Mild average air temperatures are mostly recorded throughout the year in this rural area. According to the Beaufort scale, winds with varying speeds between “calm” and “moderate breeze” (0.0-7.9 m/s) blow. The area where the village and PVPP are located is surrounded by grasslands and shrublands intersecting with steppe fields in places. Although there are some high points in the region, these points are generally at the "hill" level, and the region's land consists of plains with a slight slope in elevation (Figure 3.2).

In many regions of Turkey, there are many operational PVPPs (licensed or unlicensed) installed in various installed capacities. The selection of Sekbandemirli PVPP in accordance with this field study is a decision made by evaluating the various advantages it provides. These advantages can be listed as follows:

- The work can be carried out in a PVPP installed in a “PV power potential efficient” area according to the map in Figure 3.1(b).

- There is a distinct contribution of PVHI formations to similar studies in the literature, which can be detected in a region where mild average air temperatures are recorded, with day and night air temperatures under the influence of a moderate climate, compared to the climate of an entirely continental or desert region.

- The convenience provided by a PVPP installed in a rural area that does not have a significant land slope and an elevation difference between its plains, in PVHIE observation and analysis

- Possibility to make comparisons between the ambient meteorological conditions in the power plant field and the weather conditions in this settlement area, as a result of the PVPP's location near Sekbandemirli Village

- Within the scope of thesis projects to be explained in the following sub-section, in line with the agreements made with the residents of Sekbandemirli Village and the PVPP operator, possibility for performing long-term data monitoring and collection from the power plant and its close surroundings (both before and after the PVPP installation)

Sekbandemirli PVPP was established on an uncultivated area of 44000 $m^2$ near the village of the same name in the region in 2017 (Figure 3.2). Mono-crystalline PV modules with 18.4% efficiency and 16.6% poly-crystalline PV modules in PVPP with an installed capacity of 2.5 MW are the products of *PluraWatt* and *Ödül Solar Enerji* brands (Appendix A). The module arrays are mounted on the ground with the front edges 0.5 m above the ground and the rear edges 1.9 m above the ground, positioned south-facing with a tilt angle of 20° (Figure 3.2).

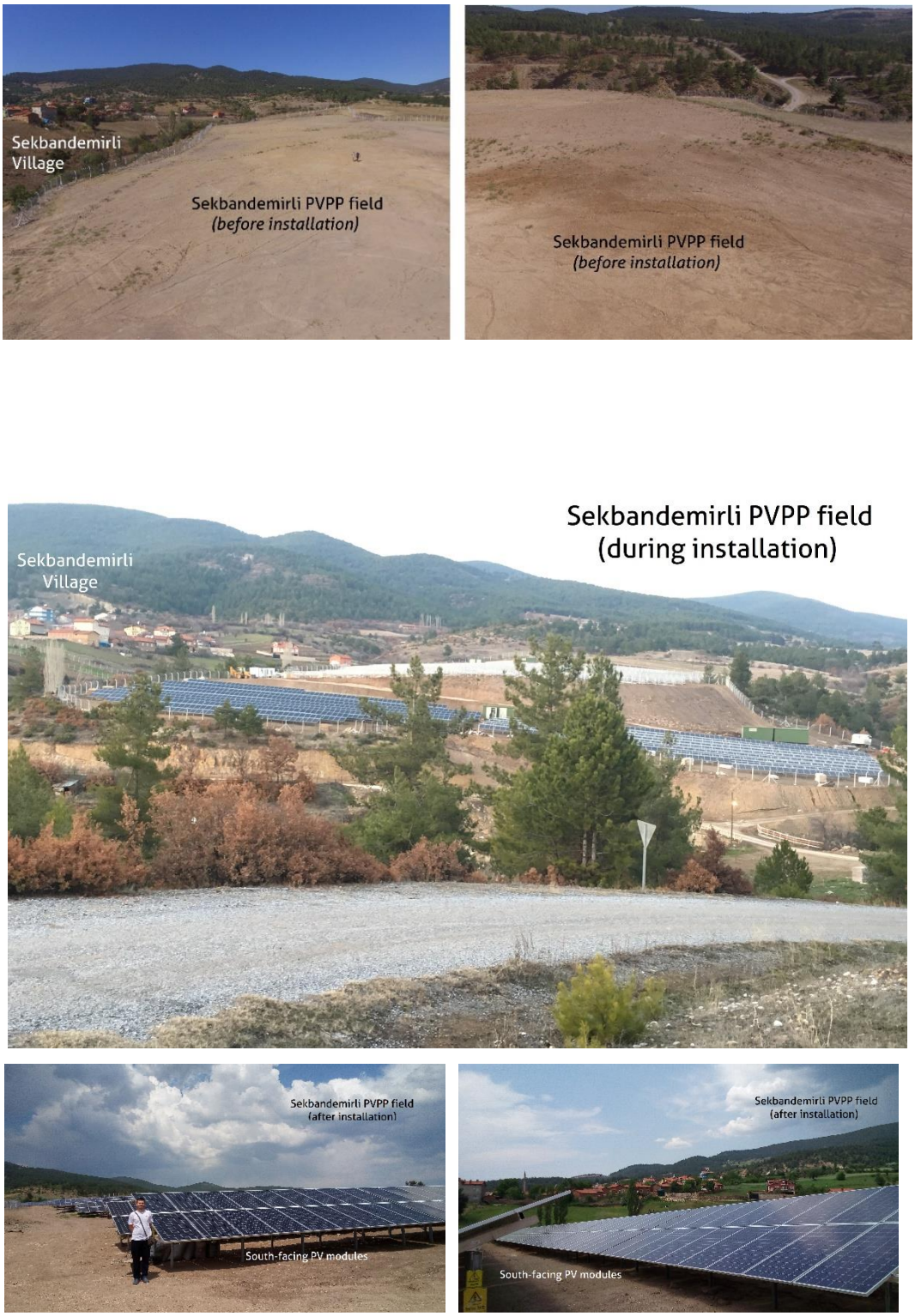


Figure 3.2. Sekbandemirli Rural Region and PVPP

When the construction plan of Sekbandemirli PVPP is examined (Figure 3.3), it can be seen that it is divided into four sub-fields. These sub-fields are included in the construction plan according to the contracts signed by the power plant operator with their stakeholders, such as private sector firms and institutions that they collaborate with before the PVPP installation. As will be explained in the next sub-titles of this Chapter, the meteorological data monitored and collected in the PVPP field during the project stages of this thesis includes the MEYSA-3, PDA-2 and MERENSE-2 sub-fields specified in the construction plan in Figure 3.3.

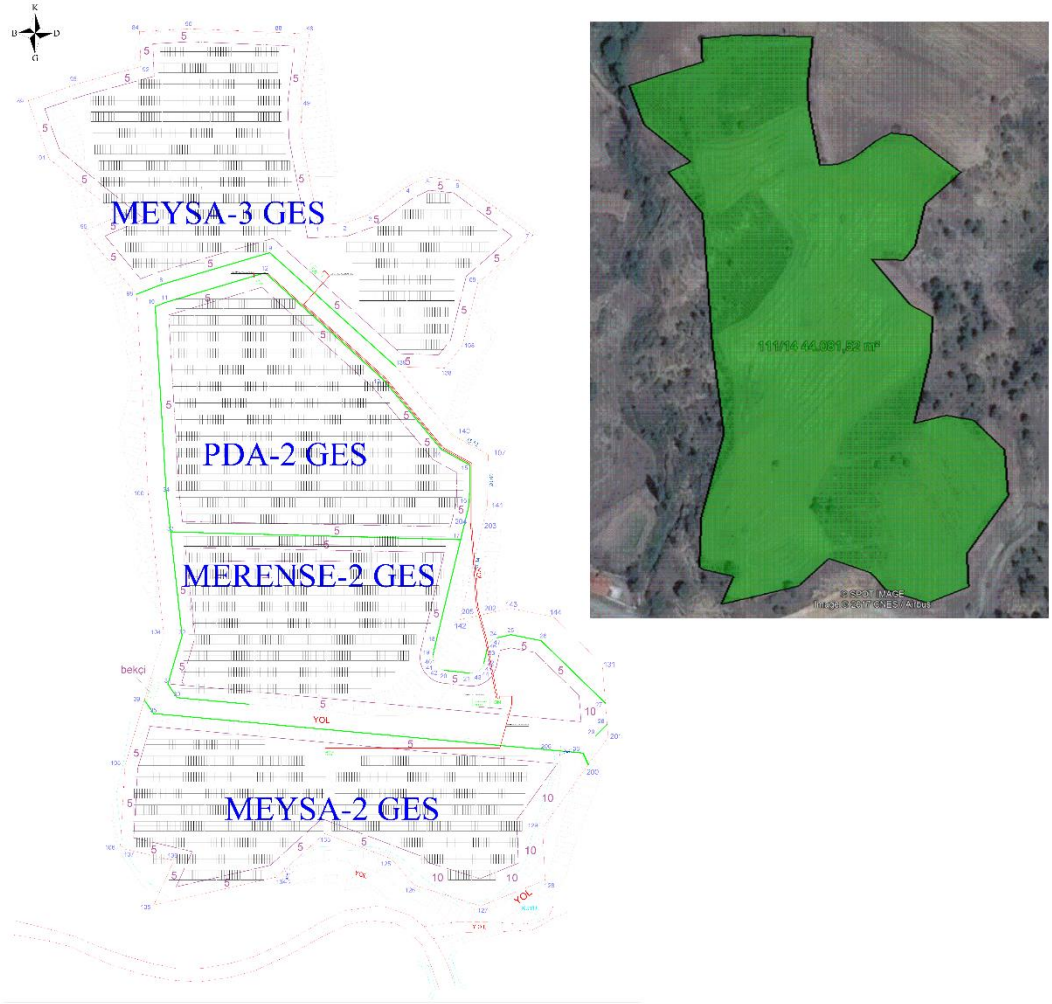


Figure 3.3. Sekbandemirli PVPP Construction Plan
*(*"GES" is the abbreviation of "PVPP" *in Turkish)*

## 3.2 Project Preparations and Supports

The location and PVPP field selection for PVHIE observations, which was explained in the previous sub-section of this Chapter, is the starting point for the preparations of this thesis. Following this selection and considering the previous similar studies in the literature, it was decided which heat island detection/observation methods specified in Table 2.2 would be used. PVHI formations

- can be examined as Surface Heat Island Effect by using the methods such as thermal imaging, modeling, etc. to consider PV module array surface temperature and longwave IR emission detection;

- can be examined as Atmospheric Heat Island Effect by using the methods such as temperature graphs and illustrations, microclimate and weather models, etc.

Since the Canopy Layer level of the regions where PVPPs are installed is usually considered in Atmospheric Heat Island observations, the methodology and the equipment selection of this study were made in such a way that data collection and monitoring would be carried out within the boundaries of this layer. In summary, the PVHI formations in the Canopy Layer were observed in the PVPP field and its close surroundings, and it was planned to use “fixed (ground-mounted) weather monitoring stations” for those observations. The brand/model and features of these weather stations used are given in the following sub-section. In addition, the interfaces where both the meteorological data collected via these weather stations and the PV module temperature and PVPP electrical power output data collected from the PVPP field are monitored on the web are explained in sub-section 3.4.

It was also planned to analyze the field study results of the thesis by microclimate simulation software. For this, a 1-year license of the *ENVI-met* microclimate software developed in Germany was purchased. The simulation of the Sekbandemirli rural region and PVPP field by *ENVI-met* and the examination of the local weather conditions of the region on this simulation are given in Chapter 6.

The financial support required to make the aforementioned preparations has been provided by two separate Scientific Project Support applications made to Middle East Technical University. These projects received support with the grant numbers BAP-07-02-2017-006 and TEZ-D-105-2020-10169 in 2017 and 2020, respectively. In this direction, the field data of the thesis started to be collected and monitored in October 2017.

## 3.3 Measurement Devices and Data Collection & Monitoring

Three fixed (ground-mounted) weather monitoring stations were used to observe heat island formations caused by the Sekbandemirli PVPP field, which might occur at the canopy layer level at certain time intervals. Two of these weather stations were obtained by renting from a private sector company (as a service purchase) with the expenditure made within the scope of Scientific Project Supports (their grant numbers were given in the previous title). As will be explained in the analysis sections of the project, the third weather station, which showed significant results in PVHIE detections, was installed in the power plant field by the PVPP operator in November 2018. The third weather station can also collect PV module temperature measurements by a temperature sensor connected to a PV module at the location where it is installed.

The features of these three stations, the meteorological parameters they can measure, and the time interval information they can measure are given in Appendix B. The brand of two rented weather stations via the project supports is *Davis*. Besides the hourly averages (calculated from the 10-minute averages between XX:00 – XX:50) of the measurements of the five meteorological parameters used in this thesis, specified in Appendix B, the Davis weather stations can also measure rainfall amount, speed, and evapotranspiration. The brand of the third station that the PVPP operator installs it to the field is *PV-met*, and it can only take solar radiation, ambient air, and PV module temperature measurements as hourly averages.

Weather data collected by the weather stations from the PVPP field, PV module temperature, and PVPP's electrical power output (daily, monthly and annual) can be monitored via two web interfaces. The parameters measured by the weather stations can be examined as numerical values and graphical demonstrations for selected dates and date intervals on the web interfaces below:

- *PlantMet*, an agricultural and meteorological data monitoring system, is used to view and download the measurements of *Davis* brand weather stations: http://web.plantmet.com.tr

- The ambient air temperature measured by the *PV-met* brand weather station, the PV module temperature collected by the temperature sensor connected to this station, and the PVPP electrical power output data are monitored via *SunnyPortal*: www.sunnyportal.com

To separate daytime and nighttime data, $WS_2$'s incoming solar radiation measurements were considered:

- A daytime value when "not zero"
- A nighttime value when "zero"

# CHAPTER 4

## STATISTICAL SIGNIFICANCE

Within the scope of the field research of this thesis, the use of "statistical significance methods" is at the forefront of the analyzes. These methods are used to categorize the daily and seasonal PVHI Effect by observing PVHI formations caused by the PVPP in the Sekbandemirli rural region, and they enable to reach the first significant findings in terms of comparing the weather data collected by the meteorological stations installed in certain locations inside and outside the PVPP field with each other.

The locations of meteorological stations in the Sekbandemirli rural region and PVPP field are given in Figure 4.1. As stated in this figure, $WS_1$ and $WS_2$ (*Davis Vantage Pro2™*) show the weather stations rented as part of the project support of the thesis project; $WS_3$ (*PV-met 150*) shows the weather station installed on the field by the power plant operator (Appendix B). While determining the locations of the three weather stations in Figure 4.1, the locations suitable for detecting PVHI formations and making comparisons with the weather conditions in Sekbandemirli Village were determined. However, in selecting the location, the PVPP's construction plan was also taken into account.

In Figure 4.1.a, Sekbandemirli's bird's-eye view is given, and in Figure 4.1.b, Google Earth view is shown. As can be seen from these two figures and Figure 3.3, $WS_1$ is located outside and northwest of MEYSA-3, one of the sub-fields of Sekbandemirli PVPP, close to Sekbandemirli Village. $WS_2$ is located at the center of the MEYSA-3 sub-field. With all its sub-fields, $WS_3$ was installed in a location (between MERENSE-2 and PDA-2) that can be considered as the center of the PVPP field where the dense PV module arrays are installed.

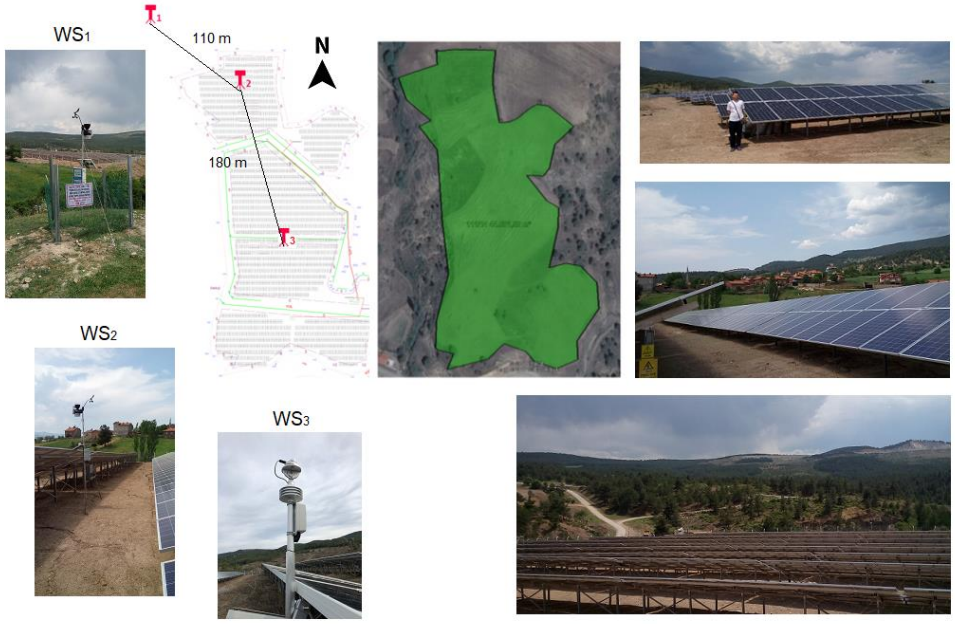


(a)


(b)

Figure 4.1. Site Plan (a) and Google Earth View (b) of the Sekbandemirli Rural Region and PVPP[1]

[1] Red drawings (a) and yellow-colored coordinates (b) show the WS locations

In addition to the distance between the locations of the three weather stations given in Figure 4.1.a, their elevations are 791 m for $WS_1$; 788 m for $WS_2$; and for $WS_3$, it is 778 m. The southern border of the PVPP field, seen in the Google Earth view in Figure 4.1.b, is at an elevation of 763-764 m, and the northern border, which is in line with the village area, is at an elevation of 792-793 m. In summary, a land structure rises with a slight slope up to a maximum difference of 30 m from the south to the north of the Sekbandemirli rural region, where the village and PVPP field are located. Considering the even smaller elevation differences between the locations of the weather stations, it is not necessary to include elevation within the PVHIE assessments of this thesis.

Considering both the short distances between the locations where they are installed (depending on the size of the land covered by the PVPP field) and the closeness of the elevations of the locations where they are located, it can be inferred that there will be no significant differences in the meteorological measurements collected by WSs. However, in an environment such as the Sekbandemirli rural region where natural or artificial external factors are relatively ineffective, it becomes easier to detect heat island formations that may arise from the PV module arrays in the PVPP field. Which meteorological variables are effective in these formations will be explained in the following titles of the thesis.

For PVHI observations, the question of the suitability of conducting field study and project by data collection and monitoring via three weather stations having low elevation differences and close distances between each other can be answered as follows: The first significant results in this direction were obtained through two statistical significance methods of the study. Thus, it has been concluded that two field projects of this thesis can be managed by using these WSs in the Sekbandemirli rural region.

The first of these statistical methods, which can be used to compare the data in large numbers with each other cumulatively, is “Analysis of Variance (ANOVA)”; the other is a Post Hoc Analysis method called “Tukey's Honest Significant Difference”.

## 4.1 Study's Statistical Methods

### 4.1.1 Analysis of Variance (ANOVA)

Analysis of Variance (ANOVA), one of the most widely used statistical techniques, shows whether there are statistically significant differences between the means of three or more independent groups. This technique was first developed by Ronald Fisher in the 20$^{th}$ century to be used in agricultural applications, and Fisher included this technique in his book, *Statistical Methods for Research Workers* [29], published in 1925.

The weather stations in this thesis represent the independent groups in the ANOVA method. Each weather station collects the unique weather data of the location where it is installed on the field (independently). The weather parameters measured by the weather stations as continuous data are independent variables in ANOVA. Whether there is statistical significance between the mean of independent groups can be analyzed separately or together for each independent variable. According to these analyses, ANOVA is divided into sub-methods in itself. The main sub-methods of ANOVA are introduced below:

- **One-Way ANOVA:** The analysis is made over an independent variable. For example, the comparison of air temperatures (as an independent variable) measured by the weather stations (independent groups) can be made by utilizing this sub-method.
- **Two-Way ANOVA:** The analysis is made over two independent variables. For example, the comparison of air temperature and relative humidity (as two independent variables) measured by the weather stations (independent groups) can be made by utilizing this sub-method.

There are also derivatives of ANOVA named ANCOVA for "covariates" and MANOVA for "dependent variables".

### 4.1.2 Post Hoc Analysis: Tukey's Honest Significant Difference (HSD)

ANOVA methods are used to determine whether there is a “statistical significance” between the independent groups whose mean values are compared. However, ANOVA does not provide information on whether the independent groups are statistically and significantly different (or not) from each other. To find these groups as pairs, applying a Post Hoc Test method such as Tukey's Honest Significant Difference (HSD) is required. After reaching the significant results in the ANOVA analysis, specific comparisons can be made between the means of groups using Tukey's HSD method. Thus, it can be found whether these means are statistically different from each other. In summary, Tukey's HSD offers the opportunity to make pairwise comparisons between the groups' means. This test was the method that enables the three weather stations (and the locations where they were installed) used within the scope of this thesis to be compared with each other.

In order to use Tukey's HSD method, the appropriate ANOVA method is selected and applied as a prerequisite. This is because the values, which should be used in Tukey's HSD test formula, are obtained from the tables prepared by ANOVA analysis. A One-Way ANOVA table structure is given in Table 4.1.

Table 4.1. Statistical values of One-Way ANOVA

| **Groups** | **Data Count** | **Data Sum** | **Average / Mean** | **Variance** |
|---|---|---|---|---|
| Group-1 | $n_1$ | $S_1$ | $Avg_1$ / $Mean_1$ | $V_1$ |
| Group-2 | $n_2$ | $S_2$ | $Avg_2$ / $Mean_2$ | $V_2$ |
| Group-3 | $n_3$ | $S_3$ | $Avg_3$ / $Mean_3$ | $V_3$ |

| **Source of Variation** | **Sum of Squares (SS)** | **Degrees of Freedom (df)** | **Mean Square (MS)** | **F statistic** | **$F_{critical}$ statistic** | **Level of Significance (p)** |
|---|---|---|---|---|---|---|
| **Between Groups** | $SS_{between}$ | $df_{between}$ | $MS_{between}$ | $F_{between}$ | $Fcri_{between}$ | $p_{between}$ |
| **Within Groups** | $SS_{within}$ | $df_{within}$ | $MS_{within}$ | $F_{within}$ | $Fcri_{within}$ | $p_{within}$ |
| **Total** | $SS_T$ | $df_T$ | $MS_T$ | $F_T$ | $Fcri_T$ | $p_T$ |

From a One-Way ANOVA results table in Table 4.1, if the preconditions in Equation 1 and 2 are met, the "HSD" statistic value calculated by Tukey's HSD test using the formula in Equation 3 can be found. Using the HSD statistical value, whether there is a statistical difference between the groups can be checked. (The value indicated by "α" in Equation 1 is the "significance level" and is generally considered as 0.05 in similar studies)

$$p_{between} < \alpha = 0.05 \quad \text{(Equation 1)}$$

$$F_{between} > Fcri_{between} \quad \text{(Equation 2)}$$

$$HSD = q\sqrt{\frac{MSwithin}{n}} \quad \text{(Equation 3)}$$

The values of "$MS_{within}$" in Equation 3 and "n" representing the Data Count of the group with the least data count can be taken from an ANOVA table like Table 4.1. Again, the Studentized Range statistic value "q" in Equation 3 can be taken from *Q Table for Tukey's HSD* [75], which is used as a reference in the literature for these calculations. The difference between the calculated HSD value and the average / mean values of the two selected groups in Table 4.1 is compared. If the absolute value of this difference is greater than the HSD value, it can be said that there is a "significant difference" between these two groups.

## 4.2 Weather Data and Statistical Significance Analysis (Part 1)

$WS_1$ and $WS_2$, whose locations are given in Figure 4.1, started to measure the weather parameters specified in Appendix B as averages in the time intervals specified in the same table, as of October 6, 2017, after they were installed on the field within the scope of this study's first project support. $WS_3$ has not yet been installed in the field by the power plant operator.

In October 2017, when the first thesis project was initiated, the mechanical assembly and electrical connection processes of the PV module arrays of Sekbandemirli PVPP had been currently under construction. As can be seen from the photographs in Figure 3.2, it can be expected that there is a significant albedo change between the naturally sandy soil surface of the region before the power plant construction and the artificial surface covered by PV module arrays after construction. Considering that the first project was launched in October 2017, before the Sekbandemirli PVPP was operational, it was possible to observe the weather conditions in the PVPP field and its close surroundings while the power plant was under construction.

Following the completion of the PV module deployment and construction processes, Sekbandemirli PVPP operationally began to generate electricity on February 5, 2018. Accordingly, the first four-month data were collected and monitored simultaneously outside the power plant via $WS_1$ (outside) until the PVPP became operational. The second four-month data was collected and monitored simultaneously from inside the power plant via $WS_2$.

The first analyses of the thesis study were made by considering the environmental conditions before and after the PVPP became operational. To make these analyses, the statistical methods described in the previous sub-section, One-Way ANOVA and Tukey's HSD test, were used. It was assessed whether there were statistical significances between the four main weather parameters measured by $WS_1$ and $WS_2$ depending on the albedo change in the power plant field depending on the PVPP construction processes. In other words, before proceeding directly to PVHIE analyses, it was aimed to determine which weather parameters are effective in possible PVHI formations.

Since at least three independent groups are required to use the statistical methods described in the previous section, another weather station was needed to enable $WS_1$ and $WS_2$ to be compared with each other. For this, the data of Tavşanlı WS ($WS_{Tav}$) belonging to TSMS, which takes measurements from a location that is closest to the Sekbandemirli rural region (bird flight 13 km away from the PVPP field), and has

the least elevation (around 50-60 meters higher than the elevation of the study's WSs) difference, and has similar specifications with the WSs of the thesis project, was included in the thesis study (Appendix C).

Three independent groups, i.e., weather stations, the study's statistical methods prerequisites, were compared according to four main weather parameters collected at 10-minute intervals for eight months. These parameters are ambient air temperature, relative humidity, barometric pressure, and wind speed. The eight-month data consists of the following two parts:

- Data collected by WSs before the PVPP became operational
  (4 months between October 6, 2017 - February 4, 2018)

- Data collected by WSs after the PVPP was operational
  (4 months between February 6, 2018 - June 5, 2018)

The field data collected from Sekbandemirli was analyzed separately in the two date ranges above, and a general analysis was made to include the entire date range.

The statistical significance comparison results were prepared after analyzing the 10-min averages of the four main weather parameters between $WS_1$, $WS_2$, and $WS_{Tav}$ by using the One-Way ANOVA and Tukey's HSD test methods (Table 4.1; Equation 1,2,3; Table 4.2). A comprehensive example of the calculations made in finding these results via *Microsoft Office Excel 2019 - Data Analysis ToolPak* will be presented in sub-section 4.4.

These initial analyses of the thesis work were presented orally at the *1st International Conference on Photovoltaic Science and Technologies (PVCon 2018)* and published as a full-paper proceeding within the IEEE-Xplore Digital Library [19].

Table 4.2. Statistical Significance Comparison Results of Weather Stations

| **Air Temperature** | 6 Oct - 4 Feb *(PVPP is under construction)* | 6 Feb - 5 Jun *(PVPP is operational)* | 6 Oct - 5 Jun |
|---|---|---|---|
| $WS_1$ - $WS_{Tav}$ | Significant | Significant | Significant |
| $WS_2$ - $WS_{Tav}$ | Significant | Significant | Significant |
| $WS_1$ - $WS_2$ | Not Significant | Not Significant | Not Significant |
| **Relative Humidity** | 6 Oct - 4 Feb *(PVPP is under construction)* | 6 Feb - 5 Jun *(PVPP is operational)* | 6 Oct - 5 Jun |
| $WS_1$ - $WS_{Tav}$ | Not Significant | Significant | Not Significant |
| $WS_2$ - $WS_{Tav}$ | Significant | Not Significant | Significant |
| $WS_1$ - $WS_2$ | Significant | Significant | Significant |
| **Barometric Pressure** | 6 Oct - 4 Feb *(PVPP is under construction)* | 6 Feb - 5 Jun *(PVPP is operational)* | 6 Oct - 5 Jun |
| $WS_1$ - $WS_{Tav}$ | Significant | Significant | Significant |
| $WS_2$ - $WS_{Tav}$ | Significant | Significant | Significant |
| $WS_1$ - $WS_2$ | Significant | Significant | Significant |
| **Wind Speed** | 6 Oct - 4 Feb *(PVPP is under construction)* | 6 Feb - 5 Jun *(PVPP is operational)* | 6 Oct - 5 Jun |
| $WS_1$ - $WS_{Tav}$ | Significant | Significant | Significant |
| $WS_2$ - $WS_{Tav}$ | Significant | Not Significant | Significant |
| $WS_1$ - $WS_2$ | Significant | Significant | Significant |

According to the results in Table 4.2, several comparisons were determined between the weather parameters' data collected by the weather stations, both with and without statistically significant differences. Based on these comparisons, the following conclusions can be remarked:

- The results denoted as "Significant" show that the two compared WSs collected significantly different measurements from each other for the respective weather parameter. This situation is vice versa for the comparisons denoted as "Not Significant".

- Considering the relatively close location of $WS_1$ and $WS_2$ at the meter level, the significant differences resulting from separately comparing them with $WS_{Tav}$ is a predictable conclusion before analysis. Because, even if the weather data measured by this station, which is 13 km away from Sekbandemirli, is not involved within the general weather forecasting, it can be statistically different from the data measured by the WSs in Sekbandemirli, considering the natural microclimatic and environmental conditions. Besides, the main aim of using the weather station in Tavşanlı is to compare $WS_1$ and $WS_2$.

- According to the explanation underlined in the previous paragraph, the following inference can be made: The comparisons of some weather parameters before and after the PVPP construction showed both "significant" and "not significant" results (e.g., $WS_1 - WS_{Tav}$ for relative humidity; $WS_2 - WS_{Tav}$ for wind speed). This result may not indicate that these weather parameters are directly affected by PV module deployment and may simply indicate some natural microclimatic changes between Tavşanlı and Sekbandemirli.

- Since these statistical comparisons are aimed to be made especially between $WS_1$ and $WS_2$, the result rows in which these two stations are compared can be examined in Table 4.2. Between $WS_1$ and $WS_2$, the “Significant” results were obtained for relative humidity, barometric pressure, and wind speed, both for the PVPP construction phase and for the period when the PVPP was operational. These results between these two stations, with a relatively short distance of 110 m, show that: The relative humidity, barometric pressure, and wind speed measurements of these two stations show significant differences even before the deployment processes of the PV modules and after they are operational. Thus, it can be said that the PVPP installation in the Sekbandemirli rural region does not affect these parameters.

- In the $WS_1$ and $WS_2$ air temperature measurements, the "Not Significant" results were obtained both for the PVPP construction phase and for the period when the PVPP was operational. In other words, opposite results were obtained in air temperature compared to relative humidity and the other two weather parameters. This finding shows that there are no significant differences between the ambient air temperature measurements of the $WS_1$ located near Sekbandemirli Village and outside the PVPP field, and the $WS_2$ located in the PVPP field and the MEYSA-3 sub-field. In summary, it can be concluded that the PV module arrays in the MEYSA-3 sub-field do not cause an alteration in the air temperature of the environment where they are installed. This inference also states that PVHIE cannot be detected at the canopy layer level in the MEYSA-3 sub-field of Sekbandemirli PVPP. However, it will be explained in sub-section 4.4 that this inference has changed with the installation of $WS_3$ in the field and that ambient air temperature is the most indicative parameter for possible PVHIE detection. In addition, "wind", which is a natural and essential source for HIE reduction, and is examined within the scope of UHI studies, will be included in the PVHIE analyses of the thesis with its "speed" and "direction" properties.

## 4.3 Error Analysis and Data Reliability

In the previous sub-section, it was stated that there were no significant differences between the measurements of $WS_1$ and $WS_2$ that could indicate possible PVHI formations. In addition, unlike the results of the other three main weather parameters, there was a particular finding that air temperature comparisons showed "not significant" results in both under-construction and operational periods of PVPP: If the air temperature measurements of $WS_1$ and $WS_2$ are statistically indistinguishably close to each other, air temperature is not affected by natural microclimatic conditions and changes compared to the results of the other three weather

parameters. Considering this finding, another WS installed at a point where the PV module arrays are denser in the PVPP field was used apart from $WS_2$. If "significant differences" are detected between this later installed WS and the air temperature measurements of the station $WS_1$ outside the power plant field, this result will show that PVHI formations from Sekbandemirli can be monitored.

The $WS_3$ was installed by the PVPP operator on November 5, 2018, at a location that could be considered as "the center of the power plant field" (between MERENSE-2 and PDA-2 sub-fields; Figure 3.3; Figure 4.1). This station can measure the incoming solar radiation (global horizontal irradiation) reaching its location, ambient air temperature, and, in addition to these weather parameters, the PV module temperature ($T_m$), which plays an important role in PVHI formations (Appendix B). Following the installation of $WS_3$ in the field, data collection in the form of "hourly averages" was made simultaneously from $WS_1$, $WS_2$, and $WS_3$ for two years (24 months) from November 2018 to October 2020.

This simultaneous data, which was collected for a much more extended period than the eight-month data used in the first analyses of the study mentioned in the previous sub-section, brought an additional question to the agenda of the study: Are the data that the three WSs recorded more than 27000 measurements in total reliable depending on

- the sensor accuracy of WSs' brand-model information given in Appendix B;

- the data losses that the WSs cannot send from the field from time to time due to technical problems and are considered as "null" in the analyses, depending on the losses?

The answer to this question is given with an error analysis and data reliability table based on all 2-year / 24-month data (November 2018 – October 2020) and prepared using the relevant formulas on *Microsoft Office Excel 2019* (Table 4.3).

Table 4.3. Error Analysis and Data Reliability Results

| | $WS_{T1}$ | $WS_{T2}$ | $WS_{T3}$ | $T_m$ | $WS_{WS1}$ | $WS_{WS2}$ | $WS_{WD1}$ | $WS_{WD2}$ |
|---|---|---|---|---|---|---|---|---|
| **Standart Deviation** | 8.4 | 8.5 | 9.5 | 14.1 | 1.1 | 1.1 | 98.2 | 90.8 |
| **Standart Error** | 0.1 | 0.1 | 0.1 | 0.1 | 0.0 | 0.0 | 0.6 | 0.6 |
| $T_{critical}$ | 2.0 | 2.0 | 2.0 | 2.0 | 2.0 | 2.0 | 2.0 | 2.0 |
| **Confidence Interval (95%)** | ±0.1°C | ±0.1°C | ±0.2°C | ±0.2°C | 0.0m/s | 0.0m/s | ±1.2° | ±1.1° |
| **WSs' Sensor Accuracy** | ±0.3°C | ±0.3°C | ±0.3°C | ±0.3°C | ±0.9m/s | ±0.9m/s | ±3.0° | ±3.0° |

The symbols indicated for air temperature, PV module temperature, and wind speed given in the column headings in Table 4.3 are the weather parameters measured by the WSs in Sekbandemirli (see the "LIST OF SYMBOLS" section). The reliability of the data collected by the WSs is checked by taking into account the 95% Confidence Intervals calculated from the standard deviation and standard error values of the error analysis [116]. If the Confidence Interval calculated for each parameter in Table 4.3 does not exceed the limit values of the WS's measurement sensor accuracies; in other words, **if Confidence Interval (95%) ≤ WSs' Sensor Accuracy** condition is met, it can be accepted that the collected data of the related parameter is reliable. This condition is ensured for all the parameters in Table 4.3.

## 4.4 Weather Data and Statistical Significance Analysis (Part 2)

Based on the fact that the most indicative parameter in the PVHIE analyses is air temperature specified in sub-section 4.2 and the data reliability results in the sub-section 4.3, the statistical significance comparison calculations in the sub-section 4.2 were made again. This time, the WS in Tavşanlı, used in the first comparisons, was replaced by $WS_3$, which was installed in the PVPP field center.

Air temperature data that $WS_3$ collected simultaneously with the other two stations ($WS_1$ and $WS_2$) for 24 months was compared via the One-Way ANOVA table (Table 4.4) prepared by using *Microsoft Office Excel 2019* - Data Analysis ToolPak, and Tukey's HSD test (Equation 4-9) applied based on the results on this table.

Table 4.4. One-Way ANOVA Results of $WS_1$, $WS_2$, $WS_3$

| **Groups** | **Data Count** | **Data Sum** | **Average / Mean** | **Variance** |
|---|---|---|---|---|
| $WS_1$ | 16524 | 221030.80 | 13.38 | 76.89 |
| $WS_2$ | 16899 | 223615.85 | 13.23 | 78.08 |
| $WS_3$ | 14210 | 201377.55 | 14.17 | 90.60 |

| **Source of Variation** | **Sum of Squares (SS)** | **Degrees of Freedom (df)** | **Mean Square (MS)** | **F statistic** | **$F_{critical}$ statistic** | **Level of Significance (p)** |
|---|---|---|---|---|---|---|
| **Between Groups** | 7683.87 | 2 | 3841.93 | 47.20 | 3.00 | 0.00 |
| **Within Groups** | 3877165.28 | 47630 | 81.40 | | | |
| **Total** | 3884849.14 | 47632 | | | | |

$$p_{between} = 0.00 < \alpha = 0.05 \text{ (Significance level)} \qquad \text{(Equation 4)}$$

$$F_{between} = 47.20 > Fcri_{between} = 3.00 \qquad \text{(Equation 5)}$$

Utilizing the One-Way ANOVA conditions in Equations 4 and 5, it has been verified that there is a statistical significance between the air temperature averages collected by the three stations. Following this, the Tukey's HSD test was performed to find out which WSs' measurements are significantly different from each other (Equation 6-9):

$$HSD = q\sqrt{\frac{MSwithin}{n}} = 3{,}31\sqrt{\frac{81{,}40}{14210}} = 0{,}25 \qquad \text{(Equation 6)}$$

$WS_{T2\_Avg}$ - $WS_{T1\_Avg}$ = 0,15 < 0,25 (Not significantly different) (Equation 7)

$WS_{T1\_Avg}$ - $WS_{T3\_Avg}$ = 0,79 > 0,25 (Significantly different) (Equation 8)

$WS_{T2\_Avg}$ - $WS_{T3\_Avg}$ = 0,94 > 0,25 (Significantly different) (Equation 9)

As can be seen from the equations above, the absolute value of the difference between the average/mean air temperature values of the WSs (Table 4.4) is compared with the calculated HSD value in Equation 6. The findings inferred after these comparisons are given below:

- There was no significant difference between the air temperature measurements of $WS_1$ and $WS_2$, as in the first part of the statistical significance analysis of the thesis (Sub-section 4.2).

- $WS_3$'s air temperature measurements differ significantly from $WS_1$ and $WS_2$. In other words, the air temperature averages measured in the center of the PVPP field show significant differences when compared with the means/averages measured both in the region with less PV module array density in the northern part of the PVPP field (MEYSA-3) and the area outside the PVPP field.

- Considering that there are no significant differences between the measurements of $WS_1$ and $WS_2$, and the short distances (Figure 4.1.a) between the three stations, it can be deduced that this situation is not caused by natural weather or environmental conditions. Therefore, the Sekbandemirli PVPP field center might be a possible PVHIE source.

# CHAPTER 5

## GRAPHICAL ANALYSIS AND REPRESENTATION

Within the scope of the analyses and comparisons in Chapter 4, the first significant findings were found regarding observing and monitoring PVHI formations at the Sekbandemirli PVPP field center, where most of the PVPP's module arrays operate. In this Chapter, the graphical representations and interpretations of the intensity of these formations, introduced with the ambient air temperature difference between $WS_{T3}$ and $WS_{T1}$, will be given.

As will be seen from the graphical analyses in the sub-sections of Chapter 5, PVHI formations can be observed as POSITIVE originating from the field center of Sekbandemirli PVPP, as well as NEGATIVE depending on the high cooling rate (duration) by longwave (IR) radiation from PV module arrays at night. The negative PVHI formations are detected when the ambient air temperature measured in the canopy layer of the PVPP field center ($WS_{T3}$) is lower than the temperature outside the field ($WS_{T1}$).

The air temperature differences ($\Delta T$), which indicate the intensity of both positive and negative PVHIE, were mostly detected in the range of "(-3) – 6°C" in line with the observations within the scope of this thesis. The graphs given under the title of this chapter have been prepared to demonstrate the monthly and seasonal distribution of heat island formations by calculating the temperature difference values in this range as a percentage. Considering the ambient air and PV module temperature as two crucial parameters within the PVHIE analysis, while preparing the graphs, the trend of change of their curves with respect to the PVHI formation distribution is also included in the graphical representation. Graphical representations are given in landscape view to allow readers to easily examine the visualization of 24-month data.

## 5.1 Monthly (Seasonal) Daytime Graphs and Temperature Curves

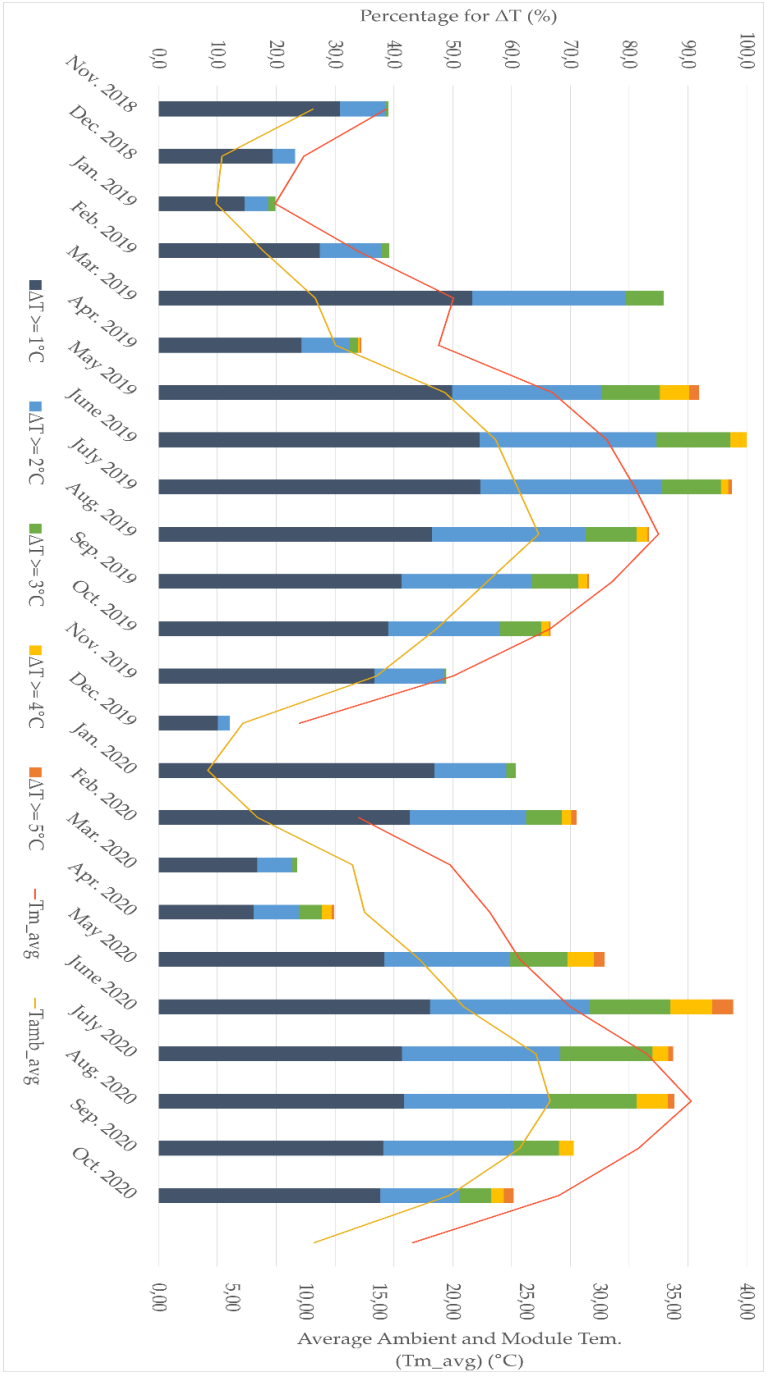


Figure 5.1. Monthly ΔT Percentages of Hourly Averages for Daytimes

*($T_m$ data couldn't be given for January 2020 due to a technical problem related to the $WS_3$'s sensor)*

On the graph in Figure 5.1, the following interpretations can be made regarding the positively detected and monitored daytime PVHIE at the Sekbandemirli PVPP field center:

- The air temperature data, which $WS_3$ recorded as 0-6°C higher than $WS_1$, is categorized as five temperature intervals for each month of the 2-year period (November 2018 – October 2020) that the simultaneous measurements had been made: $\Delta T > 1°C$ (0-1°C); $\Delta T > 2°C$ (1-2°C); $\Delta T > 3°C$ (3-4°C); $\Delta T > 4°C$ (4-5°C); $\Delta T > 5°C$ (5-6°C)

- As can be seen from the columns expressing the monthly percentage values, the number of positive PVHI formations detected at the PVPP center field increases during the daytime towards the summer months. Although less formation was detected in the winter months, there were also significant observations in specific months (e.g., February 2020). However, the overall view of the graph shows that more PVHIE observations are made in summer and less in winter.

- The formation intensities at the PVPP field center mostly vary between 0-3°C for 24 months. However, the formations that can be detected up to 6°C have been found, especially between May and October.

- Ambient air ($T_{amb}$) and PV module temperature ($T_m$) curves were added to the chart using the data collected by $WS_3$ as hourly averages.

- The $T_m$ and $T_{amb}$ curves follow a trend that is directly proportional to the height of the columns, indicating the number and intensity of PVHI formation over 24 months (during the day, PV module arrays heat up faster than the air in which they are surrounded depending on their thermal properties).

- The $T_m$ curve is trending above the $T_{amb}$ curve. When the difference between these two curves widens in the summer months, daily PVHIE becomes evident (stated in other words, PVHI formation intensity and frequency increase).

Another graphical representation supports the results and interpretations above in Figure 5.2, which shows the monthly daytime maximum air temperature changes measured by the three WSs. In this figure, the separate curves were prepared with the maximum values among the daytime ambient air temperatures recorded by the WSs in each of the 24 months. It was given in Chapter 4 that there are no significant differences between the measurements of $WS_1$ and $WS_2$; however, these differences are detected by $WS_3$ compared to the other two stations. During the 24 months, the distances between the curve trends in Figure 5.2 are consistent with these findings given in Chapter 4.


Figure 5.2. Monthly Daytime Maximum Air Temperature Changes of Hourly Averages

These findings of daytime PVHIE are the first supportive results that numerically and graphically enable to express the significantly different air temperature measurements (Chapter 4) collected by $WS_3$.

## 5.2 Monthly (Seasonal) Nighttime Graphs and Temperature Curves

In the previous sub-section, the air temperature differences between $WS_{T3}$ and $WS_{T1}$ for daytime were indicated using the expression “positive” for PVHIE observations in Sekbandemirli. The negative air temperature differences between these two stations indicate “negative PVHIE”; i.e., the ambient temperature at the PVPP field center is lower than outside the field. This situation shows when no HIE is caused by Sekbandemirli PVPP field center is observed.

Air temperature rise, which was detected to be prominent in the canopy layer atmosphere of a city / metropolitan area center, especially at night in UHI research and studies, emerges as an opposite phenomenon in the Sekbandemirli study. Plus, the intensity of this heat island effect was also recorded as smaller temperature differences compared to the effect in cities.

Figure 5.3 shows the negative air temperature differences between $WS_{T3}$ and $WS_{T1}$ monthly and in percentage, along with $T_m$ and $T_{amb\_avg}$ curve trends.

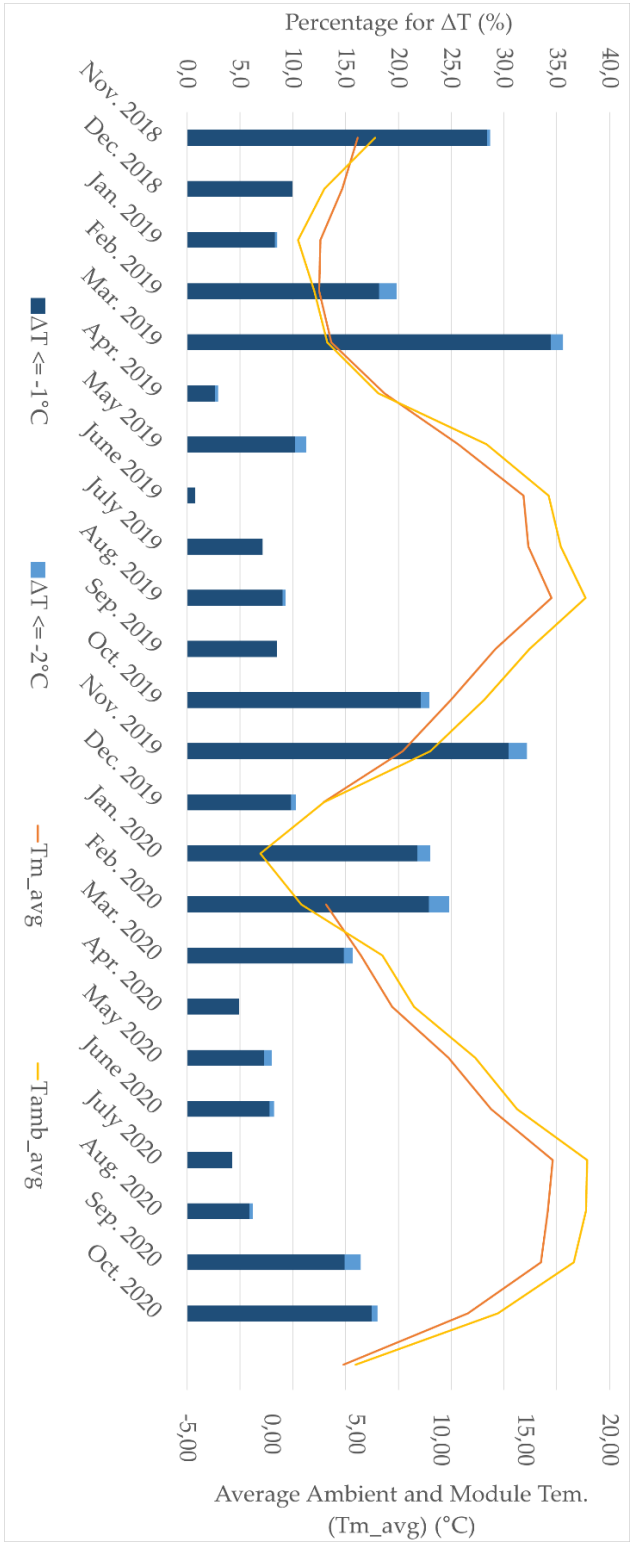


Figure 5.3. Monthly ΔT Percentages of Hourly Averages for Nighttimes

*($T_m$ data couldn't be given for January 2020 due to a technical problem related to the $WS_3$'s sensor)*

In Figure 5.3, the following interpretations can be made regarding the nighttime PVHIE, which is negatively detected and monitored at the PVPP field center:

- The air temperature data, which $WS_3$ recorded as -1-(-3)°C lower than $WS_1$, is categorized as two temperature intervals for each month of the two years (November 2018 – October 2020) that the simultaneous measurements had been made: $\Delta T < -1°C$ (-1-(-2)°C); $\Delta T < -2°C$ (-2-(-3)°C)

- As can be seen from the columns expressing the monthly percentage values, the number of negative PVHI formations increases towards the autumn and winter months. Although fewer formations were detected in the spring and summer months, the highest observations were made in March 2019. However, the overall view of the graph shows more PVHIE observations detected in autumn and winter; less detected in spring and summer. The formation intensities outside the PVPP field always ranged from 0-3°C for 24 months.

- Ambient air ($T_{amb}$) and PV module temperature ($T_m$) curves were added to the chart using the data collected by $WS_3$ as hourly averages.

- The $T_m$ and $T_{amb}$ curves follow a trend that is inversely proportional to the height of the columns, indicating the number and intensity of PVHI formation over 24 months (at night, PV module arrays cool faster than the air in which they are surrounded depending on their thermal properties).

- Depending on the fast cooling of the PV modules in spring and summer nights, the $T_{amb}$ curve is trending above the $T_m$ curve, and especially in summer months, the difference between them is widening. Considering the nights when the air in the region cools faster than the PV module arrays in the winter months, the $T_m$ curve follows a trend above the $T_{amb}$ curve.

- Unlike Figure 5.1, there is no relationship between the curve trends in Figure 5.3 and the PVHI formation intensity. Since the concept of negative PVHIE means that no heat island effect caused by Sekbandemirli PVPP is detected, it is expected that such a direct or inverse relationship has not been found.

Another graphical representation supporting the results and interpretations above in Figure 5.4 shows the monthly nighttime minimum air temperature changes measured by the three WSs. In this figure, the separate curves with minimum values were prepared among the nighttime ambient air temperatures measured by the WSs in each of the 24 months. As in Figure 5.3, there are no significant differences between the measurement trends of $WS_1$ and $WS_2$. The $WS_3$, on the other hand, recorded mostly lower minimum air temperatures over 24 months compared to the other two stations (except in March 2020). Only in the summer months, when negative PVHI formation observations are few (Figure 5.3), the measurement curves of the three stations are quite close to each other.

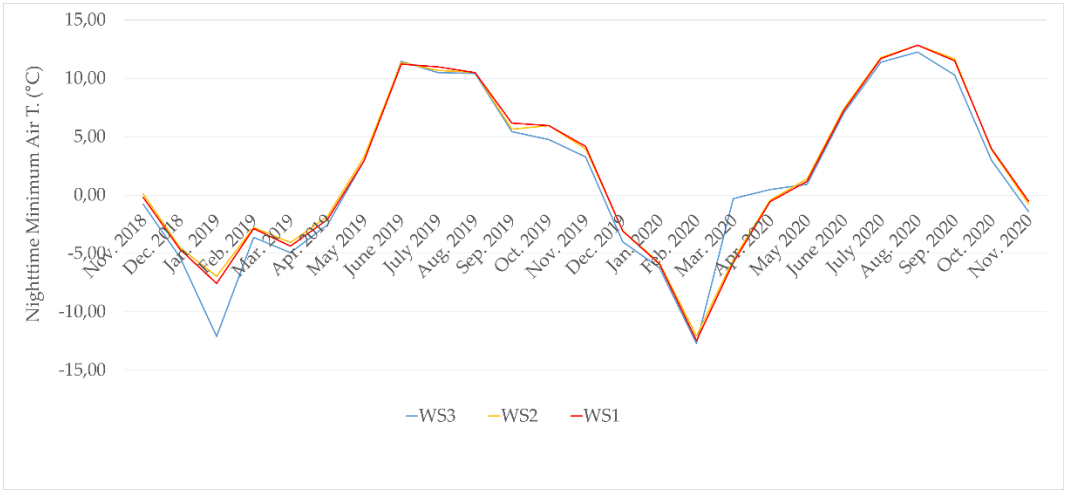


Figure 5.4. Monthly Nighttime Minimum Air Temperature Changes of Hourly Averages

## 5.3 Diurnal Temperature Variation and Representative Illustrations

Some specific graphical representations are given in this section for two selected among the daytime positive and nighttime negative PVHIE observations monitored during the 24-month field study. As shown in Figure 5.5.a and Figure 5.5.b, they are diurnal ambient air temperature variation graphs on two dates in which positive and negative PVHI formations were detected together.

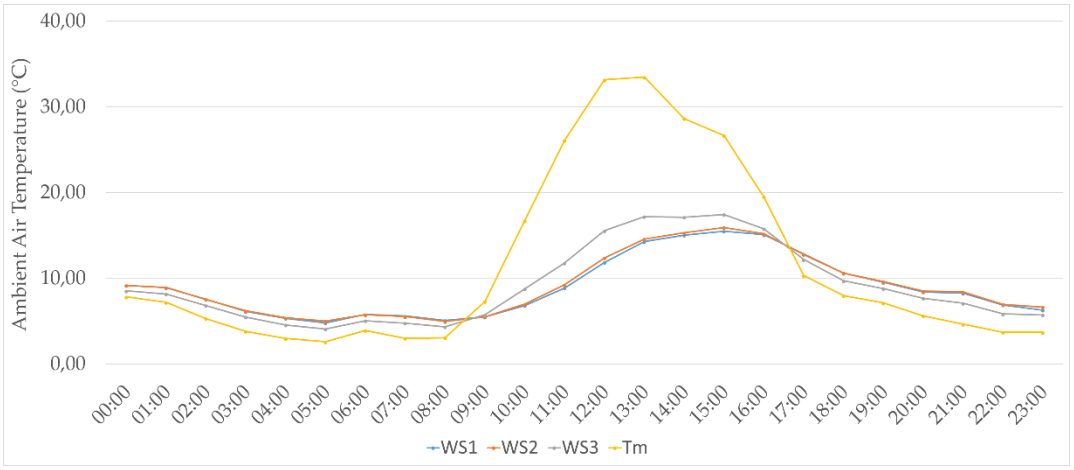


(a)

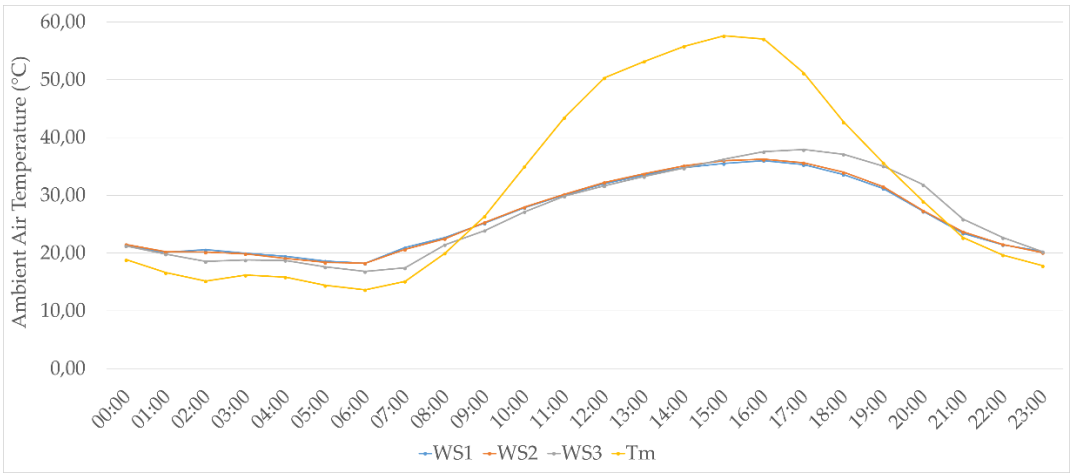


(b)

Figure 5.5. Diurnal Ambient Air Temperature Variation on 24.11.2019 (a) and 13.08.2019 (b)

Figures 5.5.a and 5.5.b show how the temperature records of each of the three WSs vary on a day in November 2019 and August 2019, respectively. In addition, the temperature variation curves of WS in those days can be compared with each other.

The graphical results in Figure 5.5 can be interpreted as below:

- • Depending on the low values recorded in the PV module temperature before sunrise and after sunset, the temperature curve of $WS_3$ is trending below that of $WS_1$ and $WS_2$ with minor differences. Thus, negative PVHI formations are detected.

- Due to the high values recorded with the increasing PV module temperature during the day, the temperature curve of $WS_3$ is trending above $WS_1$ and $WS_2$ (As in Figure 5.5.b, this trend may be prolonged due to the late sunset and later cooling of the PV modules in summer months). On this trend, major ambient air temperature differences between $WS_{T3}$ and $WS_{T1}$ are recorded, and positive PVHI formations are detected.

In Figure 5.5.a, at an hour when the PV module temperature reaches the maximum value of the day (at noon), the ambient air temperature difference between $WS_{T3}$ and $WS_{T1}$ is close to 4°C. According to this difference, a positive PVHIE formation is illustrated in Figure 5.6.a.

In Figure 5.5.b, at one of the night hours (02:00), when the PV module temperature is lower than the ambient air temperature records of the WSs, the ambient air temperature difference between $WS_{T1}$ and $WS_{T3}$ is about 2°C. According to this difference, a negative PVHIE formation is illustrated in Figure 5.6.b. The negative PVHI formation in Figure 5.6.b is at half the intensity of the positive PVHIE in Figure 5.6.a.

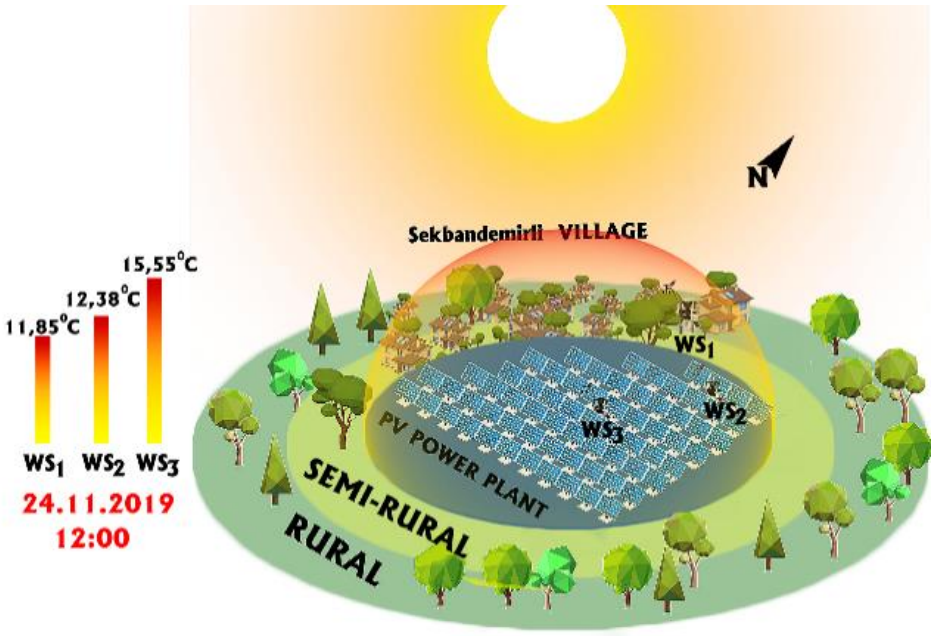


(a)

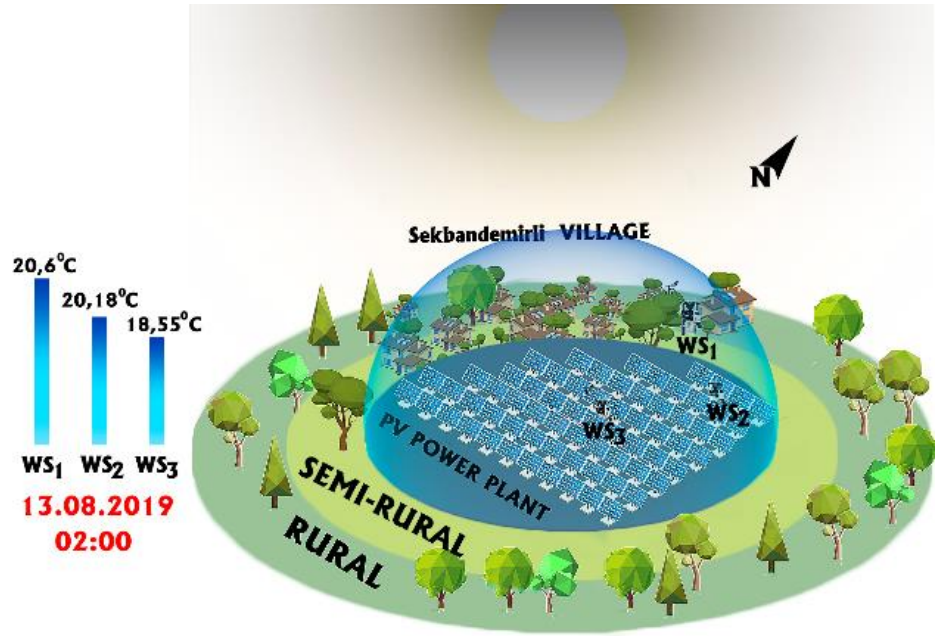


(b)

Figure 5.6. Illustrations of Positive PVHIE (a) and Negative PVHIE (b) in Sekbandemirli Rural Region

## 5.4 Local Winds and PVHI Formations

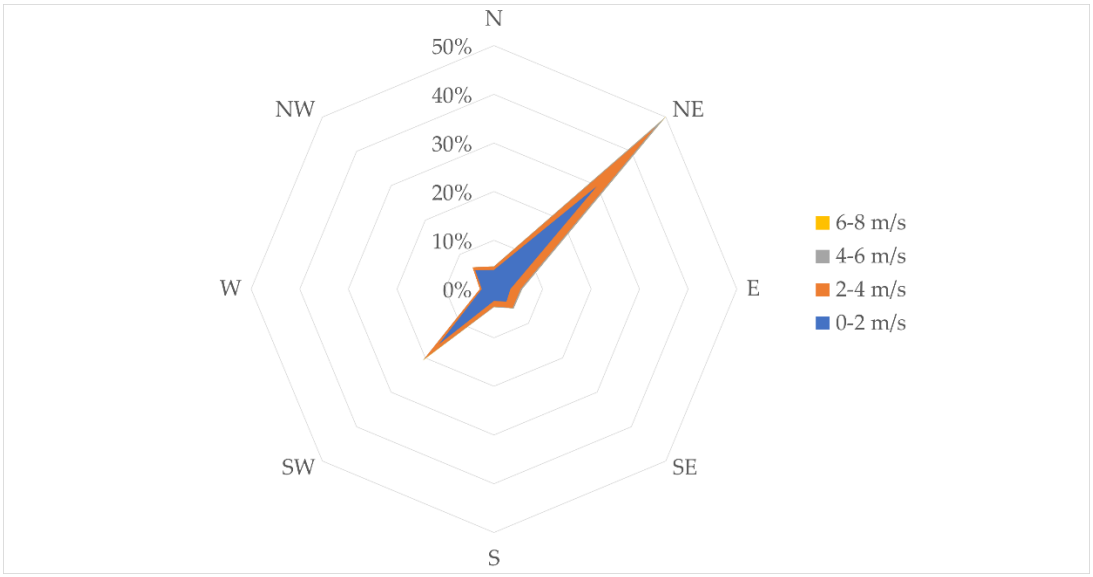


(a)

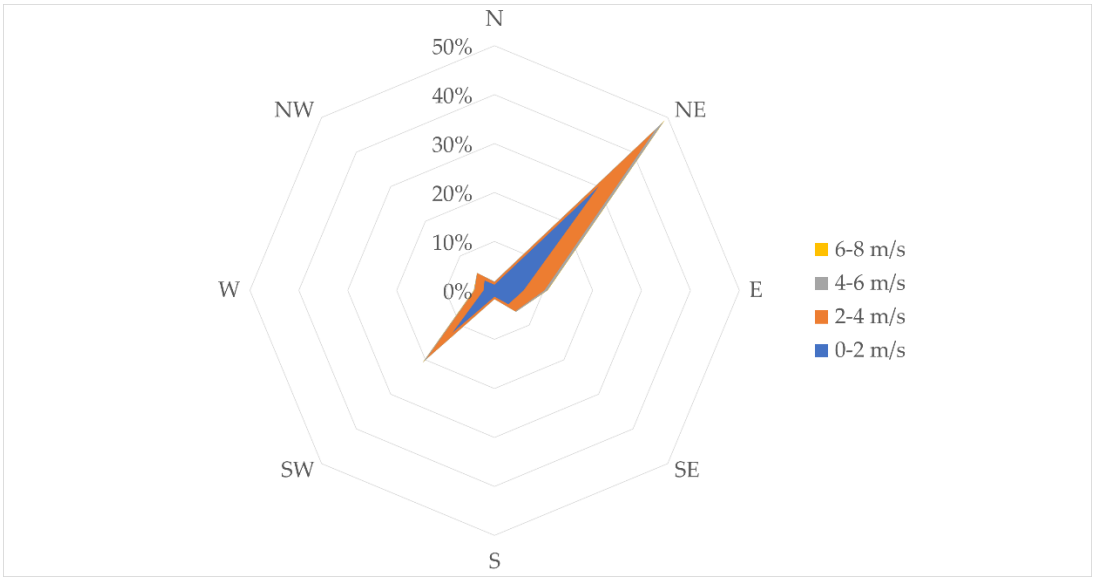


(b)

Figure 5.7. Wind Rose (Profile) of Sekbandemirli based on $WS_1$ (a) and $WS_2$ (b) Data Records

The wind measurement sensors of $WS_1$ and $WS_2$ were utilized to visualize the local wind profile inside and outside the Sekbandemirli PVPP field. The wind speed and direction data that these two WSs recorded simultaneously for three years, from October 2017 (when the thesis projects were started) to October 2020, were used. The "wind roses" prepared for both outside ($WS_1$) and inside ($WS_2$) PVPP field through the data analysis tools of *Microsoft Office Excel 2019* are given in Figure 5.7 (since $WS_3$ in Sekbandemirli PVPP field center does not have wind sensors, the wind conditions of the PVPP field were monitored via $WS_2$).

As can be seen from the wind rose graphs in Figures 5.7.a and 5.7.b, the wind profiles inside and outside the PVPP field are quite similar to each other. In both locations, the local winds mostly blow from North-East at speeds between 0-4 m/s (at "breeze" level). Again, at these speeds, but at a rate of 40% of the winds blowing from the North-West, the local winds blowing from the South-West are also observed. The recorded wind speeds higher than 4 m/s both inside and outside the PVPP field are quite low.

The prevailing wind direction of the Kütahya province is North. In addition to this information, considering the close distance between $WS_1$ and $WS_2$ in the Sekbandemirli rural region (Figure 4.1), the following inference can be made: The local winds enter Sekbandemirli rural region and PVPP field from North-East. Whether the winds entering from this direction and at breeze-level speeds might reduce PVPP-induced HIE has been examined on the graph in Figure 5.8.

The graph in Figure 5.8 has been prepared for the data collection and monitoring between November 2018 - October 2020 (considering the date of installation of WS3 at the PVPP field center). In the graph, the positive and negative PVHIE formation intensities ($\Delta T = WS_{T3} - WS_{T1}$) observed at the PVPP field center at that time are given, corresponding to the direction (0-360°) where the local winds enter the PVPP field and recorded by $WS_2$.

As seen in Figure 5.8, many positive PVHI formations were detected at various intensities while the local winds were entering and blowing the PVPP field from the 0-90° and 180-270° directions. Again, between these angles, but fewer negative PVHI formations were detected. Based on this chart:

- Considering that the local prevailing wind direction in Figure 5.7 is North-East (45°), and this value remains in the range of 0-90° where many PVHIE observations are made according to Figure 5.8;

- Considering that the local winds, according to the prevailing direction (45°), mostly interact with the rear parts of the south-facing (180°) PV modules in the PVPP field, not their heat-releasing surfaces,

it can be said that the natural cooling property of local winds is not effective in reducing PVHIE caused by Sekbandemirli PVPP. Moreover, another analysis made by utilizing the local wind speeds and using the correlation method will be presented in the next Chapter.

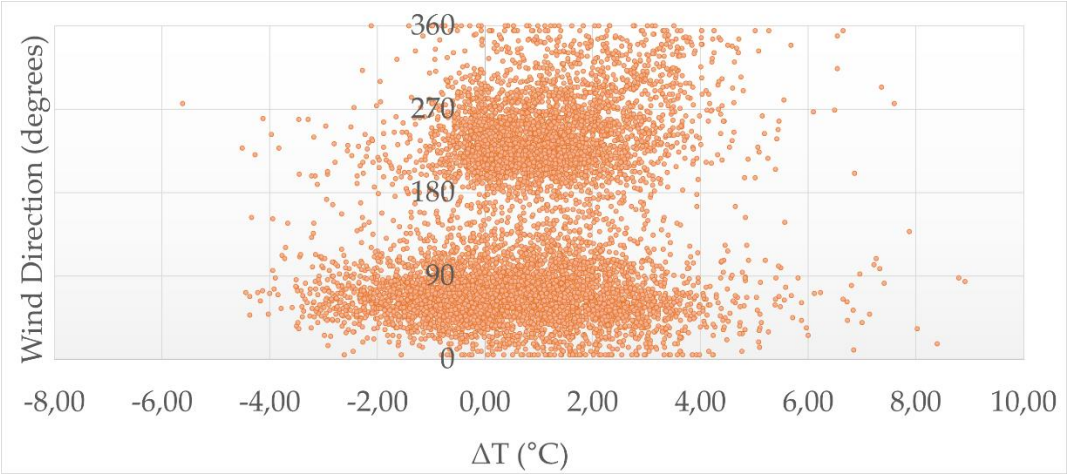


Figure 5.8. $WS_2$'s Wind Direction Data versus PVHI Formations (ΔT)

# CHAPTER 6

# CORRELATION RESULTS

The analyzes and results in Chapters 4 and 5 have shown both numerically and graphically that daily and seasonal PVHIE observations are monitored at the Sekbandemirli PVPP field center. These two chapters constitute the first part of the whole analysis techniques and results used in this thesis. The second part is introduced with the correlation results given in this chapter.

If the correlation is defined, it enables to examine in which direction and strength (degree) there is a linear statistical relationship between the two determined variables. Regarding being statistical, the question may be asked whether it is similar to the methods in Chapter 4. In a way, correlation analyses show the measurement of the dependence between these two variables and how this dependence changes over time.

One of the two variables used in the correlation analysis is $\Delta T$ ($WS_{T3} - WS_{T1}$), representing the PVHI formations in Sekbandemirli. The parameters, which are primarily examined in the formation of PVHIE, and which are correlated with $\Delta T$ separately are given below:

- PV module temperature ($T_m$)
- PVPP electrical power output (P)
- Wind speed measured by the weather stations $WS_1$ and $WS_2$ ($WS_{WS1}$ and $WS_{WS2}$) (local winds, which were found to be ineffective in terms of "direction" in reducing PVHI formations in sub-section 5.4, were included in the correlation analyzes regarding their speed)

Two methods were used to assess the correlations between $\Delta T$ and the parameters above: Pearson Correlation and Spearman Correlation.

## 6.1 Study's Correlation Methods

### 6.1.1 Pearson Correlation

The linear relationship between two variables is measured with the coefficients used in the Pearson correlation method. In other words, the degree of the linear relationship strength between these two variables can be found by this method. The Pearson correlation coefficient takes a value between (-1)-0 or 0-1, and thus, the direction of the linear relationship is specified. This direction and strength are expressed in two ways:

- The closer this coefficient is to 1, the stronger the positive linear relationship between the two variables; the closer it is to (-1), the stronger the negative linear relationship between them.

- The closer this coefficient is to 0, the weaker the positive or negative linear relationship between two variables, according to the direction of the linear relationship (+/-).

A simple example of this type of correlation can be given as follows: As the number of ground-mounted PV modules to be used in a PVPP project increases, so does the number of solar inverters used to transmit DC electricity from these PV modules to the grid as AC. The linear relationship here is determined via the Pearson method.

### 6.1.2 Spearman Correlation

Spearman correlation is based on the rank order method, and the coefficients used in this correlation are called Spearman's rank correlation coefficient. Spearman correlation specifies how the relationship between two variables can be assessed as

monotonic. The monotonic relationship shows that with the increase in the value of one variable, the value of the other variable also increases or decreases. As with Pearson Correlation, Spearman's rank correlation coefficient takes a value between (-1)-0 or 0-1.

The difference between Pearson and Spearman correlation methods is as follows: The increase/decrease rate, which is the measurement of the linear relationship between two variables in the Pearson method, is constant. In Spearman correlation, however, the direct or inverse monotonic relationship between two variables may not be at a constant rate.

The following two examples can be given to the monotonic relationship in the Spearman correlation method:

- **Directly Proportional Monotonic Relationship:** The relationship between the number of ground-mounted PV modules used in a PVPP project and the total number or amount of cleaning materials used in the surface cleaning processes of these PV modules

- **Inversely Proportional Monotonic Relationship:** The relationship between the size of a PVPP project and the electricity bill costs of consumers benefiting from the electrical power output obtained from this PVPP (considering the contribution of electricity supplied from PVPP for reducing costs in bills)

The correlation tables given in the following subtitles of this chapter have been prepared using both Pearson and Spearman correlation coefficients to provide comparative results. These coefficients were calculated separately for each of the 24 months (November 2018 – October 2020) between the variable pairs compared with each other by their monthly data. Both Pearson and Spearman correlation coefficients were calculated using the corresponding functions in *Microsoft Office Excel 2019*.

## 6.2 Daily and Monthly Correlation Tables

### 6.2.1 PV Module Temperature and PVHIE

The daytime and nighttime monthly correlation coefficients between PV module temperature ($T_m$) and PVHI formation ($\Delta T$) are given in Table 6.1.

Table 6.1. Monthly Correlation Coefficients between $T_m$ and $\Delta T$

| | Pearson | | Spearman | |
|---|---|---|---|---|
| | **Daytime** | **Nighttime** | **Daytime** | **Nighttime** |
| **November 2018** | 0.82 | 0.11 | 0.78 | 0.10 |
| **December 2018** | 0.79 | -0.04 | 0.73 | -0.05 |
| **January 2019** | 0.67 | 0.21 | 0.49 | 0.13 |
| **February 2019** | 0.67 | -0.17 | 0.69 | -0.24 |
| **March 2019** | 0.72 | 0.03 | 0.74 | 0.07 |
| **April 2019** | 0.48 | 0.37 | 0.60 | 0.13 |
| **May 2019** | 0.52 | 0.44 | 0.61 | 0.36 |
| **June 2019** | 0.61 | 0.54 | 0.65 | 0.41 |
| **July 2019** | 0.55 | 0.71 | 0.54 | 0.60 |
| **August 2019** | 0.55 | 0.65 | 0.51 | 0.58 |
| **September 2019** | 0.58 | 0.68 | 0.57 | 0.62 |
| **October 2019** | 0.57 | 0.63 | 0.58 | 0.61 |
| **November 2019** | 0.81 | -0.11 | 0.82 | -0.06 |
| **December 2019** | 0.64 | -0.04 | 0.70 | 0.07 |
| **January 2020** | - | - | - | - |
| **February 2020** | 0.56 | 0.21 | 0.52 | 0.14 |
| **March 2020** | 0.75 | -0.28 | 0.76 | -0.29 |
| **April 2020** | 0.58 | 0.59 | 0.66 | 0.52 |
| **May 2020** | 0.49 | 0.40 | 0.59 | 0.25 |
| **June 2020** | 0.55 | 0.69 | 0.64 | 0.56 |
| **July 2020** | 0.51 | 0.70 | 0.52 | 0.63 |
| **August 2020** | 0.51 | 0.83 | 0.48 | 0.73 |
| **September 2020** | 0.54 | 0.71 | 0.54 | 0.62 |
| **October 2020** | 0.53 | 0.57 | 0.58 | 0.41 |

### 6.2.2 PVPP Electrical Power Output and PVHIE

The daytime monthly correlation coefficients between PVPP electrical power output (P) and PVHI formation (ΔT) are given in Table 6.2. The table does not include a "nighttime" column as there is no production at night.

Table 6.2. Monthly Correlation Coefficients between P and ΔT

| | Pearson | Spearman |
|---|---|---|
| | Daytime | Daytime |
| **November 2018** | 0.88 | 0.91 |
| **December 2018** | 0.86 | 0.86 |
| **January 2019** | 0.62 | 0.65 |
| **February 2019** | 0.70 | 0.76 |
| **March 2019** | 0.69 | 0.72 |
| **April 2019** | 0.31 | 0.46 |
| **May 2019** | 0.34 | 0.44 |
| **June 2019** | 0.40 | 0.49 |
| **July 2019** | 0.35 | 0.38 |
| **August 2019** | 0.32 | 0.31 |
| **September 2019** | 0.31 | 0.34 |
| **October 2019** | 0.33 | 0.38 |
| **November 2019** | 0.88 | 0.91 |
| **December 2019** | 0.67 | 0.81 |
| **January 2020** | - | - |
| **February 2020** | 0.50 | 0.50 |
| **March 2020** | 0.79 | 0.85 |
| **April 2020** | 0.38 | 0.47 |
| **May 2020** | 0.31 | 0.47 |
| **June 2020** | 0.33 | 0.47 |
| **July 2020** | 0.25 | 0.27 |
| **August 2020** | 0.24 | 0.24 |
| **September 2020** | 0.32 | 0.37 |
| **October 2020** | 0.32 | 0.47 |

### 6.2.3 Local Wind Speed and PVHIE

In sub-section 5.4, it was explained that the local winds blowing mostly from North-East in Sekbandemirli are not effective in PVHIE reduction. Under the title of this section, the correlation results between local wind speed ($WS_{WS1}$, $WS_{WS2}$) recorded by $WS_1$ and $WS_2$ and PVHI formation ($\Delta T$) are given in Tables 6.3 and 6.4.

Table 6.3. Monthly Correlation Coefficients between $WS_{WS1}$ and $\Delta T$

| | Pearson | | Spearman | |
|---|---|---|---|---|
| | **Daytime** | **Nighttime** | **Daytime** | **Nighttime** |
| **November 2018** | 0.15 | 0.24 | 0.21 | 0.24 |
| **December 2018** | 0.12 | -0.09 | 0.12 | -0.12 |
| **January 2019** | 0.10 | -0.07 | 0.16 | -0.17 |
| **February 2019** | 0.08 | -0.17 | 0.14 | -0.33 |
| **March 2019** | 0.02 | 0.25 | 0.01 | 0.24 |
| **April 2019** | 0.27 | -0.04 | 0.31 | -0.07 |
| **May 2019** | 0.14 | -0.20 | 0.16 | -0.22 |
| **June 2019** | 0.36 | -0.02 | 0.39 | -0.03 |
| **July 2019** | 0.27 | -0.20 | 0.25 | -0.23 |
| **August 2019** | 0.24 | 0.02 | 0.22 | -0.06 |
| **September 2019** | 0.05 | -0.14 | -0.03 | -0.21 |
| **October 2019** | -0.14 | -0.16 | -0.13 | -0.22 |
| **November 2019** | 0.10 | 0.13 | 0.13 | 0.11 |
| **December 2019** | -0.12 | 0.02 | -0.16 | -0.08 |
| **January 2020** | - | - | - | - |
| **February 2020** | 0.00 | 0.05 | 0.09 | -0.07 |
| **March 2020** | -0.03 | -0.01 | -0.01 | -0.04 |
| **April 2020** | 0.02 | -0.17 | 0.04 | -0.25 |
| **May 2020** | 0.18 | -0.17 | 0.20 | -0.10 |
| **June 2020** | 0.39 | -0.11 | 0.43 | -0.14 |
| **July 2020** | 0.30 | -0.28 | 0.25 | -0.25 |
| **August 2020** | 0.31 | -0.20 | 0.27 | -0.20 |
| **September 2020** | 0.18 | -0.16 | 0.16 | -0.20 |
| **October 2020** | -0.20 | -0.18 | -0.16 | -0.25 |

Table 6.4. Monthly Correlation Coefficients between $WS_{WS2}$ and $\Delta T$

| | Pearson | | Spearman | |
|---|---|---|---|---|
| | **Daytime** | **Nighttime** | **Daytime** | **Nighttime** |
| **November 2018** | 0.03 | 0.28 | 0.09 | 0.26 |
| **December 2018** | 0.06 | -0.06 | 0.07 | -0.10 |
| **January 2019** | 0.12 | -0.06 | 0.17 | -0.14 |
| **February 2019** | -0.06 | -0.19 | 0.00 | -0.38 |
| **March 2019** | -0.04 | 0.26 | -0.06 | 0.23 |
| **April 2019** | 0.29 | -0.12 | 0.35 | -0.18 |
| **May 2019** | 0.12 | -0.10 | 0.15 | -0.11 |
| **June 2019** | 0.37 | 0.04 | 0.41 | 0.04 |
| **July 2019** | 0.34 | -0.18 | 0.34 | -0.18 |
| **August 2019** | 0.27 | 0.04 | 0.27 | -0.06 |
| **September 2019** | 0.12 | -0.16 | 0.09 | -0.23 |
| **October 2019** | -0.18 | -0.24 | -0.16 | -0.28 |
| **November 2019** | 0.02 | 0.14 | 0.03 | 0.12 |
| **December 2019** | -0.18 | 0.03 | -0.21 | -0.05 |
| **January 2020** | - | - | - | - |
| **February 2020** | -0.09 | 0.13 | -0.01 | 0.00 |
| **March 2020** | -0.10 | 0.04 | -0.08 | 0.01 |
| **April 2020** | 0.03 | -0.21 | 0.05 | -0.28 |
| **May 2020** | 0.00 | -0.20 | 0.02 | -0.24 |
| **June 2020** | 0.21 | -0.11 | 0.25 | -0.15 |
| **July 2020** | 0.22 | -0.30 | 0.18 | -0.33 |
| **August 2020** | 0.25 | -0.26 | 0.24 | -0.32 |
| **September 2020** | 0.25 | -0.14 | 0.27 | -0.24 |
| **October 2020** | -0.09 | -0.15 | -0.07 | -0.21 |

## 6.3 Daily and Seasonal Assessment of Correlation Tables

The correlation tables given in the subtitles of sub-section 6.2 enable the thesis project researchers to assess the three main variables taken into account in determining the PVHIE intensity, both daily and seasonally. Summary conclusions deduced from the correlational comparisons between these variables and PVHI formations separately are given below. In all tables, only the January 2020 data were not included in the calculated correlation coefficients because the Tm data recorded in January 2020 is not useable due to a technical problem with the $WS_3$ sensor.

When the monthly correlation change between $T_m$ and $\Delta T$ is examined in Table 6.1, the following interpretations can be made:

- Both the Pearson and Spearman correlation coefficients show similar results in the monthly correlation change.

- It has been determined that there are higher correlations between daytime positive PVHI formations and $T_m$, especially between November and March, in the winter months when the air temperatures drop in the Sekbandemirli rural region and when there are Autumn-Winter-Spring transitions. This correlation decreases towards summer months and Spring-Summer-Autumn transitions. This inference can also be understood from the arrows on the table showing the correlation strength change according to months (from orange (highly correlated) to blue (low correlation)).

- In Figure 5.1, it was stated that with $T_m$ rising in the summer months, PVHI formation intensity also increases. However, the correlation results in Table 6.1 show the sensitivity of the change in PVHI formation intensity relative to the sensitivity of the change in $T_m$. In other words, more intense and frequent PVHI formations are detected due to higher $T_m$ in the summer months (Figure 5.1), but in winter, the intensity change of these formations is more sensitive to the change of $T_m$.

- The reverse of the monthly correlation change between daytime positive PVHI formations and $T_m$ can be said for nighttime negative formations. It has been determined that there are lower correlations between nighttime negative PVHIE and $T_m$ during the winter months and at the times of Autumn-Winter-Spring transitions. This correlation increases towards summer months and Spring-Summer-Autumn transitions. This inference can also be understood from the arrows on the table showing the correlation strength change according to months (from orange (highly correlated) to blue (low correlation)).

- Figure 5.3 was given to show the negative PVHIE in Sekbandemirli. This figure, in other words, indicates that the PVPP field center in Sekbandemirli is cooler than outside the power plant field, and thus, there is no PVHIE formed at the PVPP field center. Again, in this figure, no direct correlation was found between $T_m$ and negative PVHIE. Besides, according to Table 6.1, it can be noted that the intensity change of negative PVHI formations is more sensitive to the change of $T_m$ in the summer months.

When the monthly correlation change between P and $\Delta T$ is examined in Table 6.2, the following interpretations can be made:

- Since there is no electricity generation via PVPP at night, the table contains daytime data.

- Both the Pearson and Spearman correlation coefficients show similar results in the monthly correlation change.

- Monthly correlation change is similar to daytime $T_m$ and $\Delta T$ in Table 6.1: It has been determined that there are higher correlations between daytime positive PVHI formations and P between November and March, during the

winter months and at the times of Autumn-Winter-Spring transitions. This correlation decreases towards summer months and Spring-Summer-Autumn transitions. This inference can also be understood from the arrows on the table showing the correlation strength change according to months (from orange (highly correlated) to blue (low correlation)).

- In general, the average increase in P towards summer months indicates less heat release and more production in PVPP, and accordingly, less HIE from PVPP is observed. The lower correlation coefficients between P and ΔT in the summer months also support this inference.

In Table 6.3 and Table 6.4, the following interpretations can be made when examining the monthly correlation change between local wind speed values ($WS_{WS1}$, $WS_{WS2}$) and ΔT:

- Both the Pearson and Spearman correlation coefficients show similar results in the monthly correlation change.

- For almost all 24 months in both tables, mostly low correlation coefficients were calculated between local wind speed and ΔT (some of these coefficients show negative correlations). Besides, positive correlations during the daytime and negative correlations at nighttime become somewhat evident in the summer months. In conclusion, no significant correlation change trend was found between daytime positive and nighttime negative PHVI formations and $WS_{WS1}$ and $WS_{WS2}$.

- Considering that the local winds in Sekbandemirli are blowing at speeds not exceeding 4 m/s (at breeze level) in all four seasons, it can be concluded that it is not effective in PVHIE reduction, as in the prevailing direction assessment (sub-section 5.4).

# CHAPTER 7

## SIMULATION OF SEKBANDEMİRLİ WEATHER AND PVHIE

This chapter has particular importance within the scope of the thesis, in terms of both being complementary to all the analysis techniques and results of the thesis study and including the simulation outputs obtained by using microclimate software (ENVI-met) for the first time in a PVPP study, which will be explained in the following sub-headings. The regional and atmospheric simulation results in this chapter can be compared with the results of PVHIE in accordance with the methods used in the previous three chapters (and the compatibility between them can be examined). The content of this chapter consists of the sub-sections specified in the paragraphs below.

Chapter 7 begins with the introduction of ENVI-met, a microclimate simulation software, and an expression of the infrastructure of this software, on which models it is built (model structure and physics). Then, the interface tools and functions of the ENVI-met software will be introduced (ENVI-guide, Projects / Workspaces, Database Manager, ENVI-core, Leonardo, and other tools). Following this part, it will be explained how the Sekbandemirli rural region (covering the PVPP field) and its weather conditions are simulated via these interface tools (ENVI-met version 4.4.5 is used).

Finally, as a complementary part of Chapter 7, the simulation-based results will be given where the Sekbandemirli's weather conditions on specific dates are simulated. These results have been prepared by considering the following weather parameters, which are primarily included in the PVHIE analysis and have a close relationship with each other:

- Incoming Shortwave Radiation
- Air Temperature

## 7.1 Introducing *ENVI-met*: A Microclimate Simulation Software

Michael Bruse initiated the development of the ENVI-met software at Ruhr-Universität Bochum in 1995. In 2014, it became the product of the company (ENVI-met GmbH), which was established in Germany with the same name. ENVI-met is a holistic microclimate modeling system that enables users to investigate microclimatic interactions within or between various settlement (urban, suburban) or natural (rural) environments on simulation. Through the interactive modules of the software, natural and artificial surfaces such as vegetation (trees, grasslands, etc.), water reservoirs (such as ponds), building parts and materials (brick or concrete walls, windows and glass, roofs and tiles, etc.), roads and road materials (pavements, asphalt road, etc.), soil profiles (such as sandy or loamy), can be determined. The interactions of these surfaces with each other and the atmosphere is analyzed via the simulations designed in space/time up to 0.5m/1-5s resolution.

ENVI-met has been a software of choice within the methodologies of various UHI studies. As an example, Perera et al. [74] published a study on thermal hotspots and UHI mitigation using ENVI-met. Ambrosini et al. [2] used ENVI-met to make the UHI mitigation assessment for the small city of Teramo in Italy. On the other hand, Sodoudi et al. [83] used ENVI-met for a study area in Tehran, the capital of Iran. Huttner et al. [42] simulated the impact of global warming on the microclimate of a model area representing the central European cities. Ozkeresteci et al. [72] prepared an experimental study for a linear park in Arizona in line with environmental design and planning. As stated on the website, there are more than 3000 scientific publications and independent studies using ENVI-met. However, for the first time within the scope of this thesis, a simulation of a PVPP and its close/surrounding environment was designed via ENVI-met, and the PVHIE was assessed on this software.

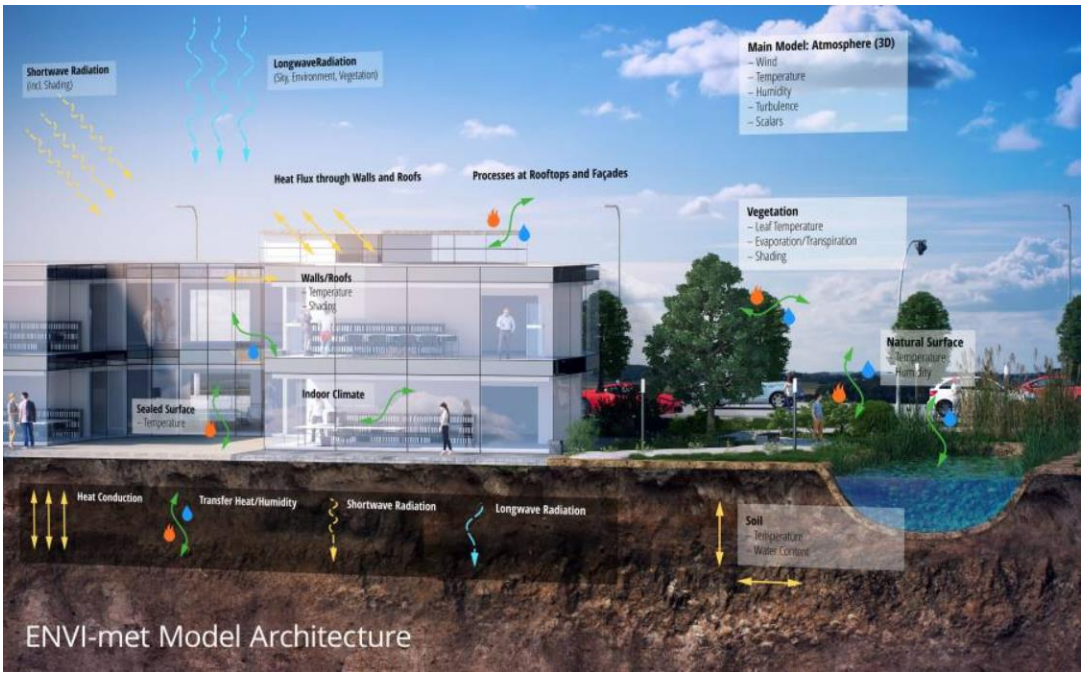


Figure 7.1. ENVI-met Model Architecture [26]

In Figure 7.1, the model architecture of ENVI-met is visualized by specifying the interactions between the residential areas and the natural and artificial environments that surround these areas. The resolution and time period ranges of small/micro-scale analyzes that can be made using ENVI-met on this model architecture are indicated on the software's website as follows:

- Possibility to work with a horizontal resolution of 0.5-10 m
- Possibility to work with a time frame between 24-48 hours and a time-step between 1-5s
- Simulation of a whole month or year, according to the working time and computer hardware

ENVI-met provides simulation results to the user by making calculations of the interactions between natural areas, atmospheric environment, and buildings, which are also exemplified in Figure 7.1. Some of these interactions are described below:

- Shortwave and longwave radiation fluxes (considering shading, reflection, and re-radiation from the sources such as buildings and vegetation)
- Soil-Vegetation-Air Interactions: Water and heat exchanges inside soil (e.g., plant water uptake); sensible heat flux, transpiration, and evaporation (including some physical processes of plants such as photosynthesis)
- Dynamic surface temperature and wall temperature calculations (façade and roof elements separately)
- Gas and particle dispersion
- Biometeorological parameters (e.g., mean radiant temperature)

In Figure 7.2, the micro-model layout of ENVI-met, which also has a 3D numerical model structure, is given. Basically, the ENVI-met's main model is based on the x and y horizontal dimensions and the z vertical dimension. The sub-models (1-D and soil) covered by this basic layout can also be seen in the same figure.

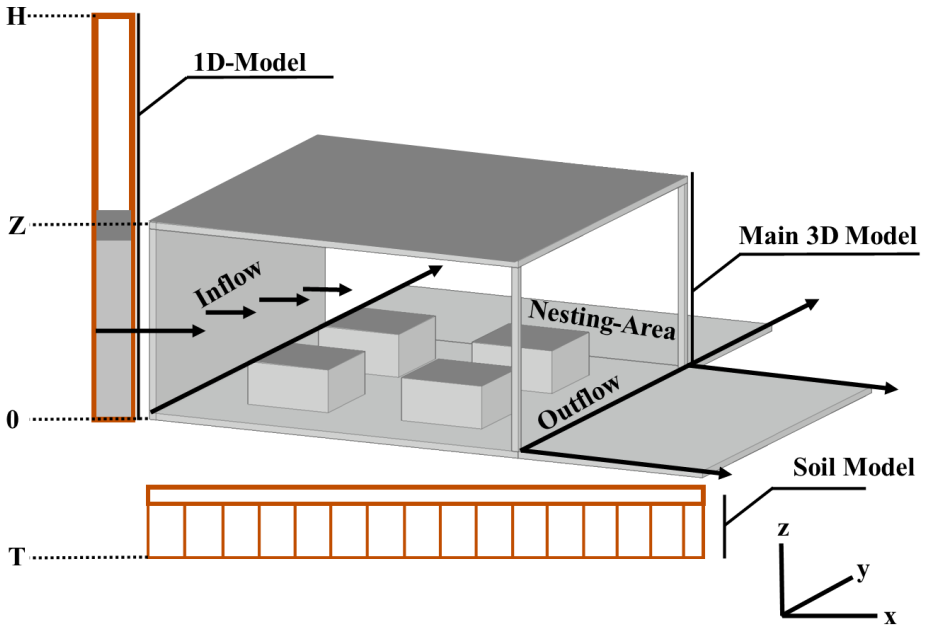


Figure 7.2. ENVI-met Basic Model Layout [27] *(modified)*

The model structure in Figure 7.2 includes the areas such as buildings, vegetation, various surface types, etc. These areas are prepared with the “grid” cells in ENVI-met. The smaller a single grid cell is defined in the software, the higher the model's resolution. However, as the grid cells get smaller, the number of cells used to design an area also increases. For example, an area with 500 x 500 m can be designed with 500 x 500 grid cells of 1 x 1 m. The same area can be prepared with 100 x 100 grid cells of 5 x 5 m. The numbers and dimensions of the grid cells used to design areas in ENVI-met may increase or decrease the simulation time. This increase/decrease also depends on the hardware of the computer running ENVI-met and the CPU usage intensity.

## 7.2 Atmospheric Model Structure and Other Models of *ENVI-met*

When the simulations of the Sekbandemirli study are taken into account, the weather data collected from the field and defined as inputs to ENVI-met is analyzed with the calculations that build the atmospheric model structure of the software. The weather parameters building this atmospheric model structure and the physical equations behind this model are as follow [12] [43]:

- **Air/Wind Flow:** One sub-model that builds the atmospheric model of ENVI-met is *3D Computational Fluid Dynamics (CFD).* Within the scope of this model, t*he Reynolds-averaged Navier-Stokes equations (non-hydrostatic)* are solved for each grid defined to each time step and space. Building physics and vegetation effect are also included in these analyses and calculations.

- **Air Temperature and Humidity:** Different sensible heat and vapor sources and sinks (such as leaves, ground surfaces) within the scope of the atmospheric model enable the determination of air temperature and specific humidity. Air advection and diffusion are simulated in a 3D wind field. Building walls and roofs in the model are surfaces that exchange heat with the atmosphere. However, if green roof or façade applications are also

included in the simulation, these walls and roofs may also be a humidity source. Accordingly, *the combined Advection-Diffusion equation* is used for calculations in the model. In ENVI-met, phase transitions between water and water vapor are not included in the modeling. Thus, the relative humidity is always below 100%.

- **Atmospheric Turbulence:** In ENVI-met, turbulence occurs when air/wind flow interacts with building walls or vegetation. This turbulence may be transported by mean airflow in windy conditions, and its intensity increases accordingly. To simulate the turbulence effect, ENVI-met uses the *1.5 order Turbulence Closure Model* (including local turbulence and its dissipation rate).

- **Radiative Fluxes:** For the environment simulated in ENVI-met, shortwave and longwave radiation analyses can be made within the atmospheric model of the software. These analyses can also include reflection from complex building or other artificial surface geometries, vegetation and radiation, and shading. Radiative flux calculations are included in the model via a *Two-Stream Approximation in Combination*. Within the scope of the 3D model, the radiative fluxes are modified by considering buildings and plants and flux reduction coefficients. These coefficients take a value between 0-1, and 0 indicates “total absorption”.

In addition to the above factors and equations, which build the Atmospheric Model of ENVI-met used in the Sekbandemirli study, "pollutant dispersion" is also included in the same model.

The other models and scopes that form the structure of ENVI-met are given below:

- Soil Model
    - Surface and Soil Temperature
    - Soil Water Content
    - Vegetation Water Supply
    - Water Bodies and Pounds
- Vegetation Model
    - 3D Plant Geometry
    - Foliage Temperature
    - Exchange Processes with the Environment
    - Vegetation Health Assessment / TreePass / Wind Risk Assessment
- Built Environment & Building System
    - Full 3D Building Geometry & Single Walls
    - Detailed Building Materials
    - High-Resolution Building Physics
    - Building Energy Performance
    - Green Wall and Roof Systems

## 7.3 Simulation Work for Sekbandemirli Rural Region and PVPP

In accordance with the simulation work for the Sekbandemirli rural region and PVPP in ENVI-met using the atmospheric model calculations indicated in the previous sub-section, the preliminary preparations were made utilizing some tools on the software's main menu (Figure 7.3).

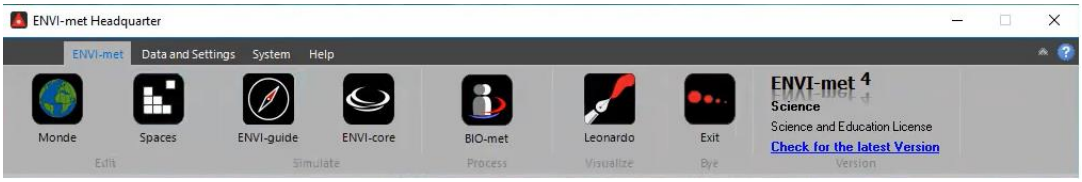


Figure 7.3. ENVI-met Main Menu

The ENVI-met main menu given in Figure 7.3 consists of five parts:

- **Edit:** It includes "Spaces", where the region to be simulated in ENVI-met is digitized as "grid by grid" on the software, and "Monde", where this design is prepared as vector-based. “Spaces” was used for the simulation of Sekbandemirli.

- **Simulate:** This part consists of 2 sub-parts. “ENVI-Guide” is the part where the date range (with the start time) and the total simulation duration are selected for the region digitized in Spaces. Here, the meteorological boundary and initial conditions are also defined, and the measured data is entered as hourly inputs via the “Simple Forcing” or Full Forcing” options. Then, the simulation process can be checked or directly run by using the "ENVI-core" option. The simulation time may vary depending on the date interval selected in the ENVI-Guide and the hardware of the computer running ENVI-met. The simulation process and calculations for 1 hour of a date interval chosen approximately take 1 hour on the workstation (computer) used for this thesis work.

- **Process:** “BIO-met”, the only option in this menu section, is a tool where Human Thermal Comfort Indices calculations are made. It was not used for the Sekbandemirli study.

- **Visualize:** The only option in this section, "Leonardo", is the tool/program that allows viewing the graphical results of the simulations run in ENVI-met. These results can be visualized for various weather parameters separately and by changing the spatial values of the simulated area, such as height (z) or aspect ratio (x-y). The graphical results of the Sekbandemirli simulation work were obtained through this program (sub-section 7.4).

- **Bye:** Users quit ENVI-met via this option.

ENVI-met Spaces enables “coordinate” search from Geonames or Google database. The Sekbandemirli region is introduced to the software in this way (Figure 7.4).

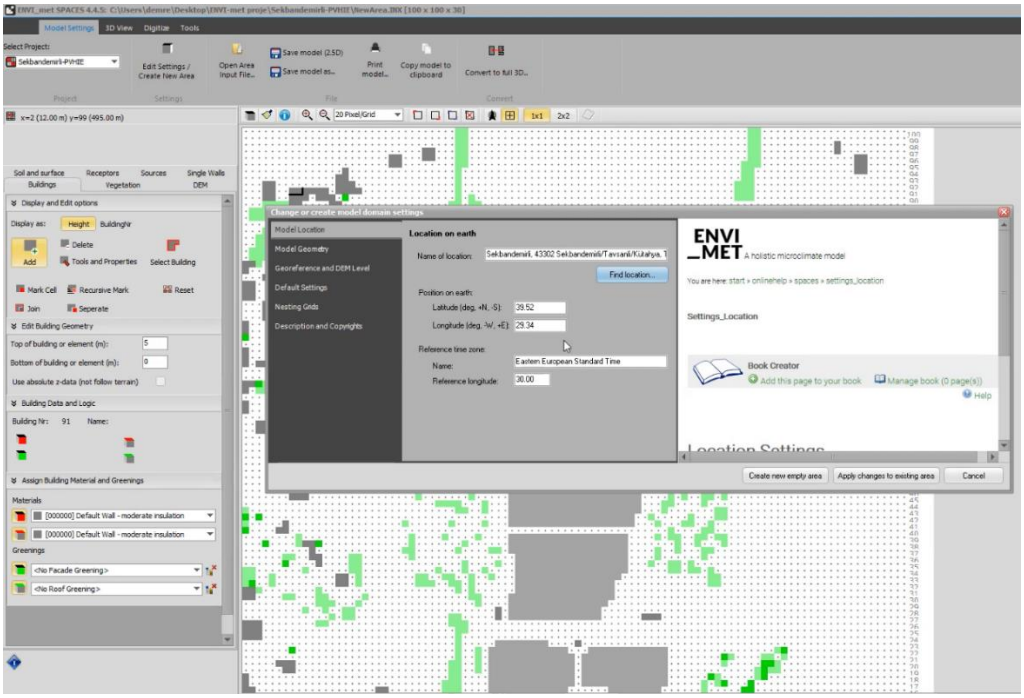


Figure 7.4. ENVI-met Spaces and Location Database

After the area size (600x500m)[2] to be simulated by considering the Sekbandemirli PVPP field and its close surroundings (including Sekbandemirli Village) was determined on Google Earth, it was introduced to ENVI-met Spaces as a bitmap file. This bitmap (Figure 7.5.a) file taken from Google Earth view and the grid-based digitization view (Figure 7.5b) prepared in Spaces can be seen in Figure 7.5. The elevation difference of the land structure (a rise with a slight slope from the south to the north of the investigated area) is negligible to be considered in the simulation analyses (a maximum difference of 30 m; please see Chapter 4). Therefore, the

[2] Model Dimensions: x-y-z Grids = 100-100-30 & Size of Grid Cells (dx-dy-dz) = 6-5-4 meter

Digital Elevation Model (DEM) part of ENVI-met Spaces (Figure 7.4) is not included in the digitization process.

(a)

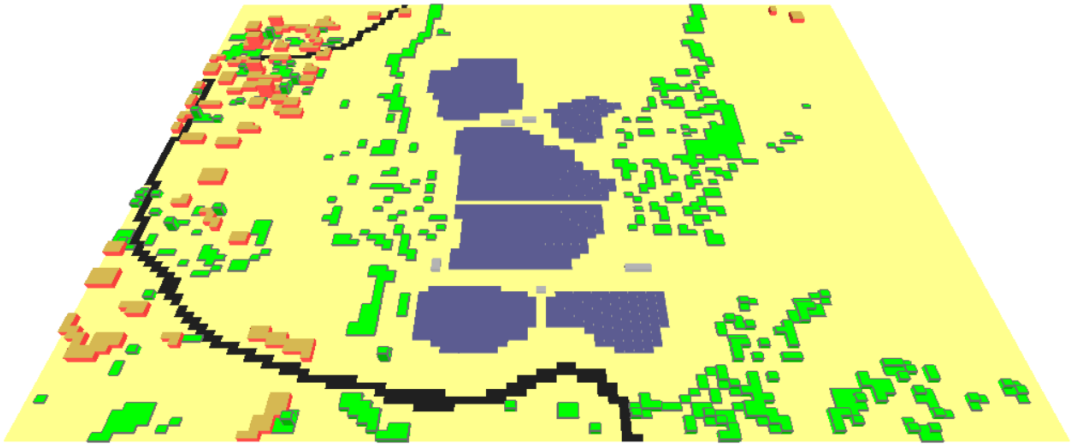

Roughness Length = 0.10; Albedo = 0.17; Emissivity = 0.75

(b)

Figure 7.5. Area Size in Google Earth View (a) and Digitization (b) of the Sekbandemirli Rural Region

On the bitmap in Figure 7.5.a, the relevant area in Sekbandemirli has been digitized using the elements in the Soil and Surface, Buildings, and Vegetation categories (Figure 7.4) in Spaces (Figure 7.5.b). In the digitization process of Sekbandemirli geography, a few elements have been used regarding its natural environment and non-complex fabric compared to cities. These elements are available in the "Database Manager" section of the "Data and Settings" menu and can be added to the design in Spaces as grids:

- **Soil and Surface:**
    - Sandy Soil (as the surface of Sekbandemirli's natural environment)
    - Asphalt Road (leading to the Sekbandemirli Village)
    - PV module arrays (in the Sekbandemirli PVPP)

- **Buildings** (in the Sekbandemirli Village)**:**
    - Walls: Brick
    - Roofing: Tile
    - Building height: between 5-10 m

- **Vegetation** (in the Sekbandemirli rural region)**:**
    - Grasslandsshrublands
    - Small trees

Materials not in the ENVI-met's current database can be defined to the software by introducing their physical properties. Since the PV modules are not found in the Database Manager, this method has been applied (the components of the PV modules in Figure 1.12.b, the dimensions in Appendix A, and the parameters in Figure 7.6 are considered, accordingly). The introduction of the artificial surface formed by the PV modules in Sekbandemirli PVPP to the Database Manager of the software (Figure 7.6) is the first study using this feature of ENVI-met. In other words, for the first time, the heat island formations originating from a PVPP were investigated on an

ENVI-met-based simulation within the content of this thesis study. In this respect, this study can also make a significant contribution to the publications related to ENVI-met.

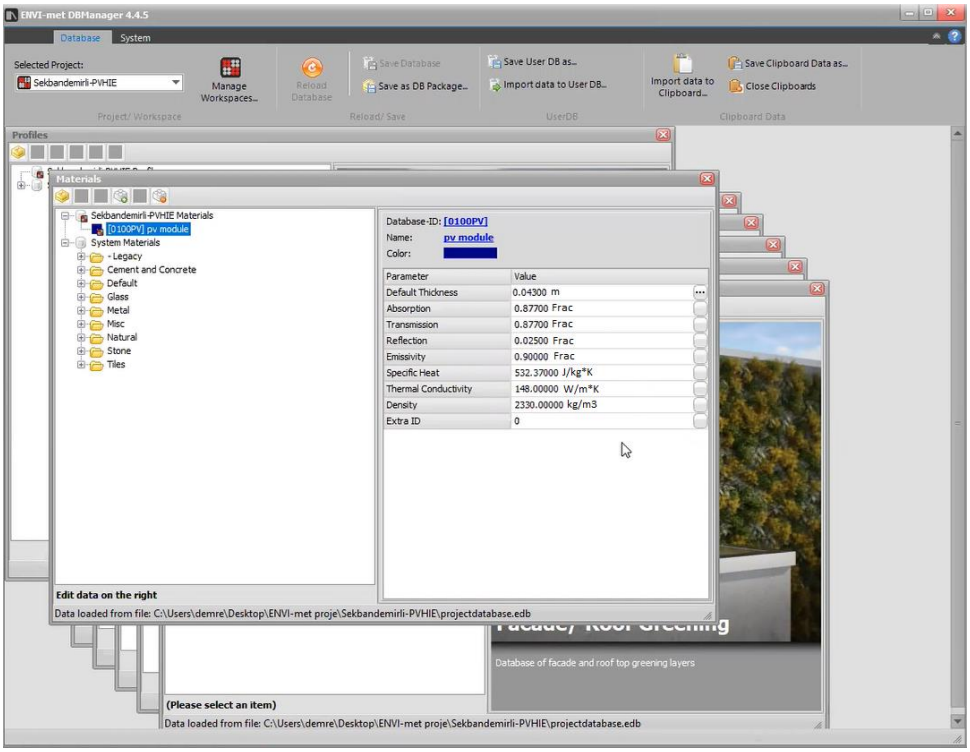


Figure 7.6. ENVI-met Database Manager and PV Module Parameters

Some inputs are defined for Start Date, Start Time, and Total Simulation Time sections in ENVI-met to examine the changes in local weather of the digitized area in Figure 7.5.b on simulation. Total Simulation Time shows how many hours the simulation will cover for the relevant date range. Then, the weather data collected by the WSs in Sekbandemirli at the specified dates and times are entered as inputs (using the Simple Forcing option in ENVI-met) as the meteorological boundary and initial conditions (Figure 7.7).

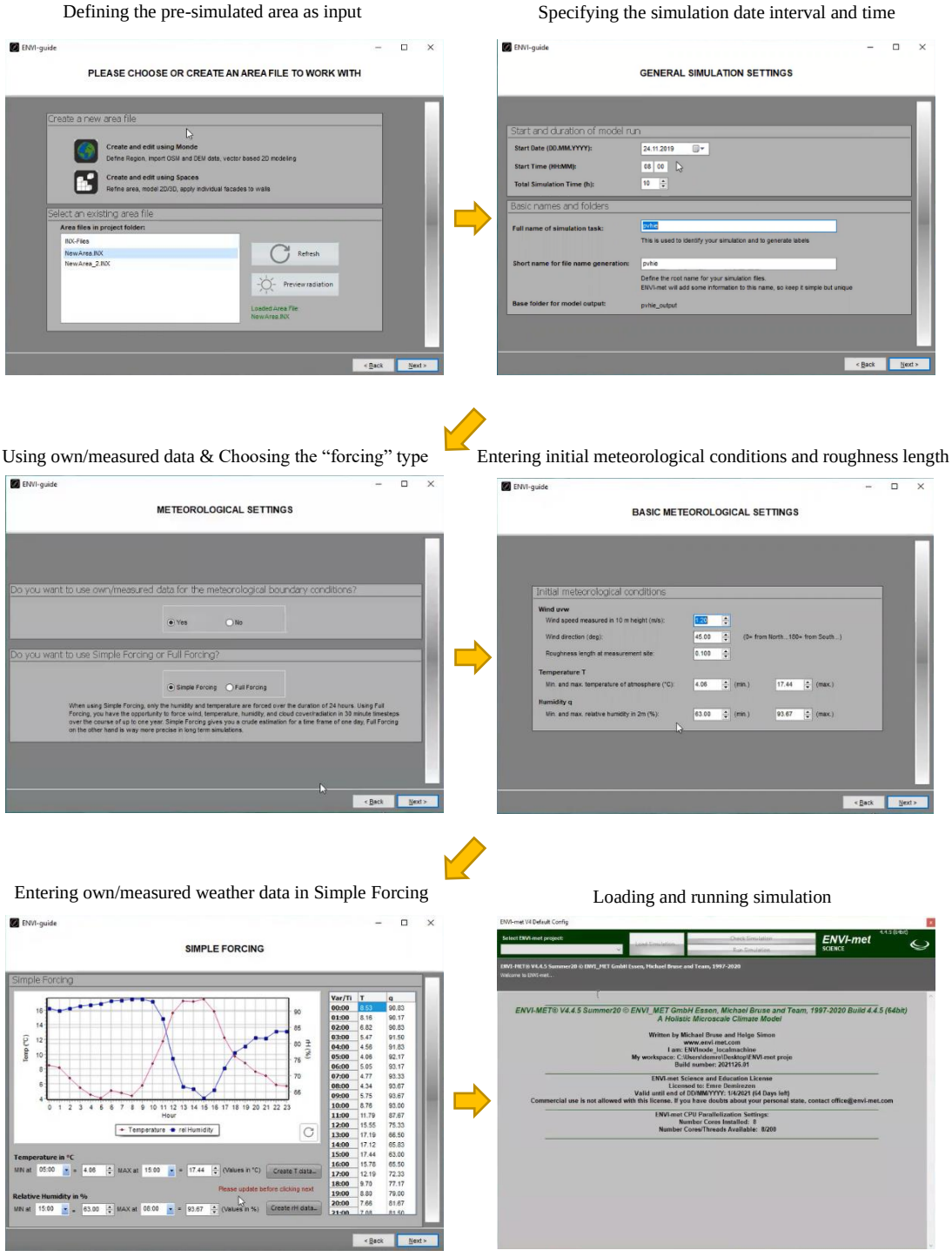


Figure 7.7. ENVI-met Pre-Simulation Menu Flow Chart

## 7.4 Simulation-based Weather Analysis and Results

Following the digitization work in Figure 7.5.b and the steps in Figure 7.7, the local weather conditions in the Sekbandemirli rural region were simulated for specific dates. The output files obtained from these simulation results are visualized through ENVI-met's "Leonardo" program. In this sub-section, the simulation results of the weather parameters given below are compared with the field data of the WSs.

The four different dates on which positive and negative PVHI formations were detected in Sekbandemirli according to field data were considered as follows:

- Positive PVHIE: 20 July 2019 / 14:00 & 11 June 2020 / 11:00
- Negative PVHIE: 13 August 2019 / 03:00 & 29 September 2020 / 02:00

### 7.4.1 Solar Radiation and Albedo

In analyzing the incoming solar radiation data reaching the Sekbandemirli PVPP field, the measurements taken with the irradiance sensor (Kipp & Zonen CMP3) in $WS_3$ were considered. Since the PVHIE observations are made at the field center, the daytime radiation budget in this location was investigated due to a ground surface albedo alteration caused by the PV module arrays. Direct, diffuse, and reflected shortwave radiation distribution were viewed separately on the simulation results visualized in ENVI-met Leonardo (Figure 7.8 and 7.9).

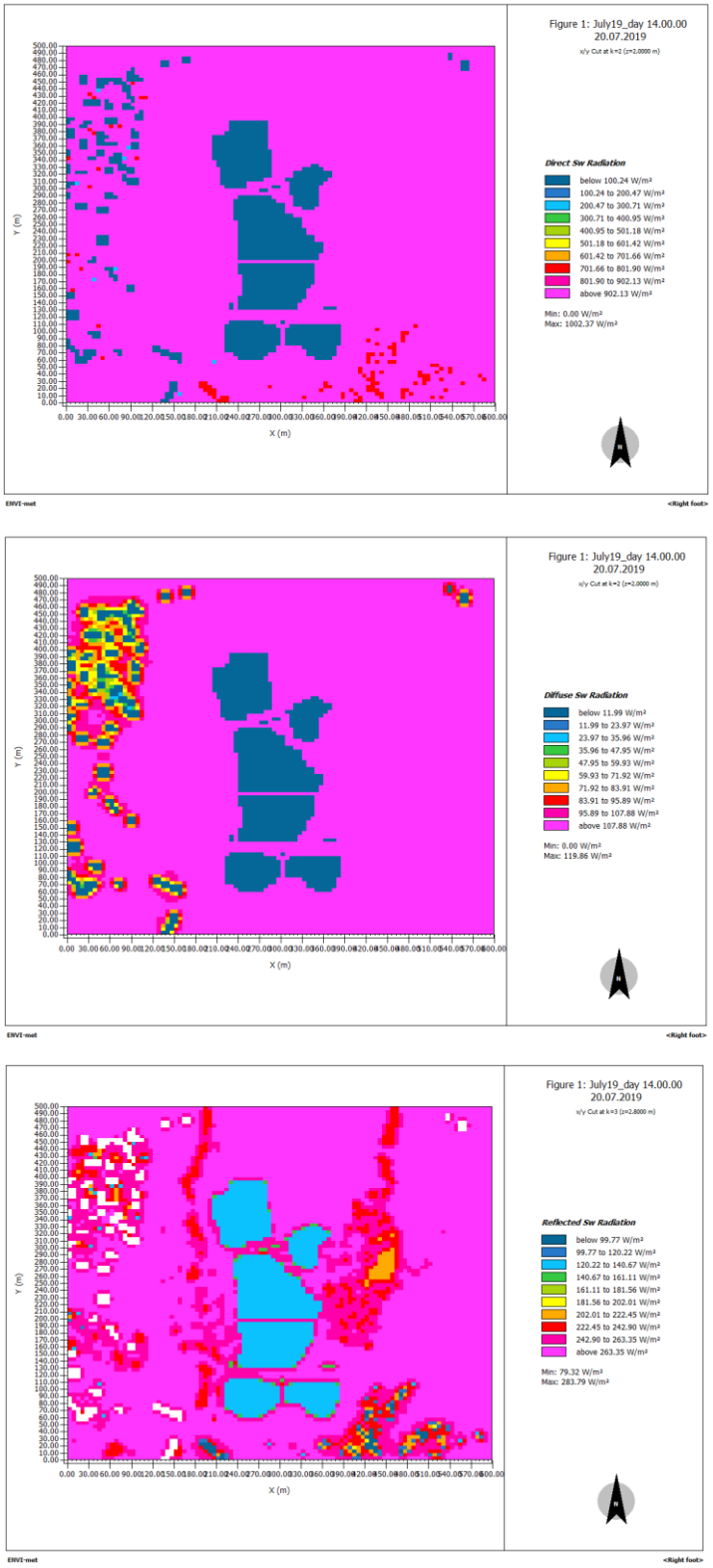


Figure 7.8. Solar Radiation Components on Leonardo (20 July 2019 / 14:00)

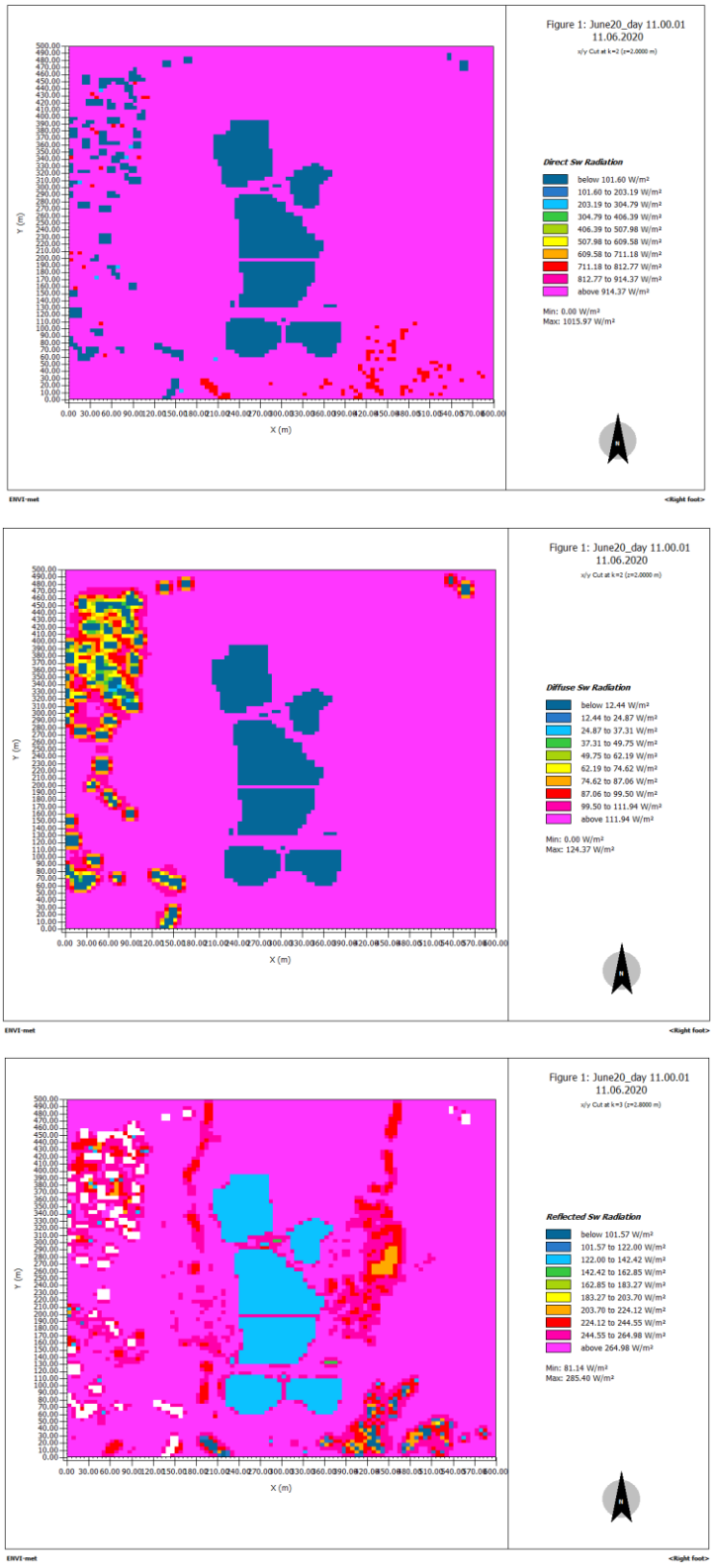


Figure 7.9. Solar Radiation Components on Leonardo (11 June 2020 / 11:00)

In Figures 7.8 and 7.9, the value ranges for the incoming shortwave solar radiation components on two selected dates from the summer months are categorized. As seen in the figures, the direct and diffuse radiation distribution is displayed at the height of 2 meters from the ground. Since this height is below the roof heights (5-10 m) of the Sekbandemirli Village buildings and equals the highest point (2 m) of the PV module arrays, direct and diffuse radiation reach these locations at low rates. For this reason, the radiation values on the natural ground surface (pink parts) are considered for the direct and diffuse radiation reaching the Sekbandemirli rural region and PVPP field (in the reflected radiation graphics, the reflection data at 2.8 m was not calculated for the roofs of village buildings located at the higher locations (white colors)). Comparing the global (or plane of array) irradiance measurement of $WS_3$ with the sum of these direct and diffuse radiation results from ENVI-met Leonardo, it is understood that the field data and simulation results are compatible with each other:

**20 July 2019 / 14:00**

- Direct Sw radiation results on Leonardo: 902.13 $W/m^2$ - 1002.37 $W/m^2$
- Diffuse Sw radiation results on Leonardo: 107.88 $W/m^2$ - 119.86 $W/m^2$
- Global radiation *(based on the results above)*: 1010.01 $W/m^2$ - 1122.23 $W/m^2$
- $WS_3$'s measurement: 1420.33 $W/m^2$

**11 June 2020 / 11:00**

- Direct Sw radiation results on Leonardo: 914.37 $W/m^2$ - 1015.97 $W/m^2$
- Diffuse Sw radiation results on Leonardo: 111.94 $W/m^2$ - 124.37 $W/m^2$
- Global radiation *(based on the results above)*: 1026.31 $W/m^2$ - 1140.34 $W/m^2$
- $WS_3$'s measurement: 1036.11 $W/m^2$

The reflected radiation results in Figure 7.8 and 7.9 (from a height of 2.8m) can be used to calculate how much shortwave radiation reflects from the Sekbandemirli PVPP field surface compared to the natural ground surface (sandy soil) neighboring the power plant field (The WSs in Sekbandemirli can't take reflected radiation measurements). As can be seen from the results below, the positive PVHIE observed at the relevant hours on both dates occurs due to the change in ground reflectivity by half:

**20 July 2019 / 14:00**

- Global radiation: 1010.01 W/m$^2$ - 1122.23 W/m$^2$
- Reflected Sw radiation from the natural ground surface (sandy soil): 263.35 W/m$^2$ – 283.79 W/m$^2$
- **Reflectivity (Albedo): 25-26%**

- Global radiation: 1010.01 W/m$^2$ - 1122.23 W/m$^2$
- Reflected Sw radiation from the PV module arrays: 120.22 W/m$^2$ – 142.42 W/m$^2$
- **Reflectivity (Albedo): 12-13%**

**11 June 2020 / 11:00**

- Global radiation: 1026.31 W/m$^2$ - 1140.34 W/m$^2$
- Reflected Sw radiation from the natural ground surface (sandy soil): 264.98 W/m$^2$ – 285.40 W/m$^2$
- **Reflectivity (Albedo): 25-26%**

- Global radiation: 1026.31 W/m$^2$ - 1140.34 W/m$^2$
- Reflected Sw radiation from the PV module arrays: 122.00 W/m$^2$ – 140.67 W/m$^2$
- **Reflectivity (Albedo): 12%**

### 7.4.2 Air Temperature

The positive PVHIE occurrences detected due to shortwave radiation changes and albedo alteration (sub-section 7.4.1) are given in Figures 7.10 and 11. The PVPP field highlighted in pink on the figures represents the ambient air temperature zone of the field. In other words, this zone represents the temperature of the overlying atmosphere surrounding the PV module arrays. Because these simulation results are calculated as "potential air temperature (θ)" on ENVI-met, a conversion equation (Eq. 10) is required to compare the field data and simulation with each other.

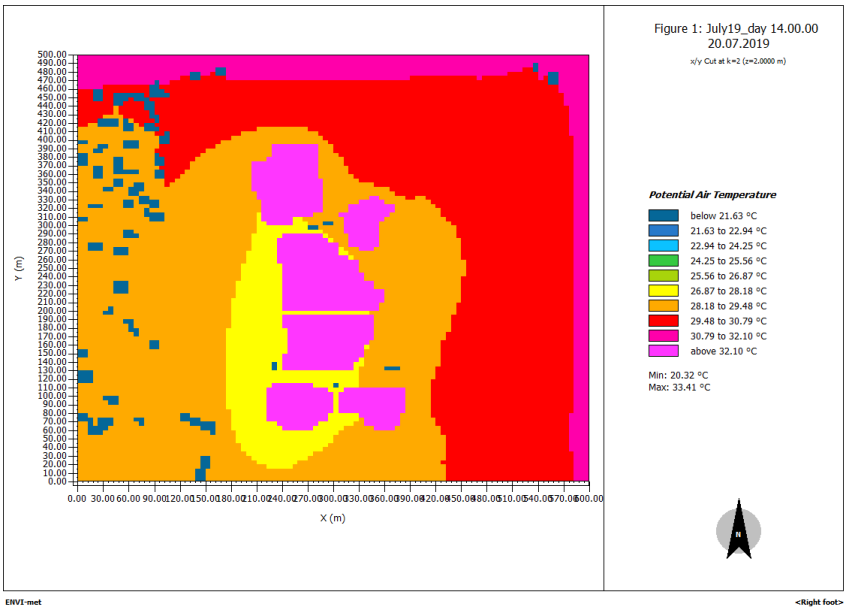


Figure 7.10. Potential Air Temperature on Leonardo (20 July 2019 / 14:00)

<u>According to Figure 7.10:</u>

$$\theta = T(p_0/p)^{\kappa},$$ (Equation 10 and LIST OF SYMBOLS)

$\Delta T_{simulation}$ = 32.76°C / (1000 mbar / 924.17 mbar)$^{0.286}$ – 30.14°C / (1000 mbar / 924.63 mbar)$^{0.286}$ = **2.56°C**

$\Delta T_{field\_data}$ = $WS_{T3}$ – $WS_{T1}$ = 30.92 – 28.83 = **2.09 °C**

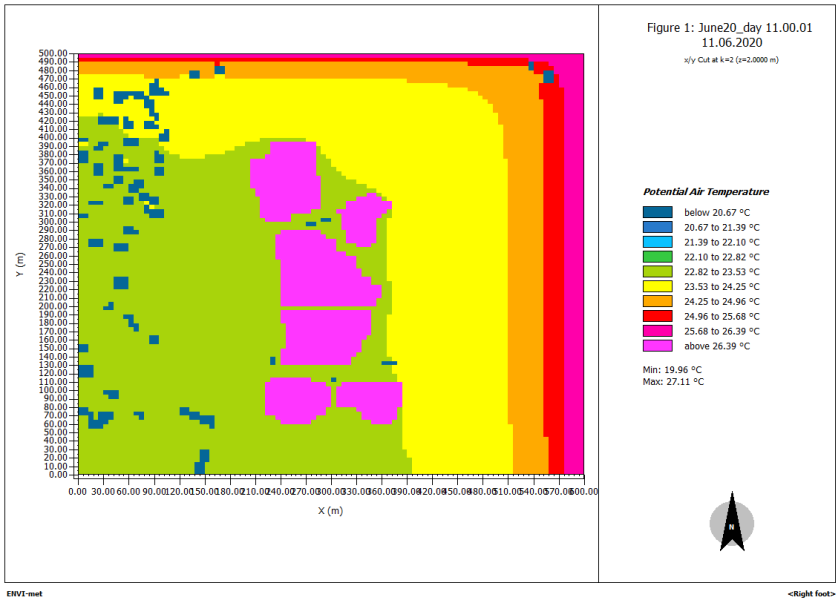


Figure 7.11. Potential Air Temperature on Leonardo (11 June 2020 / 11:00)

<u>According to Figure 7.11:</u>

$$\theta = T(p_0/p)^{\kappa}, \qquad \text{(Equation 10)}$$

$\Delta T_{simulation}$ = 26.75°C / (1000 mbar / 918.33 mbar)$^{0.286}$ – 23.89°C / (1000 mbar / 919.12 mbar)$^{0.286}$ = **2.79°C**

$\Delta T_{field\_data}$ = $WS_{T3}$ – $WS_{T1}$ = 30.92 – 28.83 = **3.48 °C**

By comparing the field data and simulation results on both summer dates, it can be concluded that they are again compatible with each other.

The negative PVHI formations observed especially at night and whose intensity is lower than the positive ones have also been simulated. The field data in two selected dates and hours were determined accordingly, and the graphical simulation results in Leonardo are given in Figures 12 and 13. The results are again compatible.

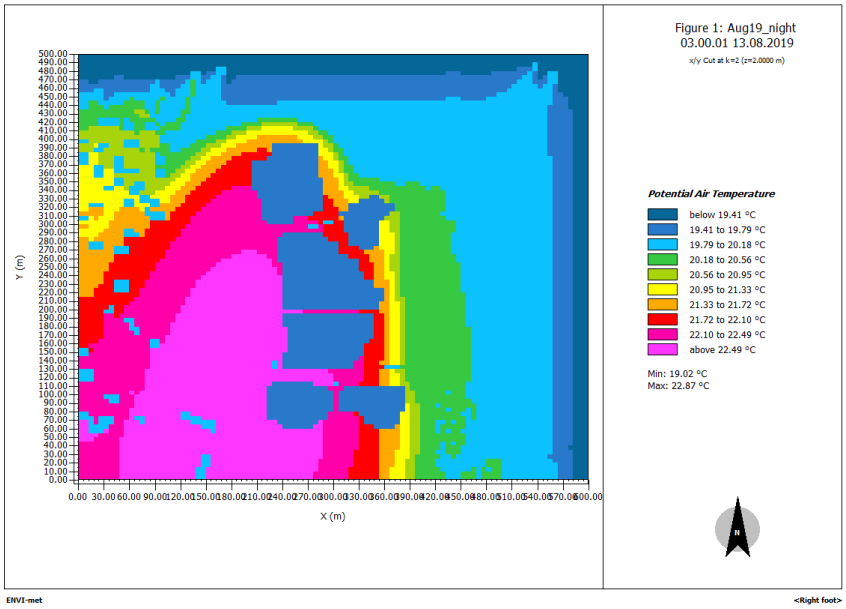


Figure 7.12. Potential Air Temperature on Leonardo (13 August 2019 / 03:00)

<u>According to Figure 7.12:</u>

$$\theta = T(p_0/p)^{\kappa}, \qquad \text{(Equation 10)}$$

$\Delta T_{simulation}$ = 19.60°C / (1000 mbar / 921.20 mbar)$^{0.286}$ – 19.99°C / (1000 mbar / 921.77 mbar)$^{0.286}$ = **- 0.38°C**

$\Delta T_{field\_data}$ = $WS_{T3}$ – $WS_{T1}$ = 18.82 – 19.96 = **- 1.14°C**

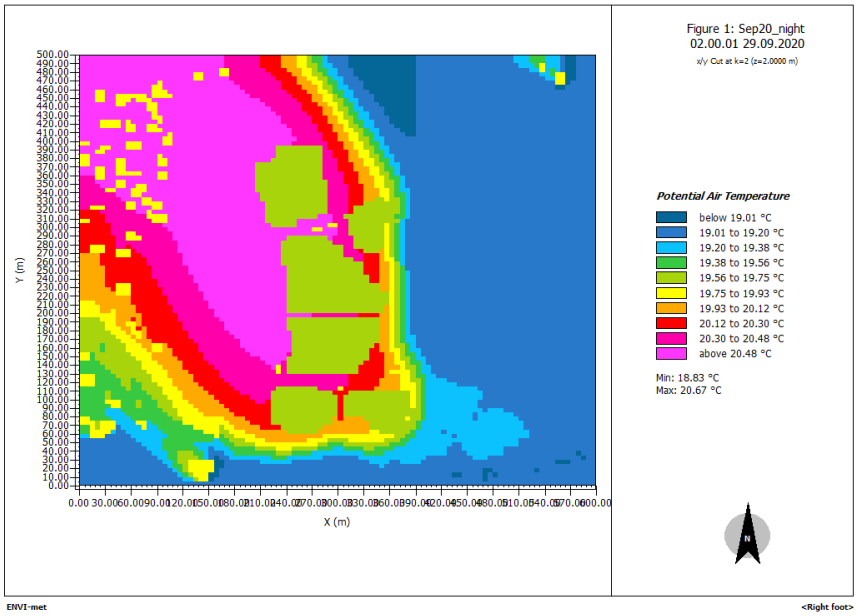


Figure 7.13. Potential Air Temperature on Leonardo (29 Sept 2020 / 02:00)

<u>According to Figure 7.13:</u>

$\Delta T_{simulation}$ = 19.66°C / (1000 mbar / 926.29 mbar)$^{0.286}$ – 20.58°C / (1000 mbar / 927.28 mbar)$^{0.286}$ = **- 0.91°C**

$\Delta T_{field\_data}$ = $WS_{T3}$ – $WS_{T1}$ = 19.00 – 20.33 = **- 1.33°C**

# CHAPTER 8

# CONCLUSION AND RECOMMENDATIONS

The infrastructure of sustainable development-oriented interactions between society, environment, and economy is established with proper and efficient policy implementations in various sectors such as “energy”. The energy sector has a particular place in solving environmental issues and debates at global and regional levels, especially on climate change. Reducing the use of fossil fuels, which are the primary energy sources in many countries (or the development of more efficient combustion technologies); energy efficiency; increasing the share allocated to renewable energy utilization strengthen the contribution of this sector to "sustainability". Today, solar energy technologies, which have many applications among renewable energy conversion techniques, play a significant role in increasing this share.

While making developments and improvements in these technologies, researchers, policy-makers, and stakeholders should also pay attention to their negative environmental side-effects, including Photovoltaic Heat Island Effect (PVHIE) caused by Solar PhotoVoltaic Power Plants (Solar PVPP). PVHIE emerges due to the albedo alteration on the natural land type covered by the PVPPs constructed onto different continental and water surfaces in the world geography.

This thesis study was carried out to contribute to the literature on PVHIE publications and conduct the first field study of this environmental issue in Turkey. Considering its geographical characteristics, the Sekbandemirli rural region of Tavşanlı district of Kütahya and a PVPP constructed in this region were chosen as the field study location. The field data were collected and monitored both during the PVPP was operational and under construction.

The three weather stations installed inside and outside the PVPP field were used for the field data collection and monitoring, which covers an extended period, i.e., three years. These weather stations measure weather parameters such as incoming solar radiation, ambient air temperature, wind speed & direction. Through this comprehensive data collection and monitoring, it has been possible to detect positive (more observations) and negative (fewer observations) PVHI formations at the Sekbandemirli PVPP field center, varying daily and seasonally. When a higher (ambient) air temperature is measured (at the PVPP field center) than outside the PVPP field, this measurement is expressed as a "positive" PVHIE detection/observation (whereas "negative" PVHIE indicates the opposite). These heat island results were obtained after analyzing the Sekbandemirli field data via the appropriate statistical methods, graphical representations, correlation results, and simulations.

Following these analyses, the positive PVHIE is monthly and seasonally observable at the PVPP field center with 1-6°C higher air temperatures than those measured outside the PVPP field. The inverse but less-effective negative PVHIE is detectable with 1-3°C higher air temperatures outside the field. All these PVHI formations correlate with PV module temperature ($T_m$) and PVPP electrical power output (P), and change monthly (from season to season) with specific formation frequencies (Chapter 6).

Last but not least, it is important to consider the local wind speed and directions characteristics for the location of a PVPP field before PV module installment and orientation because wind reduces heat island effect by natural cooling. On the other hand, the prevailing wind direction as North-East (NE) and the breeze speeds varying mostly between 0-4 m/s are not sufficiently effective to reduce PVHIE monitored at the PVPP field center.

Although the daily and seasonal PVHI formations at the Sekbandemirli PVPP field center are "transient" (not continuous), some recommendations can also be made related to the reduction of this transient PVHIE.

How efficiently PV modules convert solar energy to electricity while operating is closely related to how much heat they absorb and release to their close environment and surroundings. In other words, PVPPs may be a PVHIE source as well as an electrical power facility. Outdoor tests on performance and degradation of PV module types give an idea to project managers and power plant operators in terms of the selection of these solar modules used to build the arrays in PVPPs [69] [70] [71] [79].

While new components are added to the assemblies and new manufacturing technologies are developed by the improvements in the physical structure of the PV module components (Figure 1.12), the product range of different PV module technologies also expands. In this context, bifacial modules [24] that provide energy yield from the rear surface of a PV module like its front surface and support of these modules with solar tracking systems [73] can be given as an example.

On the development of PV modules that absorb and release less heat (and provide more solar electricity yield), the efforts to increase the research efficiency of solar cells [11] and the technologies developed using some new production techniques (e.g., PERC, IBC, Bifacial, HJT, TOPCon) also contribute to the reduction of heat island effect.

The land requirements for solar energy conversion systems or facilities such as solar PV power plants and the determination of construction site/location in this direction should be considered. It would be beneficial to examine some studies related to various countries/cities regarding this land use and site choice. Ven et al. [102] calculated the potential land requirement for solar energy utilization for EU, India, South Korea, and Japan, and how much carbon release could occur depending on the change in land use (occupation). Oudes and Stremke [68] analyzed landscape changes due to solar power plant installations for the 11 locations in the Netherlands, UK, Germany, and Italy in terms of visibility, multifunctionality, and temporality via a comparative study. Devitt et al. [20] assessed the potential environmental impacts of utility-scale solar energy systems on land resources in West Texas, US.

Geographic Information System (GIS) and Analytic Hierarchy Process (AHP) methods are also utilized in land suitability and site/location determination assessments for the construction and installation processes of solar power plants [7] [34] [64] [66] [67] [76] [90] [99]. Moreover, some studies are carried out to develop software such as SOlAR TURnKEY [51], where feasibility analyses can be made technically and economically according to solar energy projects' location and capacity information.

The term "agrivoltaics", which expresses the use of PVPPs in agricultural applications, plays a key role in reducing the heat island effect caused by these systems [15] [37] [38] [94] [106] [114]. PV modules installed on or between plants and crops can increase agricultural quality and efficiency in yield with some factors such as shading. Transpiration, a natural/organic process of plants and crops, provides cooling of the PV modules.

ENVI-met software, which is utilized in UHI analyses and included in the methodology of many research studies published on this topic, was used for the first time to prepare the simulation of a PVPP and its close environment within the scope of this thesis. The compatibility of the PVHIE results obtained from this simulation with the field data of the thesis study also shows that: For some HIE studies planned on PVPPs where it is not possible to take direct field measurements, a microclimate simulation software such as ENVI-met can be used as a study technique.

ENVI-met is a comprehensive and practical software with its comparable simulation outputs close to the weather station measurements in the Sekbandemirli region. However, as can be understood from the simulation studies given in Chapter 7, the developers of software such as ENVI-met should be able to integrate the components of PVPPs (e.g., PV modules) and similar energy systems/facilities into the database and other related tools of their software (not only by letting users define physical properties of these components via their software tools). ENVI-met should also be improved/updated by considering artificial sloping surface types like building roof pitches or tilted PV modules.

In Turkey and the world, there are solar power plants that cover a much larger land (or water) surface area than Sekbandemirli PVPP, where the field study projects of this thesis were conducted. In accordance with the relevant policy regulations, environmental impact assessments, including HIE, should be a prerequisite for these existing power plants' operation and PVPP projects under construction/installation or implementation.

## REFERENCES


[1] Alstom: Reliable, consistent, concentrated solar power (CSP) from industry experts. (2021). Retrieved 14 December 2021, from https://helioscsp.com/alstom-reliable-consistent-concentrated-solar-power-csp-from-industry-experts

[2] Ambrosini, D., Galli, G., Mancini, B., Nardi, I., Sfarra, S. (2014). Evaluating Mitigation Effects of Urban Heat Islands in a Historical Small Center with the ENVI-Met® Climate Model. Sustainability, 6(10), 7013-7029. doi: 10.3390/su6107013

[3] Amindin, A., Pouyan, S., Pourghasemi, H., Yousefi, S., Tiefenbacher, J. (2021). Spatial and temporal analysis of urban heat island using Landsat satellite images. Environmental Science And Pollution Research, 28(30), 41439-41450. doi: 10.1007/s11356-021-13693-0

[4] Aris, A., Syaf, H., Yusuf, D. N., Nurgiantoro. Analysis of urban heat island intensity using multi temporal landsat data; case study of Kendari City, Indonesia Paper presented at Geomatics International Conference 2019, Surabaya, Indonesia.

[5] Armstrong, A., Waldron, S., Whitaker, J., Ostle, N. (2014).Wind farm and solar park effects on plant-soil carbon cycling: Uncertain impacts of changes in ground-level microclimate. Global Change Biology, 20(6), 1699-1706. doi: 10.1111/gcb.12437

[6] Athukorala, D. & Murayama, Y. (2021). Urban Heat Island Formation in Greater Cairo: Spatio-Temporal Analysis of Daytime and Nighttime Land Surface Temperatures along the Urban–Rural Gradient. Remote Sensing, 13(7), 1396. doi: 10.3390/rs13071396

[7] Ayday, C., Yaman, N., Sabah, L., Höke, O. (2016). Site Selection of Solar Power Plant by Using Open Source GIS for Eskişehir Province. In 6. Uzaktan Algılama ve Coğrafi Bilgi Sistemleri Sempozyumu (pp. 510-520). Çukurova, Adana.

[8] Barron-Gafford, G. A., Minor, R. L., Allen, N. A., Cronin, A. D., Brooks, A. E., Pavao-Zuckerman, M. A. (2016). The Photovoltaic Heat Island Effect: Larger solar power plants increase local temperatures. Scientific Reports, 6(1). doi: 10.1038/srep35070

[9] Barron-Gafford, G. A., Pavao-Zuckerman, M.A., Minor, R.L. et al. (2019). Agrivoltaics provide mutual benefits across the food–energy–water nexus in drylands. Nat Sustain 2, 2, 848–855. doi: 10.1038/s41893-019-0364-5

[10] Beck, H., Zimmermann, N., McVicar, T. et al. (2018). Present and future Köppen-Geiger climate classification maps at 1-km resolution. Sci Data 5, 180214. https://doi.org/10.1038/sdata.2018.214

[11] Best Research-Cell Efficiency Chart. (2021). Retrieved 14 December 2021, from https://www.nrel.gov/pv/cell-efficiency.html

[12] Bruse, Michael. (2004). ENVI-met 3.0: Updated Model Overview.

[13] Burg, B., Ruch, P., Paredes, S., Michel, B. (2017). Effects of radiative forcing of building integrated photovoltaic systems in different urban climates. Solar Energy, 147, 399-405. doi: 10.1016/j.solener.2017.03.004

[14] Canan, F. (2017). Kent Geometrisine Bağlı Olarak Kentsel Isı Adası Etkisinin Belirlenmesi: Konya Örneği. Journal of the Faculty of Engineering and Architecture (Çukurova University), 32(3), 69-80. doi: 10.21605/cukurovaummfd.357202

[15] Chamara, R. & Beneragama, C. (2020). Agrivoltaic systems and its potential to optimize agricultural land use for energy production in Sri Lanka: A Review. Journal of Solar Energy Research (JSER), 5(2), 417-431. doi: 10.22059/JSER.2020.302720.1154

[16] Concentrating Solar Power Projects. (2021). Retrieved 14 December 2021, from https://solarpaces.nrel.gov/by-country

[17] Coseo, P. & Larsen, L. (2014). How factors of land use/land cover, building configuration, and adjacent heat sources and sinks explain Urban Heat Islands in Chicago. Landscape and Urban Planning, 125, 117–129. doi: 10.1016/j.landurbplan.2014.02.019

[18] Deilami, K., Kamruzzaman, Md., Liu, Y. (2018). Urban heat island effect: A systematic review of spatio-temporal factors, data, methods, and mitigation measures. International Journal of Applied Earth Observation and Geoinformation, 67, 30–42. doi: 10.1016/j.jag.2017.12.009

[19] Demirezen, E., Ozden, T., Akinoglu, B. G. (2018). Impacts of a Photovoltaic Power Plant for Possible Heat Island Effect Paper presented at the 1st International Conference on Photovoltaic Science and Technologies (PVCon2018), Ankara, Turkey. doi: 10.1109/PVCon.2018.8523937 (IEEE-Xplore Digital Library

[20] Devitt, D., Young, M., Pierre, J. (2020). Assessing the potential for greater solar development in West Texas, USA. Energy Strategy Reviews, 29, 100490. doi: 10.1016/j.esr.2020.100490

[21] Dihkan, M. (2015). Kentsel Isı Adalarının (KIA) Uydu Görüntüleri ile Konumsal Olarak Modellenmesi, (Doctoral dissertation). Turkey: Karadeniz Technical University

[22] Dorer, V., Allegrini, J., Orehounig, K., Moonen, P., Upadhyay, G., Kämpf, J., Carmeliet, J. (2013). Modelling the Urban Microclimate and Its Impact on the Energy Demand of Buildings and Building Clusters Paper presented at 13th Conference of International Building Performance Simulation Association, Chambéry, France.

[23] Duman Yüksel, Ü. & Yılmaz, O. (2008). Ankara Kentinde Kentsel Isı Adası Etkisinin Yaz Aylarında Uzaktan Algılama ve Meteorolojik Gözlemlere Dayalı Olarak Saptanması ve Değerlendirilmesi. Journal of the Faculty of Engineering and Architecture of Gazi University, 23(4), 937-952.

[24] Durusoy, B., Ozden, T., Akinoglu, B. G. (2020). Solar irradiation on the rear surface of bifacial solar modules: a modeling approach. Scientific Reports, 10(1). doi: 10.1038/s41598-020-70235-3

[25] Dwivedi, A. & Khire, M. V. (2014). Measurement Technologies for Urban Heat Islands. International Journal of Emerging Technology and Advanced Engineering, 4(10), 539-545.

[26] ENVI-met: Model Concept. (2021). Retrieved 14 December 2021, from https://envi-met.info/doku.php?id=intro:modelconept

[27] ENVI-met: Model Layout. (2021). Retrieved 14 December 2021, from https://envi-met.info/doku.php?id=kb:modellayout

[28] Fan, C. & Huang, X. (2020). Satellite-observed changes of surface spectral reflectances due to solar farming and the implication for radiation budget. Environmental Research Letters, 15(11), 114047. doi: 10.1088/1748-9326/abbdea

[29] Fisher, R. (1925). Statistical Methods for Research Workers. Oliver and Boyd.

[30] Fthenakis, V. & Yu, Y. (2013). Analysis of the potential for a heat island effect in large solar farms Paper presented at IEEE 39th Photovoltaic Specialists Conference (PVSC), Florida, US. doi: 10.1109/PVSC.2013.6745171

[31] Gambone, S. (2021). The Difference Between Off-Grid and On-Grid Solar Energy. Retrieved 14 December 2021, from https://www.paradisesolarenergy.com/blog/difference-between-off-grid-and-on-grid-solar-energy

[32] Gifford, J. (2021). Australia's rooftop installations above 2017's record-breaking year. Retrieved 14 December 2021, from https://www.pv-magazine.com/2018/03/09/australias-rooftop-installations-above-2017s-record-breaking-year

[33] Gokmen, N., Hu, W., Hou, P., Chen, Z., Sera, D., Spataru, S. (2016). Investigation of wind speed cooling effect on PV panels in windy locations. Renewable Energy, 90, 283-290. doi: 10.1016/j.renene.2016.01.017

[34] Günen, M. (2021). Determination of the suitable sites for constructing solar photovoltaic (PV) power plants in Kayseri, Turkey using GIS-based ranking and AHP methods. Environmental Science And Pollution Research, 28(40), 57232-57247. doi: 10.1007/s11356-021-14622-x

[35] Hadjimitsis, D., Retalis, A., Michaelides, S., Tymvios, F., Paronis, D., Themistocleous, K., Agapiou, A. (2013). Satellite and Ground Measurements for Studying the Urban Heat Island Effect in Cyprus. Remote Sensing of Environment - Integrated Approaches. (pp. 1-24). Cyprus: IntechOpen. doi.org/10.5772/39313

[36] Hardin, A.W., Liu, Y., Cao, G., Vanos, J. K. (2018). Urban heat island intensity and spatial variability by synoptic weather type in the northeast U.S. Urban Climate, 24, 747–762. doi: 10.1016/j.uclim.2017.09.001

[37] Hassanpour Adeh, E., Selker, J., Higgins, C. (2018). Remarkable agrivoltaic influence on soil moisture, micrometeorology and water-use efficiency. PLOS ONE, 13(11). doi: 10.1371/journal.pone.0203256

[38] Hassanpour Adeh, E, Good, S., Calaf, M., Higgins, C. (2019). Solar PV Power Potential is Greatest Over Croplands. Scientific Reports, 9(11442). doi: 10.1038/s41598-019-47803-3

[39] Hernandez, R. R., Easter, S. B., Murphy-Mariscal, M. L., Maestre, F. T., Tavassoli, M., Allen, E. B., Barrows, C. W., Belnap, J., Ochoa-Hueso, R., Ravi, S., Allen, M. F. (2014). Environmental impacts of utility-scale solar energy. Renewable and Sustainable Energy Reviews, 29, 766-779. doi: 10.1016/j.rser.2013.08.041

[40] Homadi, A. (2016). Effect of Elevation and Wind Direction on Silicon Solar Panel Efficiency. International Journal of Energy and Power Engineering, 10, 1205-1212.

[41] Honsberg, C., & Bowden, S. (2021). Heat Generation in PV Modules. Retrieved 14 December 2021, from https://www.pveducation.org/pvcdrom/modules-and-arrays/heat-generation-in-pv-modules

[42] Huttner, S., Bruse, M., Dostal, P. (2008). Using ENVI-met to simulate the impact of global warming on the microclimate in central European cities. 5th Japanese-German Meeting on Urban Climatology. 18.

[43] Huttner, S. (2012). Further development and application of the 3D microclimate simulation ENVI-met, (Doctoral dissertation). Germany: Johannes Gutenberg University of Mainz.

[44] IEA, IRENA, UN Statistics Division, The World Bank, WHO. (2021). Tracking SDG7 - The Energy Progress Report 2021 (p. 89).

[45] International Renewable Energy Agency. (2021). Renewable Power Generation Costs in 2020 (p. 13).

[46] Intergovernmental Panel on Climate Change. (2020). Climate Change and Land (p. 8).

[47] International Energy Agency. (2021). Net Zero by 2050 - A Roadmap for the Global Energy Sector (p. 39).

[48] International Energy Agency. (2020). Renewables 2020 - Analysis and Forecast to 2025 (pp. 37-38).

[49] Jäger-Waldau, A. (2021). Rooftop PV And Self Consumption Of Electricity In Europe. Retrieved 14 December 2021, from http://www.europeanenergyinnovation.eu/Articles/Autumn-2018/Rooftop-PV-and-self-consumption-of-electricity-in-Europe

[50] Jiang, J., Gao, X., Lv, Q., Li, Z., Li, P. (2021). Observed impacts of utility-scale photovoltaic plant on local air temperature and energy partitioning in the barren areas. Renewable Energy, 174, 157-169. doi: 10.1016/j.renene.2021.03.148

[51] Karaveli, A. B. (2018). Development of the Algorithm of SOlAR TURnKEY: Solar Electricity Software for Turkey, (Doctoral dissertation). Turkey: Middle East Technical University.

[52] Keetels, S. Solar panels reduce the urban heat island. TU Delft & Deerns.

[53] Kershaw, T. (2017). Climate Change Resilience in the Urban Environment (pp. 4-1 - 4-44). IOP Science.

[54] Kiris, B., Bingol, O., Senol, R., Altintas, A. (2016). Solar Array System Layout Optimization for Reducing Partial Shading Effect. Special Issue of the 2nd International Conference on Computational and Experimental Science and Engineering (ICCESEN 2015), Acta Physica Polonica A, 130. doi: 10.12693/APhysPolA.130.55

[55] Kotharkar, R. & Surawar, M. (2016). Land Use, Land Cover, and Population Density Impact on the Formation of Canopy Urban Heat Islands through Traverse Survey in the Nagpur Urban Area. Journal of Urban Planning and Development, 142(1), 1-13. doi: 10.1061/(ASCE)UP.1943-5444.0000277

[56] Lempriere, M. (2021). India adds 883MW of rooftop solar in first nine months of 2020 despite COVID-19. Retrieved 14 December 2021, from https://www.pv-tech.org/india-adds-883mw-of-rooftop-solar-in-first-nine-months-of-2020-despite-covid-19/

[57] Lobera, D. T. & Valkealahti, S. (2013). Dynamic thermal model of solar PV systems under varying climatic conditions. Solar Energy, 93, 183-194. doi: 10.1016/j.solener.2013.03.028

[58] Lu, L., Weng, Q., Xiao, D., Guo, H., Li, Q., & Hui, W. (2020). Spatiotemporal Variation of Surface Urban Heat Islands in Relation to Land Cover Composition and Configuration: A Multi-Scale Case Study of Xi'an, China. Remote Sensing, 12(17), 2713. doi: 10.3390/rs12172713

[59] Masson, V., Bonhomme, M., Salagnac, J. L., Briottet, X., Lemonsu, A. (2014). Solar panels reduce both global warming and urban heat island. Frontiers in Environmental Science, 2(14). doi: 10.3389/fenvs.2014.00014

[60] Matai, K. (2020). Influence of SPV Installations on the Thermal Character of the Urban Milieu. J - Multidisciplinary Scientific Journal, 3(3), 343-357. doi: 10.3390/j3030027

[61] Met Office. Microclimates - National Meteorological Library and Archive Fact Sheet 14.

[62] Millstein, V. & Menon, S. (2011). Regional climate consequences of large-scale cool roof and photovoltaic array deployment. Environmental Research Letters, 6. doi: 10.1088/1748-9326/6/3/034001

[63] Mirzaei, P.A. (2015). Recent challenges in modeling of urban heat island. Sustainable Cities and Society, 19, 200–206. doi: 10.1016/j.scs.2015.04.001

[64] Mokarram, M., Mokarram, M., Khosravi, M., Saber, A., Rahideh, A. (2020). Determination of the optimal location for constructing solar photovoltaic farms based on multi-criteria decision system and Dempster–Shafer theory. Scientific Reports, 10(8200). doi: 10.1038/s41598-020-65165-z

[65] Montaner-Fernández, D., Morales-Salinas, L., Rodriguez, J., Cárdenas-Jirón, L., Huete, A., Fuentes-Jaque, G. et al. (2020). Spatio-Temporal Variation of the Urban Heat Island in Santiago, Chile during Summers 2005–2017. Remote Sensing, 12(20), 3345. doi: 10.3390/rs12203345

[66] Noorollahi, E., Fadai, D., Akbarpour Shirazi, M., Ghodsipour, S. (2016). Land Suitability Analysis for Solar Farms Exploitation Using GIS and Fuzzy Analytic Hierarchy Process (FAHP) - A Case Study of Iran. Energies, 9(8), 643. doi: 10.3390/en9080643

[67] Omoloso, O., Alaigba, D., Aboyeji, O., Balogun, I., Akande, S. (2020). Optimal Site Suitability for Large Scale Solar Farms in Osun East District, Nigeria. 15. 24-37.

[68] Oudes, D. & Stremke, S. (2021). Next generation solar power plants? A comparative analysis of frontrunner solar landscapes in Europe. Renewable And Sustainable Energy Reviews, 145, 111101. doi: 10.1016/j.rser.2021.111101

[69] Ozden, T., Yardım, U., Akinoglu, B., Turan, R. (2015). Outdoor efficiency analyses and comparison of on-grid CdTe and µc-Si/a-Si thin-film PV systems for three years in Ankara - Turkey. Physica Status Solidi (C), 12(9-11), 1283-1287. doi: 10.1002/pssc.201510077

[70] Ozden, T., Akinoglu, B., Turan, R. (2017). Long term outdoor performances of three different on-grid PV arrays in central Anatolia – An extended analysis. Renewable Energy, 101, 182-195. doi: 10.1016/j.renene.2016.08.045

[71] Ozden, T. & Akinoglu, B. G. (2018). Preliminary investigations on two different procedures to calculate the efficiency and performance ratio of PV modules. International Journal of Environmental Science and Technology, 16(9), 5171–5176. doi: 10.1007/s13762-018-2003-5

[72] Ozkeresteci, I. & Crewe, K. (2003). Use and evaluation of the ENVI-met model for environmental design and planning: an experiment on linear parks. Cartographic Renaissance.

[73] Patel, T., Ahmed, M., Imran, H., Butt, N., Khan, M., Alam, M. (2020). Optimum design of tracking bifacial solar farms -- A comprehensive global analysis of next-generation PV.

[74] Perera, T., Nayanajith, T., Jayasinghe, G., Premasiri, H. (2021). Identification of thermal hotspots through heat index determination and urban heat island mitigation using ENVImet numerical micro climate model. Modeling Earth Systems And Environment. doi: 10.1007/s40808-021-01091-x

[75] Q Table for Tukey's HSD. (2021). Retrieved 14 December 2021, from https://www2.stat.duke.edu/courses/Spring98/sta110c/qtable.html

[76] Rediske, G., Siluk, J., Michels, L., Rigo, P., Rosa, C., Cugler, G. (2020). Multi-criteria decision-making model for assessment of large photovoltaic farms in Brazil. Energy, 197, 117167. doi: 10.1016/j.energy.2020.117167

[77] Reduce Urban Heat Island Effect. (2021). Retrieved 14 December 2021, from https://www.epa.gov/green-infrastructure/reduce-urban-heat-island-effect

[78] REN21. (2021). Renewables 2021 Global Status Report (p. 36).

[79] Saadsaoud, M., Ahmed, A. H., Er, Z., Rouabah, Z. (2017). Experimental Study of Degradation Modes and Their Effects on Reliability of Photovoltaic Modules after 12 Years of Field Operation in the Steppe Region. Special Issue of the 3rd International Conference on Computational and Experimental Science and Engineering (ICCESEN 2016), Acta Physica Polonica A, 132. doi: 10.12693/APhysPolA.132.930

[80] Siddiqui, M. U. & Arif, A. F. M. (2013). Electrical, thermal and structural performance of a cooled PV module: Transient analysis using a multiphysics model. Applied Energy, 112, 300-312. doi: 10.1016/j.apenergy.2013.06.030

[81] Şimşek Kuşçu, C. & Şengezer, B. (2012). İstanbul Metropoliten Alanında Kentsel Isınmanın Azaltılmasında Yeşil Alanların Önemi. Megaron, 7(2), 116-128.

[82] Smets, A., Narayan, N. (2013). PV Systems: PV Modules II – Temperature dependency of PV output. DelftX: ET3034TUx Solar Energy. Delft University of Technology. Retrieved from https://www.youtube.com/watch?v=v8nbwvC8aBg&t=2s&ab_channel=3rabGeeks

[83] Sodoudi, S., Shahmohamadi, P., Vollack, K., Cubasch, U., Che-Ani, A. (2014). Mitigating the Urban Heat Island Effect in Megacity Tehran. Advances in Meteorology, 1-19. doi: 10.1155/2014/547974

[84] SolarPower Europe. (2021). Global Market Outlook for Solar Power 2021-2025.

[85] Song, B. & Park, K. (2014). Validation of ASTER Surface Temperature Data withIn SituMeasurements to Evaluate Heat Islands in Complex Urban Areas. Advances In Meteorology, 2014, 1-12. doi: 10.1155/2014/620410

[86] Stewart, I. & Oke, T. (2012). Local Climate Zones for Urban Temperature Studies. Bulletin Of The American Meteorological Society, 93(12), 1879-1900. doi: 10.1175/bams-d-11-00019.1

[87] Svarc, J. (2021). Most Efficient Solar Panels 2021 - Clean Energy Reviews. Retrieved 14 December 2021, from https://www.cleanenergyreviews.info/blog/most-efficient-solar-panels

[88] T.R. Ministry of Environment, Urbanisation and Climate Change. Turkey Climate Change Strategy 2010 - 2023.

[89] Tachev, V. (2021). Renewable Energy Investments in Vietnam - Asia's Next Clean Energy Powerhouse. Retrieved 14 December 2021, from https://energytracker.asia/renewable-energy-investments-in-vietnam-asias-next-clean-energy-powerhouse

[90] Taoufik, M., Laghlimi, M., Fekri, A. (2021). Land suitability analysis for solar farms exploitation using the GIS and Analytic Hierarchy Process (AHP) – a case study of Morocco. Polityka Energetyczna – Energy Policy Journal, 24(2), 79-96. doi: 10.33223/epj/133474

[91] Tawalbeh, M., Al-Othman, A., Kafiah, F., Abdelsalam, E., Almomani, F., Alkasrawi, M. (2021). Environmental impacts of solar photovoltaic systems: A critical review of recent progress and future outlook. Science Of The Total Environment, 759, 143528. doi: 10.1016/j.scitotenv.2020.143528

[92] TEİAŞ. (2020). Kurulu Güç Raporu - Ekim 2020.

[93] TMMOB EMO. (2021). Türkiye Elektrik İstatistikleri - Şubat 2021.

[94] Toledo, C. & Scognamiglio, A. (2021). Agrivoltaic Systems Design and Assessment: A Critical Review, and a Descriptive Model towards a Sustainable Landscape Vision (Three-Dimensional Agrivoltaic Patterns). Sustainability, 13(12), 6871. doi: 10.3390/su13126871

[95] Tollefson, J. (2021). How hot will Earth get by 2100?. Retrieved 14 December 2021, from https://www.nature.com/articles/d41586-020-01125-x

[96] Tuncel, B., Ozden, T., Akinoglu, B. G., Balog, R. S. (2018). Thermal Modeling and Verification of PV Module Temperature and Energy Yield Using Outdoor Measurements for Ankara, Turkey Paper presented at the 1st International Conference on Photovoltaic Science and Technologies (PVCon2018), Ankara, Turkey. doi: 10.1109/PVCon.2018.8523953

[97] Tuncel, B., Ozden, T., Balog, R., Akinoglu, B. G. (2020). Dynamic thermal modelling of PV performance and effect of heat capacity on the module temperature. Case Studies in Thermal Engineering, 22, 100754. doi: 10.1016/j.csite.2020.100754

[98] Turney, D. & Fthenakis, V. (2011). Environmental impacts from the installation and operation of large-scale solar power plants. Renewable and Sustainable Energy Reviews, 15(6), 3261–3270. doi: 10.1016/j.rser.2011.04.023

[99] Türk, S., Koç, A., Şahin, G. (2021). Multi-criteria of PV solar site selection problem using GIS-intuitionistic fuzzy based approach in Erzurum province/Turkey. Scientific Reports, 11(1). doi: 10.1038/s41598-021-84257-y

[100] Tsoutsos, T., Frantzeskaki, N., Gekas, V. (2005). Environmental impacts from the Solar Energy Technologies. Energy Policy, 33(3), 289-296. doi: 10.1016/s0301-4215(03)00241-6

[101] Türkiye'nin güneş enerjisi kurulu gücü 7 GW'a yaklaştı - Gensed - Güneş Enerjisi Sanayicileri ve Endüstrisi Derneği. (2021). Retrieved 14 December 2021, from https://www.gensed.org/basin/t%C3%BCrkiyenin-g%C3%BCne%C5%9F-enerjisi-kurulu-g%C3%BCc%C3%BC-7-gwa-yakla%C5%9Ft%C4%B1

[102] van de Ven, D., Capellan-Peréz, I., Arto, I., Cazcarro, I., de Castro, C., Patel, P., Gonzalez-Eguino, M. (2021). The potential land requirements and related land use change emissions of solar energy. Scientific Reports, 11(1). doi: 10.1038/s41598-021-82042-5

[103] Voogt, J. (2008). How Researchers Measure Urban Heat Islands. US Environmental Protection Agency. Retrieved from https://19january2017snapshot.epa.gov/sites/production/files/2014-07/documents/epa_how_to_measure_a_uhi.pdf

[104] Vrînceanu, A., Grigorescu, I., Dumitrașcu, M., Mocanu, I., Dumitrică, C., Micu, D. et al. (2019). Impacts of Photovoltaic Farms on the Environment in the Romanian Plain. Energies, 12(13), 2533. doi: 10.3390/en12132533

[105] Vrînceanu, A., Dumitrașcu, M., Mocanu, I., Grigorescu, I., Șerban, P., Mitrică, B., Dumitrică, C. (2020). Environmental and Socio-Economic Impacts of Photovoltaic Parks in the Centre Development Region. Romania. In International Scientific Conference GEOBALCANICA 2020. Ohrid, North Macedonia.

[106] Walston, L., Li, Y., Hartmann, H., Macknick, J., Hanson, A., Nootenboom, C. et al. (2021). Modeling the ecosystem services of native vegetation management practices at solar energy facilities in the Midwestern United States. Ecosystem Services, 47, 101227. doi: 10.1016/j.ecoser.2020.101227

[107] What is Earth's Energy Budget? Five Questions with a Guy Who Knows. (2021). Retrieved 14 December 2021, from https://www.nasa.gov/feature/langley/what-is-earth-s-energy-budget-five-questions-with-a-guy-who-knows

[108] World Meteorological Organization. (2020). State of the Global Climate 2020.

[109] World Meteorological Organization. (2020). The State of Greenhouse Gases in the Atmosphere Based on Global Observations through 2019 (p. 2).

[110] World Wildlife Fund. (2010). Türkiye'nin Yarınları Projesi Sonuç Raporu.

[111] Wu, W., Yue, S., Zhou, X., Guo, M., Wang, J., Ren, L., Yuan, B. (2020). Observational Study on the Impact of Large-Scale Photovoltaic Development in Deserts on Local Air Temperature and Humidity. Sustainability, 12(3403). doi: 10.3390/su12083403

[112] Xu, M., Bruelisauer, M., Berger, M. (2017). Development of a new urban heat island modeling tool: Kent Vale case study Paper presented at International Conference on Computational Science (ICCS 2017), Zurich, Switzerland. doi: 10.1016/j.procs.2017.05.282

[113] Yılmaz, E. (2015). Landsat Görüntüleri ile Adana Yüzey Isı Adası. Coğrafi Bilimler Dergisi (Ankara University), 13(2), 115-138. doi: 10.1501/Cogbil_0000000167

[114] Yue, S., Guo, M., Zou, P., Wu, W., Zhou, X. (2021). Effects of photovoltaic panels on soil temperature and moisture in desert areas. Environmental Science And Pollution Research, 28(14), 17506-17518. doi: 10.1007/s11356-020-11742-8

[115] (2014). Reducing Urban Heat Islands: Compendium of Strategies. US Environmental Protection Agency (US EPA). Retrieved from https://www.epa.gov/sites/production/files/2014-06/documents/basicscompendium.pdf

[116] (2022). Content - Calculating confidence intervals. (2022). Retrieved 19 January 2022, from http://amsi.org.au/ESA_Senior_Years/SeniorTopic4/4h/4h_2content_11.html#:~:text=For%20a%2095%25%20confidence%20interval,%2C%20we%20use%20z%3D1.64

# APPENDICES

## A. PV Module Brand and Model Information

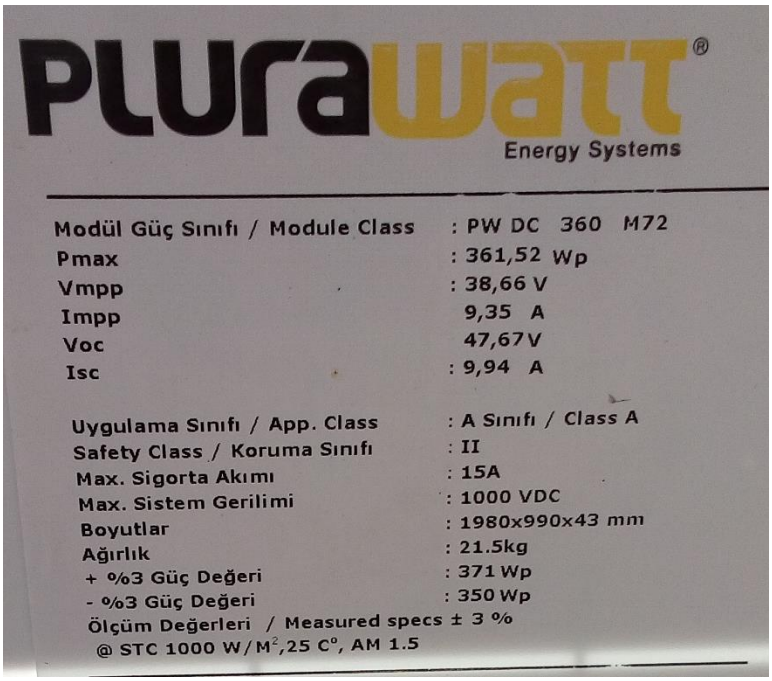


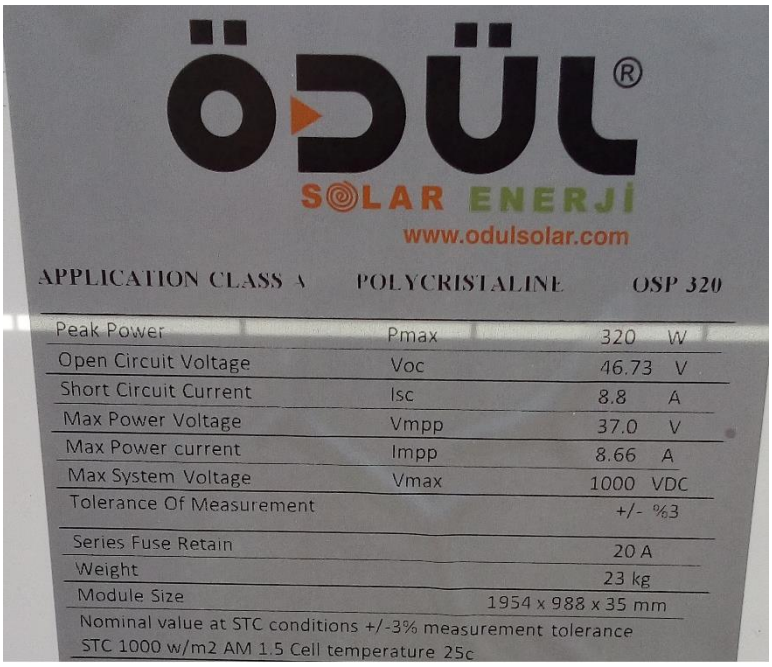

## B. Weather Station Equipment

| Photo | Brand / Model | Weather Data | Time Interval |
|---|---|---|---|
|  | Davis / Vantage Pro2™ | *Solar Radiation*<br>0 to 1800 W/m$^2$ (acc. ±5%)<br>*Air Temperature*<br>-40° to +65°C (acc. ±0.3°C)<br>*Relative Humidity*<br>1 to 100 % (acc. ±2%)<br>*Barometric Pressure*<br>540 to 1100 hPa/mb (acc. ±1.0 hPa/mb)<br>*Wind Dir. & Speed*<br>540 to 1100 hPa/mb (acc. ±1.0 hPa/mb)<br>1 - 360° (acc. ±3°) | 10-minutes<br>Hourly<br>Daily<br>Weekly<br>Monthly |
|  | PV-met / 150 | *Solar Radiation*<br>0 to 2000 W/m$^2$ (acc. ±5%)<br>*Ambient Air Temp.*<br>-40° to 80°C (acc. ±0.3°C) | Hourly |
|  | PV-met / A2101 | *PV Module Temp.*<br>-40° to 80°C (acc. ±0.3°C) | Hourly |

## C. TSMS's Acceptance Letter *(in Turkish)*

T.C.
ORMAN VE SU İŞLERİ BAKANLIĞI
Meteoroloji Genel Müdürlüğü
Meteorolojik Veri İşlem Dairesi Başkanlığı

Sayı : 95579059-107-E.15826 20/04/2018
Konu : Meteorolojik Bilgi

ODTÜ GÜNEŞ ENERJİSİ ARAŞTIRMA VE UYGULAMA MERKEZİNE
ODTÜ Kampüsü Üniversiteler Mah. Dumlupınar Bulvarı No:1
06800 Çankaya / ANKARA

İlgi : ODTÜ Güneş Enerjisi Araştırma ve Uygulama Merkezi' nin 17.04.2018 tarihli ve 19464727/GÜNAM-2018-75 sayılı ve 15310 EBYS kayıt nolu yazısı.

İlgi yazı ile istenilen bilgiler, Tavşanlı Otomatik Meteoroloji Gözlem İstasyonumuz ile birlikte, civarda yakın olan ve güneşlenme ile buharlaşma ölçümlerinin yapıldığı Afyonkarahisar ve Kütahya Meteoroloji İstasyonlarımızın mevcut kayıtlarından çıkartılarak ekte gönderilmiş olup Tavşanlı Otomatik Meteoroloji Gözlem İstasyonumuzun koordinatları, istasyonda bulunan bütün algılayıcılar marka modelleri, ölçüm yükseklik bilgileri hazırlanarak aşağıda sunulmuştur.

Bilgilerinizi rica ederim.

Cemal OKTAR
Genel Müdür a.
Meteorolojik Veri İşlem Dairesi Başkanı

| Kurulu OMGİ Adı | Enlem | Boylam | Yükseklik(m) |
|---|---|---|---|
| Tavşanlı | 39,538395 | 29,494086 | 833 |

| Algılayıcı | Marka ve Modeli | Yerden Yüksekliği |
|---|---|---|
| Rüzgar Yön ve Hızı | Lastem DNA011<br>Lastem DNA002 | 10 Metre |
| Sıcaklık | Rotronic MP101A | 2 Metre |
| Nem | Rotronic MP101A | 2 Metre |
| Yağış | Lastem DQA031 | 1 Metre |
| Basınç | DRUCK RPT200 | 1,5 Metre |
| Toprak Sıcaklıkları | Campbell PT100 3 Telli | +5, -5, -10, -20, -50, -100 cm |
| Toprak Nemi | Campbell CS616 | -10 cm |

Ek: CD (1 Adet)

Bu evrak 5070 sayılı Elektronik İmza Kanunu'na göre elektronik olarak imzalanmıştır. http://ebys.mgm.gov.tr/dogrulama.aspx adresi üzerinden K3W23030258D1 kodu ile doğrulama yapabilirsiniz.

Kütükçü Alibey Caddesi No: 4
06120 Kalaba/ANKARA
Tel/Faks:0 312 359 75 45/360 25 51
www.mgm.gov.tr
Kep:meteorolojigenelmudurlugu@hs01.kep.tr

Ayrıntılı Bilgi: E.Poyraz - Rasatçı
Tel: 0 312 203 24 44
E-posta: epoyraz@mgm.gov.tr

## CURRICULUM VITAE

Surname, Name: Demirezen, Emre
Nationality: Turkish (TC)
Date and Place of Birth: 18 August 1985, Ankara
Marital Status: Single
Phone: +90 506 327 36 99
email: demre@metu.edu.tr / emre.foton@gmail.com

### EDUCATION

| Degree | Institution | Year of Graduation |
|---|---|---|
| MS | METU Science and Tech. Policy Studies | 2014 |
| BS | Hacettepe Univ. Physics Engineering | 2008 |
| High School | Etimesgut Anadolu High School, Ank. | 2003 |

### WORK EXPERIENCE

| Year | Place | Enrollment |
|---|---|---|
| 2016-Present | ODTÜ-GÜNAM | Research Assistant |
| 2012-2016 | ODTÜ-FEAS | Research & Computer Assistant |
| 2009-2010 | MYLASER | Optical Design and Test Engineer |

### FOREIGN LANGUAGES

Advanced English

## PUBLICATIONS

1. Demirezen, E., Ozden, T., Akinoglu, B. G. (2018). "Impacts of a Photovoltaic Power Plant for Possible Heat Island Effect Paper" presented at the 1st International Conference on Photovoltaic Science and Technologies (PVCon2018), Ankara, Turkey. doi: 10.1109/PVCon.2018.8523937 (IEEE-Xplore Digital Library)

2. Demirezen, E., Ozden, T., Akinoglu, B. G. (2019). "In Situ Measurements of Photovoltaic Heat Island Effect (PV-HIE) and Findings from Sekbandemirli Solar Power Plant in Tavsanli, Kutahya" presented at the 6th International Conference on Computational and Experimental Science and Engineering. Antalya, Turkey.

3. Demirezen, E., Ozden, T., Akinoglu, B. G. (2020). "Monitoring and Assessment of Daily and Seasonal Photovoltaic Heat Island Effect on Sekbandemirli Rural Region in Kütahya, Turkey" presented at the 2nd International Conference on Photovoltaic Science and Technologies (PVCon2020), Ankara, Turkey.

## PUBLICATION PREPARATIONS

The part of this thesis study entitled "Analysis and Assessment of Daily and Seasonal Photovoltaic Heat Island Effect on Sekbandemirli Rural Region by Local Weather Data Records" and the ENVI-met simulation results will be separately submitted for journal article applications.